University of Alberta

Collaborative Beamforming for Wireless Sensor Networks

by

Mohammed F. A. Ahmed

A thesis submitted to the Faculty of Graduate Studies and Research
in partial fulfillment of the requirements for the degree of

Doctor of Philosophy

Department of Electrical and Computer Engineering

Spring 2011
Edmonton, Alberta

Examining Committee

Sergiy A. Vorobyov, Electrical and Computer Engineering

Sofiéne Affes, Institut National de la Recherche Scientifique (INRS), University of Quebec

Peter Hooper, Mathematical and Statistical Sciences

Chinta Tellambura, Electrical and Computer Engineering

Masoud Ardakani, Electrical and Computer Engineering

To my parents,
and to the martyrs of the Egyptian revolution.

Abstract

Many Wireless Sensor Network (WSN) applications require sensor nodes to be deployed over a remote area to collect data from the surrounding environment and communicate it to far Base Stations or Access Points (BSs/APs). The limited power and hardware capabilities of individual sensor nodes prevent direct transmission to far away destinations. However, the inherent high density deployment of sensor nodes can be exploited to increase the transmission range. Collaborative Beamforming (CB) has been introduced in WSNs context as a power-efficient communication scheme that increases the transmission range using a cluster of sensor nodes. However, CB inherits some challenges from the distributed nature of WSNs. Namely, the randomness of sensor node locations and the need for distributed schemes. The randomness of sensor node locations results in different beampatterns for different network realizations.

In this thesis, we first study the average behavior of CB for a given spatial distribution of sensor nodes. Gaussian Probability Density Function (pdf) is used to model the spatial distribution of sensor nodes in a cluster of WSN. It is shown that Gaussian pdf is more suitable in many WSN applications than, for example, uniform pdf which is commonly used for flat ad-hoc networks. The average CB beampattern and its characteristics are derived using the theory of random arrays. The distribution function of the beampattern level in the sidelobe region and the upper bound on the outage probability of sidelobes are found and compared with the corresponding characteristics resulting from uniform distributed sensor nodes. For any particular realization of sensor node locations, the mainlobe of the beampattern matches precisely the mainlobe of the average beampattern. Therefore, the mainlobe behavior can be considered to be deterministic. This suggests that the average beampattern characteristics are suitable for describing the mainlobe of a sample

beampattern. However, the CB beampattern is still random in the sidelobe region and severely depends on the particular sensor node locations.

In the case of WSN with multiple BSs/APs, high level sidelobes can cause unacceptable interference to unintended BSs/APs. By controlling the power level in the sidelobe region and limiting the interference to unintended BSs/APs, the network capacity can be increased if Space Division Multiple Access (SDMA) is employed. To apply traditional sidelobe control techniques in the context of WSNs, a central processing node or a BS/AP has to collect the nodes location information and Channel State Information (CSI) from all sensor nodes. Then it can design the beamforming weights and communicate them back to the collaborative nodes for the beamforming step. However, this is impractical for distributed sensor nodes especially for a densely populated WSN because the overhead needed to communicate with each node individually grows unacceptably high. Therefore, we propose a node selection scheme for CB sidelobe control which aims at minimizing the interference at unintended BSs/APs. A selection algorithm with low implementation complexity and low feedback is developed to search over different sensor node combinations. If in random network coding, the inherent randomness of the channels is used, out algorithm is based on both the use of the randomness of the channels and a low feedback that approves/rejects tested random node combinations. The performance of the proposed algorithm is analyzed in terms of the average number of trials and the achieved interference suppression. Simulation results match the analytical approximations and show the effectiveness of node selection for controlling the sidelobes and limiting the interference.

Finally, we study the energy consumption behavior in WSNs and aim at optimizing it through the CB with power control. Since the transmission is the major energy consuming task in sensor nodes, it is important to study the effect of CB with power control on the energy consumption of WSNs. When CB distributes the energy consumption among the collaborative sensor nodes, it has to take into account that the energy at each sensor node is not the same. Indeed, different sensor nodes may perform different tasks and not equally frequently. Clearly the assignment of different CB weight powers will result in changing the individual sensor nodes' lifetimes. Thus, we propose a distributed algorithm for CB with power control that is based on the Residual Energy Information (REI) at each sensor node while achieving the required average SNR at the BS/AP. The resulting power control have low

computational complexity and maximizes the network lifetime. The effectiveness of the proposed CB with power control algorithm is illustrated by simulations.

Acknowledgements

I express my sincere gratitude to my supervisor Prof. Sergiy A. Vorobyov for his supervision, continuous advice, encouragement, and providing an excellent research environment. His enthusiasm, approachability and patience were essential to the completion of this dissertation. In addition, I would like to thank my supervisory committee members, Prof. Chinta Tellambura and Prof. Masoud Ardakani, for their precious comments and suggestions and for being helpful. I am sincerely thankful to Prof. Sofiéne Affes and Prof. Peter Hooper for serving in my examination committee. I appreciate the time they devoted in reading my thesis and their cooperation and contributive comments. I would like to acknowledge Dr. Aboulnasr Hassanien and Dr. Amir Masoud Rabiei for the insightful comments, valuable advices, and useful suggestions. Moreover, I would like to give thanks to all my colleagues at University of Alberta who have contributed greatly to provide a supportive and exciting research atmosphere. The assistance from other members and staff at the ECE Department at University of Alberta is also appreciated. I would like to thank all my friends in the lab and in Edmonton who made me feel home. Special thanks are due to the Egyptian Students Association (ESA) who were there for me whenever I needed them and provided countless support and help to me. I would like to sincerely thank my parents and siblings, Marwa, Mostafa, and Mona, for their endless support and continuous encouragement throughout my life. Finally, I am grateful to the Government of Egypt for the financial support. I am greatly obligated to the Bureau of Cultural and Educational Affairs of Egypt in Canada for being supportive and conscientious.

Table of Contents

List of Tables

List of Figures

List of Abbreviations

WSNs	Wireless Sensor Networks
CB	Collaborative Beamforming
RF	Radio Frequency
SoC	Development of System-on-Chip
MEMSs	Micro-Electro-Mechanical-Systems
DSP	Digital Signal Processing
BSs/APs	Base Stations or Access Points
DT	Direct Transmission
MAC	Media Access Control
SNR	Signal-to-Noise Ratio
SDMA	Space Division Multiple Access
DAR	Distributed Array Radar
pdf	Probability Density Function
iid	Independent Identically Distributed
PLL	Phase Locked Loop
DS-CDMA	Direct Sequence Code Division Multiple Access
TDD	Time-Division Duplexing
TDMA	Time-Division Multiple Access
FDMA	Frequency-Division Multiple Access
OFDMA	Orthogonal Frequency-Division Multiple Access
CDMA	Code Division Multiple Access
NDMA	Network-Assisted Diversity Multiple Access
MIMO	Multiple-Input Multiple-Output
ALLIANCES	ALLow Improved Access in the Network via Cooperation and Energy Savings
MAC-PHY	Medium Access Control-Physical

SINR	Signal-to-Interference-plus-Noise Ratio
CSI	Channel State Information
2D	2 Dimensional
LOS	Line-Of-Sight
CCDF	Complementary Cumulative Distribution Function
ID	Identification
AWGN	Additive White Gaussian Noise
INR	Interference-to-Noise Ratio
REI	Residual Energy Information

List of Symbols

λ	the signal wavelength
j	$\sqrt{-1}$
x_r	the x coordinates for the rth antenna element
y_r	the y coordinates for the rth antenna element
ρ_r	the distance from the origin to the rth antenna element
ϕ_r	the azimuth direction for the rth antenna element
θ_r	the elevation direction for the rth antenna element
ρ	the radial distance in the spherical coordinates
ϕ	the azimuth direction in the spherical coordinates
θ	the elevation direction in the spherical coordinates
ϱ	the distance from the origin to the BS/AP
φ	the azimuth direction of the BS/AP
ϑ	the elevation direction of the BS/AP
$f(\cdot)$	the probability density function
$\mathbb{F}(\cdot)$	the array factor
$\mathbb{P}(\cdot)$	the beampattern
N	the number of collaborative sensor nodes
m	the mean of random variable
σ^2	the variance of random variable
$\delta_r(\phi, \theta)$	the distance between the rth sensor node and point (ϱ, ϕ, θ)
$\boldsymbol{\rho}$	the radial distance vector of sensor nodes
$\boldsymbol{\phi}$	the azimuth direction vector of sensor nodes
ψ_k	the initial phase of the rth sensor node's carrier
α	the azimuth direction parameter
z_r	the rth sensor node location parameter

$\mathbf{z}$	the location parameter vector of sensor nodes
$\mathbb{P}_{\text{av}}(\cdot)$	the average beampattern
R	the radius of the cluster
$\tilde{R}$	the radius of the cluster normalized to λ
ϕ_{3dB}	the 3dB beamwidth
ϕ_{SL}	the 3dB sidelobe region start angle
$D(\cdot)$	the directivity
D_{av}	the average directivity
D^*_{av}	the lower bound on the average directivity
${}_1F_1(\cdot)$	the hypergeometric function of the first kind
${}_2F_3(\cdot)$	the generalized hypergeometric function
X	the real part of the array factor approximation at angle ϕ
Y	the imaginary part of the array factor approximation at angle ϕ
$Q_M(\cdot)$	the first-order Marcum-Q function
Pr_{out}	the outage probability
$\mathcal{D}$	the set of BSs/APs
d_k	the kth BS/AP
$\mathcal{S}$	the set of source sensor nodes
s_k	the kth source sensor node
$K+1$	the number of source–destination pairs
$\mathcal{M}^k$	the set of nodes in the coverage area of the node s_k
c_r	the rth collaborative node
P_r	the transmit power of the rth sensor node
ψ_r^k	the initial phase of the rth node's carrier targeting d_k
$\psi_r(\phi)$	the phase delay due to propagation at the point (ϱ, ϕ)
h_{rk}	the channel coefficient between the rth node and the kth BS/AP
a_{rk}	the flactuation/shadowing effect in the channel coefficient h_{rk}
b_{rk}	the attenuation/path loss effect due to propagation distance in the channel coefficient h_{rk}
z_k	the data symbol broadcasted from the source node s_k
t_r	the transmitted signal by the collaborative node c_r

$g(\phi)$	the received signal at angle ϕ from $\mathcal{M}^k$
g_{k^*}	the received signal at the BS/AP d_{k^*} from $\mathcal{M}^k$
w	the AWGN received at BSs/AP
σ_w^2	the power of the AWGN received at BSs/AP
$\mathcal{R}\{\cdot\}$	the real part of a complex number
$\mathcal{I}\{\cdot\}$	the imaginary part of a complex number
$\mathcal{N}^k$	the set of collaborative nodes to target d_k
η	the INR
M	the number of nodes in the coverage area of s_k
L	the size of one group of nodes to be tested in each trial
$\mathcal{L}^k$	the set of candidate nodes from $\mathcal{M}^k$
γ	the CB transmission power normalized to σ_w^2
$I\left(\varphi_k \vert \mathcal{L}_l^{k^*}\right)$	the interference power received at d_k from the set $\mathcal{L}_l^{k^*}$
σ_a^2	the variance of a_{rk}
m_a^2	the mean of a_{rk}
η_{thr}	the INR threshold value
p'	the probability of approval of a candidate set of nodes
$\text{Q}(\cdot)$	the Q-function of the Gaussian distribution
$\gamma_{\text{ML}}^{k^*}$	the average SINR at the intended BS/AP d_{k^*} for the proposed multi-link CB with node selection
$2\sigma_I^2$	the interference from single BS/AP
C_{ML}	the transmission rate in bits/sec/Hz of the multi-link CB
$\bar{\gamma}_{\text{ML}}^{k^*}$	the average SINR at the intended BS/AP d_{k^*} for the multi-link CB without node selection
$\gamma_{\text{SL}}^{k^*}$	the SNR at the intended BS/AP d_{k^*} in the single-link CB
C_{SL}	the transmission rate in the single-link CB
$\max\{\cdot\}$	the maximum value of a function
$E\{\cdot\}$	the statistical average
$J_1(\cdot)$	the first order Bessel function of the first kind.
$\text{card}(\cdot)$	the cardinality of a set
$\vert\cdot\vert$	the magnitude of a complex number
E_{tx}^{e}	the energy consumption of the transmitter electronics
E^{a}	the energy consumed by the transmit power amplifier
E_{rx}^{e}	the energy consumption of the receiver electronics

$\boldsymbol{u}$	the normalized CB weight vector
w_{max}	the maximum CB weight
$\boldsymbol{w}$	the CB weight vector
$\boldsymbol{E}$	the REI vector
E_{max}	the maximum energy available at each node
$\bar{\gamma}$	the required average SNR at the targeted BS/AP
m_E	the mean of REI
σ_E^2	the variance of REI

Chapter 1

Introduction

1.1 Thesis Overview

Wireless Sensor Networks (WSNs) technology is a promising technology that attracted considerable research attention in recent years [1]–[4]. The low-cost of sensor nodes and flexible deployment of WSNs allow for new applications that were expensive or not realistic in the past [5]. Moreover, unlike traditional sensors, modern wireless sensor nodes have sensing, processing, and wireless transmitting capabilities, and thus are able to perform more than just sensing function of the surrounding environment [6]. Raw data can be pre-processed, compressed, or fused at sensor nodes or central point before data is transmitted to the destination [7], [8] and thus, the transmission energy consumption and system response time can be reduced [9]. Sensor nodes' cheap price and self-configuring ability allow for dense deployment that can increase the accuracy of the collected data and increase the fault tolerance [10], [11].

However, the distributed nature of WSNs along with the limited resources available at sensor nodes introduce new challenges to the communication system design [12]. Existing communication schemes are not specifically designed to meet the WSN requirements or consider its constraints and can not be directly applied to WSNs [13]. One major constraint in WSNs is the short transmission range of individual sensor nodes resulting from its limited energy and hardware simplicity [12]. A recent solution to this problem is to apply Collaborative Beamforming (CB) in the context of WSNs to achieve directional transmission and distribute power consumption over a group of sensor nodes. Since each sensor node is equipped with single omni-directional antenna, sensor nodes coordinate their transmissions and act collaboratively as an antenna array. Given that sensor nodes are able to share data

and synchronize their carrier's phase and frequency, the data can be transmitted coherently.

Unlike traditional antenna arrays with predetermined geometry, the deployment of sensor nodes in WSNs is ad-hoc and results in randomly located sensor nodes. Thus, the beampatten of such random array of sensor nodes is random and changes for each realization of sensor nodes' locations. The CB beampatten behavior is studied and its performance for data transmission is proved to be reliable [14], [15]. The focus of this thesis is on studying the behavior of the CB beampattern and determining its reliability for achieving direct link transmissions in WSNs. First, we study the effects of spatial distribution of sensor nodes on the beampattern characteristics. We compare the beampattern characteristics for two different spatial distributions of sensor node locations, namely, the uniform and Gaussian spatial distributions. The influence of spatial distribution parameters such as cluster area and number of sensor nodes is analyzed which is useful for designing good deployment strategies. It is shown that both the uniform and Gaussian sensor node deployments behave qualitatively in a similar way in terms of the beamwidths and sidelobe levels of average beampattern, while the Gaussian deployment gives wider mainlobe and has lower chance of large sidelobes. We go one step further and propose a method to control, up to a certain extend, the randomness of the CB beampattern at unintended directions of the sidelobe region. The improvement of the CB performance due to beampattern control is studied in terms of the data rate increase. The energy consumption is considered afterwards and a CB weight design algorithm is proposed to extend the WSN lifetime. Since sensor nodes are responsible for different tasks such as sensing, data pre-processing, and communication, the energy consumption is not the same at individual sensor nodes and the remaining energy at each sensor node is different. The argument is that the transmission hardware at sensor nodes is the most energy consuming part. Thus, good choice of CB weight amplitudes at sensor nodes can extent overall WSN lifetime.

1.2 Wireless Sensor Networks

In this chapter, we introduce the WSNs and discuss the specific scenarios for implementing WSNs. The requirements and constraints for data communication in WSNs are reviewed. We give a brief background on the theory of random arrays and presents its main results. Afterwards, the motivation and the contributions of

our research are stated. Finally, we give the outline of the thesis.

1.2.1 Definition and Tasks of WSNs

In the recent years, WSNs technology is becoming a practical technology and a number of its potential applications is growing rapidly. Moreover, the cost of deploying large-scale networks decreases rapidly due to the advances in different engineering areas [16]–[19]. WSNs consist of a potentially large number of sensor nodes that are deployed over an area of interest and connected to each other through wireless links. Sensor nodes are capable of collecting data from the surrounding environment and communicating the collected data to a central point for further processing or decision making. Sensor node has at least four basic components: sensing unit, processor, Radio Frequency (RF) transceiver, and energy source (battery). Different types of sensors can be used in sensor nodes such as mechanical, thermal, biological, chemical, optical, magnetic, visual, and infrared sensors [20]. Advances in different engineering fields had directly affected the practicality of WSNs. Development of System-on-Chip (SoC) and Micro-Electro-Mechanical-Systems (MEMSs) technologies provide small-size, low-power, and low-complexity nodes with sensing, computation, and communication capabilities at reasonable price [17]. Also, in the Digital Signal Processing (DSP) area, many algorithms have been proposed to match distributed applications, and the computations are optimized for low-complexity hardware [21]–[24]. Collaborative signal processing algorithms that have been developed for WSNs include time synchronization [25]–[27], localization [28], [29], target tracking [30], [31], and distributed source coding [32], [33]. Moreover, RF circuits and wireless standards, such as ZigBee [34], are introduced for low-power communications over short distances as the demand for new applications grows [35].

1.2.2 Applications of WSNs

WSNs opened the door to many potential applications where different tasks can be performed with the collected data, such as object tracking, classification, parameter estimation, etc. [36]–[39]. While it is difficult to list all WSNs applications, some applications are briefly overviewed here:

- **Environmental Applications:** WSNs are used to detect natural disasters such as landslide [40], forest fires [41], [42], floods [43], or hurricanes [44]. Also, it allows to monitor various parameters such as temperature, pressure, or air

quality [45]. Additionally, WSNs can be used to collect data for scientific research. For instance, in the SensorScope project [46], a WSN is deployed in a harsh mountain environment to study the requirements of the environmental monitoring. Other WSN projects are reported in [47] for measuring temperature, light, and soil moisture for environmental monitoring in greenhouses, and in [48] for measuring the soil moisture changes due to rainfall.

- **Industrial Applications:** WSNs are used for real-time data acquisition and control in industrial applications [6], [49]–[52]. Wireless sensor nodes are replacing the traditional wired sensors due to its flexible configuration [53] and are deployed to measure temperature, pressure, impedance, or other quantities [54]. Different tasks have to be performed in the industrial applications such as surveillance [55], automation [56], and equipment faults detection [57].

- **Military and Security Applications:** Sensor nodes can be scattered in a battlefield to gather information about enemy movements or detect the occurrence of events of interest such as nuclear, biological or chemical attacks. Examples for military and security applications includes intrusion detection [58], video surveillance [59], [60], boarder monitoring [61], and fire rescue [62].

- **Health Applications:** Health care systems use sensor nodes to monitor vital signs such as temperature, pulse rate, respiration rate, and blood pressure for patients and seniors in real-time [63], [64]. The data can be recorded and used for diagnostic and treatment purposes.

More applications are being proposed with the new advances achieved everyday in the WSN research.

1.2.3 WSNs Design Factors and Challenges

WSNs are used in many applications with different requirements and there is no single standard design [65]. Selecting design factors like topology, sensor hardware, wireless technology, energy source, deployment method, and etc. depend significantly on a particular application. Knowledge of different challenges related to the sensor nodes hardware and deployment is important to develop techniques targeting WSNs. WSN design factors include:

- **Scalability:** Some applications require very large area coverage and the WSN could consist of hundreds, thousands, or even millions of sensor nodes. The

sensor nodes density varies depending on the required amount and quality of measurements, the phenomenon field to be monitored, and the deployment strategy. In some situations, it is required to deploy more sensor nodes to improve the network functionality in terms of improving the network connectivity or even to replacing dead sensor nodes.

- **Power Efficiency:** Sensor nodes are required to operate with low power to extend the battery lifetime, and hence the overall WSN lifetime [66]–[68]. The same requirement applies for sensor nodes powered by energy-harvesting because of the limited energy generated from the surrounding environment. Power-aware protocols and algorithms are the most important requirements for WSNs.

- **Sensor Node Hardware:** The cost of individual sensor node determines the total cost of the WSN. It is critical to reduce the sensor node price and make the WSN financially feasible [17], [69]. Manufacturing cheap sensor nodes require using low-complexity hardware. Moreover, the size of sensor nodes hardware must be small to facilitate easier and flexible deployment. Depending on the application, some extra components can be added to achieve certain requirements for the application, such as a positioning and location-aware unit or a mobilizer.

- **Wireless Technology:** Wireless standards commonly used in WSN are 802.15.4 and ZigBee [34], [70], [71]. Sensor nodes RF circuits enable short distance wireless communication with low power consumption and can usually achieve a data rate up to hundreds of Kbps [72].

- **Topology:** Once deployed, sensor nodes are unattended therefor, the WSN should be self-organizing. Sensor nodes have cooperate while the topology of the network changes dynamically due to failure of sensor nodes or deployment of new sensor nodes. Sensor nodes can be stationary, which is the most common case, or mobile. In the latter case, sensor nodes are able to move and re-position according to the physical phenomena they monitor [35]. On the other side, WSNs can consist of few sensor nodes that are deployed at specific locations with fixed topology.

- **Deployment:** Sensor nodes are typically deployed very close the monitored phenomenon. Deployment can be done in ad-hoc fashion or in terms of one by one placement in a predetermined locations. Ad hoc deployment is used when WSN has a large number of sensor nodes which are deployed in mass by, for example, dropping them from a plane in the area to be monitored. When the WSN has few sensor nodes in an easy to access place, one by one placement by a human or a robot can be used. Dense deployment of sensor nodes improves the data accuracy/reliablity and increase the WSN robustness against sensor nodes failure.

- **Distributed:** WSNs are infrastructure-free networks with all processing and communication tasks being distributed. Moreover, distributed processing and communication is suitable for the limited resources and simple hardware typical for such sensor nodes.

- **Data Collection:** Sensor nodes communicate the collected data to a central point or data fusion center that can be fixed or mobile depending on the application scenario. Moreover, sensor nodes can process the collected data before transmitting to the central data destination. The processing can be performed locally at each sensor node or cooperatively among different sensor nodes in WSN.

- **Fault Tolerance:** Protocols, schemes, and algorithms designed for WSNs should be fault tolerant to sustain the functionality of the network [11]. Indeed, sensor nodes can stop working because of physical damage or energy depletion. However, the overall performance of WSN should not depend on the failure of individual sensor nodes.

- **Maintenance:** In most of WSNs applications, sensor nodes are deployed in difficult-to-access locations and they are left unattended after deployment. WSN maintenance is performed by deploying new sensor nodes to replace dead sensor nodes, sustain connectivity, or improve network coverage.

It is essential to determine the appropriate assumptions, deployment scenario, and design factors before designing protocols, algorithms, or schemes for WSNs.

1.3 Scenario of Interest

In this thesis, we focus on the scenario where sensor nodes are deployed in an ad-hoc fashion over large and remote area to collect information form the surrounding neighborhood. Sensor nodes transmit the collected data to a far Base Stations or Access Points (BSs/APs) which are located far away and out of the transmission range of individual senor nodes. In some applications, the collected data are redundant and sensor nodes refine them locally before transmitting the data to the BSs/APs. In other applications, the sensor nodes remain inactive most of the time and activate when certain event is detected. On either case, the traffic has low-rate and burst nature. In such scenario, sensor nodes are usually deployed at the ground level, thus, the channel path loss for individual node is high and the slow rate shadowing is the dominant factor in the channel variations. The aforementioned scenario is found in applications like environmental and habitat monitoring [65], [73], [74]. Challenges for data communication in such scenario are quite different from the traditional wireless ad-hoc networks [18]. The main constraints are the sensor node's limited resources and the ad-hoc deployment. In order to keep the production cost of the sensor node reasonable, sensor nodes used for this kind of applications are required to be small size with very simple hardware. Therefore, all proposed methods should be distributed or at least semi-distributed and be charachterized by minimum possible computational complexity. Each sensor node is equipped with one omnidirectional antenna and transmission is performed in half-duplex mode. The WSN is densely deployed to capture more data and improve the reliability of the network. Communication schemes designed for WSNs should be scalable, because the size of the network can vary from hundreds to millions of sensor nodes. The network topology is dynamic because of possible failure of sensor nodes or due to deployment of new sensor nodes. For achieving robust WSN operation, it is desired that the WSN performance does not depend on individual sensor nodes. Energy in sensor nodes can be supplied from batteries or energy harvesting devices [75]–[77]. In the case of battery-powered sensor nodes, the battery often cannot be replaced, thus, the sensor node lifetime is limited by the battery lifetime and the available battery technology results in bulky batteries. Energy harvesting is currently developed as alternative solution to power sensor nodes by equipping them with a device capable to convert one form of surrounding energy into electric energy. Electric

energy is typically obtained from:

- **Solar energy:** Photovoltaic cells are know in many other applications and are well established. It is based on the photovoltaic effect where incoming photons are converted into electricity.
- **Motion and Vibration:** This method is based on the electrostatic, piezoelectric, or electromagnetic transduction to convert motion or vibration into voltage.
- **RF Energy:** In this case, sensor node extract RF energy radiated from wireless networks like GSM, WLAN, or TV station.
- **Temperature Differences:** This method is based on the fact that a junction of two different conductors at different temperatures generates a voltage.

However, with the current technology, the price of the harvesting device is high and will increase the total cost of the sensor node. Moreover, the energy generated by energy harvesting is low and still remains to be a limited resource. In both cases of using battery or energy harvesting, the energy consumption of sensor nodes should be minimized as much as possible to prolong the overall network lifetime.

1.4 Data Transmission in WSNs

Sensor nodes are deployed close to the phenomena monitored and the collected data are sent to a central station. Long-distance Direct Transmission (DT) to the BSs/APs is expensive in terms of energy consumption and the transmitted signal decay dramatically because of deployment on the ground and short antenna heights. Moreover, RF transceiver circuit is the main energy consuming part in the sensor node, and long-distance transmission is not feasible with the available technology. It is critical to design alternative communication schemes which would be still practical for WSNs. By practical, we specifically mean, energy-efficient, low-complex, distributed, scalable. Low complexity and high energy-efficiency are the most critical constraints in designing communication protocols and physical layer techniques. Data transmission in WSNs is addressed at the media access and network layers, through multi-hop relay transmission, or at the physical layer, through directional coherent transmission.

1.4.1 Multi-hop Relay Transmission

The energy consumed in data transmission increases for long distance transmission. On the same time, WSN is characterized by the high density deployment of sensor nodes. Therefore, it is natural to use short distance transmissions between neighboring sensor nodes to relay data from the source sensor node to the destination. In multi-hop relay transmission, sensor nodes broadcast the data only to the sensor nodes in its coverage area and data is routed through different relays from the source to the destination. Multi-hop relay communication requires Media Access Control (MAC) [78] and routing protocols [79], [80]. MAC protocols organize the transmissions from different sensor nodes through the wireless channel. Routing protocols are designed to find the shortest path between the source and the destination. Scalability and dynamic topology of the WSN is considered in the routing protocols design. Moreover, energy-aware algorithms are proposed to find the minimum energy route from the source to the destination.

While multi-hop relay transmission successfully meets the constraints of the WSNs, the data overhead associated with the MAC and routing protocols reduces communication spectral efficiency and data throughput [3], [81], [82]. Moreover, the system performance degrades with increasing the number of sensor nodes [83]. The omnidirectional transmissions cause unnecessary interference to other sensor nodes and limit the available number of simultaneous transmissions. Additionally, MAC and routing protocols for multi-hop relay communication can be impractical for WSNs which consist of sensor nodes with simple hardware [81]. Indeed, in this case, sensor nodes close to the data destination are part of most of the routes and, hence, suffer from energy depletion earlier than other sensor nodes. Finally, multi-hop relay communication principle can not be used if long distance hop is required in the transmission path [84], [85], [86].

Hierarchical routing can be used to address some of the aforementioned issues [80], [87]. In this case, the WSN is organized into clusters in a hierarchical architecture where certain sensor nodes are assigned as cluster heads. Cluster heads are responsible for coordination among the sensor nodes within the cluster, collecting data, and communicating the data to the BS/AP. Cluster head assignment/rotation algorithms are used to balance power consumptions in the sensor nodes. While this method reduces the multi-hop into two-hop relay transmission, it still assumes long

distance transmission from the cluster head to the BS/AP.

1.4.2 Coherent Transmission

Another method of data communication in WSNs is using coherent transmission for increasing the transmission range and achieving directional gain. Moreover, directional transmission increases the throughput in the wireless networks because it reduces the unwanted interference and allows for spatial reuse [88]. It is critical to bring the advantages of directional transmission to the WSNs without adding extra antennas to the sensor nodes. Sensor nodes are limited to one omnidirectional antenna to reduce size, hardware complexity, and price. The inherent dense deployment of sensor nodes has been used to introduce CB for the uplink communication to a BS/AP [14], [89]. Particularly, sensor nodes are organized into clusters and sensor nodes from one cluster act collaboratively as distributed antenna array to form a beam toward the direction(s) of the intended BS(s)/AP(s). Given that sensor nodes are distributed and operate in half-duplex mode, CB is performed in two stages. In the first stage, the data from source node(s) in a cluster is shared with all other collaborative nodes, while in the second stage, this data is transmitted by all sensor nodes simultaneously and coherently. In the latter stage, sensor nodes adjust the initial phase of their carriers so that the individual signals from different sensor nodes arrive in phase and constructively add at the intended BS/AP. In this way, CB is able to increase the area coverage of WSNs and, therefore, can be also viewed as an alternative scheme to the multi-hop relay communications.

Moreover, as compared to the multi-hop relay communications, CB brings the following advantages.

(i) For CB, there is no dependency of communication quality on individual nodes [90]. Thus, the communication link is more reliable than in the multi-hop relay communication method .

(ii) CB distributes the power consumptions over large number of sensor nodes and balances the lifetimes of individual nodes [90], [91]. Each node then transmits with less power than in the case of DT and, therefore, CB prolongs the network lifetime.

(iii) CB enables to create a direct single-hop uplink to the intended BS(s)/AP(s). Thus, it reduces the communication delay and data overhead.

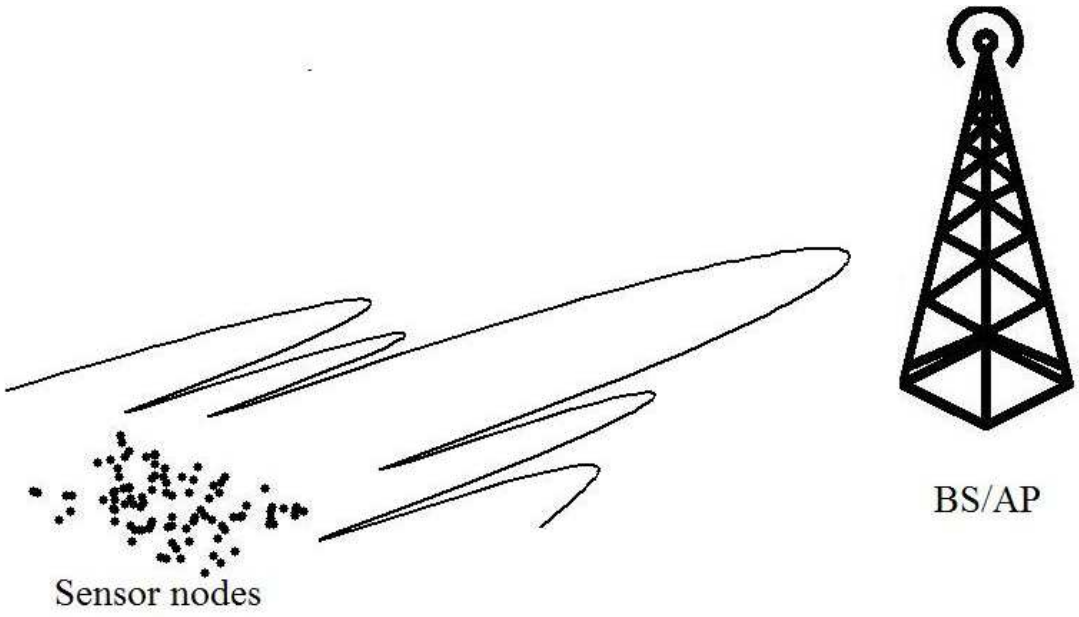

Figure 1.1. CB of a cluster of sensor nodes.

(iv) CB achieves higher connectivity than that of the omnidirectional transmission with the same transmit power [92].

(v) CB improves the Signal-to-Noise Ratio (SNR) at the BS/AP and extends the transmission range of a cluster of sensor nodes. Therefore, it enables to increase the capacity and the area coverage of WSNs.

(vi) CB is scalable and deployment of more sensor nodes in the network does not add complexity to the communication part.

(vii) CB concentrates the radiation power in a certain direction and reduces the power lose in other directions. This helps to introduce security and interference reduction features.

(viii) CB allows frequency reuse based on Space Division Multiple Access (SDMA) [93].

From the network layer point of view, CB is similar to hierarchical routing, but with replacing the omnidirectional transmissions of the cluster head by the directional transmissions of the cluster sensor nodes. Cluster of sensor nodes is basically a distributed random arrays which is similar to traditional centralized random array.

1.5 Random Arrays

The literature on random arrays started as early as the 1960's (see [94]–[98]). Antenna arrays are motivated by the need of achieving sidelobe level suppression and beamwidth reduction. Equally spaced antenna array has a periodic beampattern with deterministic sidelobes. Grating lobes, which are sidelobes with level equal to the mainlobe, occur when the element spacing is much greater than a half wavelength. On the other hand, antenna elements in random arrays are distributed over a linear [99], planer [100], or spherical [101], [102] aperture with unequal spacing. Random antenna arrays produce beampattern with random sidelobes levels lower than the mainlobe level [99]. Due to flexibility of spacing in random arrays, it provides more controlled beamwidth and sidelobe levels over equally spaced arrays [103].

Different applications adopted the random antenna arrays for achieving specific beampattern requirements. Random arrays are used, for example, in Distributed Array Radar (DAR), where identical coherent transceiver units deployed on the

ground or over an aircraft or ship [104], [105]. It offers better performance over traditional radar systems in terms of the target localization accuracy. It also offers minimum echoes and interference [106], [107]. Moreover, random arrays are used in coherent MIMO radar [108], distributed space-based radar [109]–[111], multiple beam satellite applications [112], and ultrawideband transmission [113], [114]. In addition, ultrasound random arrays have been used to produce beampatter with very low sidelobe levels for medical diagnostic, therapeutic, and surgical applications [115], [116].

Different random arrays synthesis techniques are introduced to determine the array element positions. Synthesis techniques aims at achieving narrower beamwidths, sidelobe level suppression [117], null control [118], or minimizing the number of the antenna elements [102], [119]–[121]. These techniques can be classified into [122]:

- **Iterative procedures:** Such as genetic algorithms [123]–[125], differential evolution algorithms [126], simulated annealing [127], [128], particle swarm optimization [129], and tabu search [99].
- **Non-iterative methods:** Based on mathematical approaches [102], [130]–[132], linear programming [133], nonlinear minimax optimization [134].
- **Statistical methods :** Different methods are proposed to achieve beampattern with certain characteristics sch as lower sidelobe [135] or the distribution of the desired mainlobe beamwidth and sidelobe levels [94], [136]. Upper bound on the sidelobe peak level of the random array is derived in [137],

1.6 Motivation

CB is introduced in the context of WSNs in [14]. The theory of random arrays [94] is used to find the average characteristics and distribution of the beampattern of randomly located sensor nodes. It is shown that if randomly located sensor nodes collaborate to achieve coherent transmission, the radiated power can be directed at a predetermined direction. While the work of [14] has established the performance baseline for the CB in the WSNs, it also pointed out some open problems. One problem is the randomness of the CB sample beampattern and its dependency on the sensor nodes' locations. It is required to achieve more predictable CB beampattern and move from analyzing the average beampattern to establishing a predetermined

sample beampattern. Since the sample CB beampattern in WSNs depends on the sensor node locations, we aim at inspecting the effect of the sensor node locations spatial distribution on the CB beampattern. The results in [14] are based on the assumption that sensor nodes in one cluster of WSN are uniformly distributed. It is critical to establish that the CB beampatten has acceptable characteristics with sensor nodes randomly located according to other spatial distributions. We analyze the CB beampattern of Gaussian spatially distributed sensor nodes and explore the changes in its characteristics compared to the case of uniformly spatially distributed sensor nodes. The practical implementation of CB transmission schemes is affected by the sidelobes of the sample CB beampatterns. Sidelobe control reduces cross interference when multiple CB beampatterns coexist and improves the overall performance of the WSN. Proposed algorithms for sidelobe control should consider the distributed nature of WSNs and limited resources at individual sensor nodes. Another important issue in applying CB to the WSNs is the energy consumption corresponding to CB transmission. The original CB scheme assumes equal transmitted power from each sensor node and, thus, CB inherently balance energy consumption among the collaborative sensor nodes. However, different sensor nodes perform different tasks according to the surrounding circumstances and, thus, the energy at each sensor node is different. CB weight power assignment can be designed to consider different remaining energies at the sensor nodes to extend the WSN lifetime.

1.7 Contribution of Thesis

We propose Gaussian Probability Density Function (pdf) as a more realistic model for spatial distribution of the sensor nodes' locations in a cluster of WSN. Gaussian pdf is more suitable in many WSN applications than, for example, uniform pdf which is commonly used for flat ad-hoc networks. Indeed, in WSN applications such as rural areas monitoring, the actual sensor node distribution depends on the deployment method. To cover a wide area, large number of sensor nodes must be deployed simultaneously in an ad-hoc manner which cannot guarantee uniform distribution over the area. For example, if the deployment is done by dropping a group of sensor nodes from an airplane, their spatial distribution is likely to be Gaussian according to the central limit theory [138].

The average beampattern and its characteristics, the distribution of the beam-

pattern level in the sidelobe region, and the distribution of the maximum sidelobe peak are derived using the theory of random arrays. We show that both the uniform and Gaussian sensor node deployments behave qualitatively in a similar way with respect to the beamwidths and sidelobe levels, while the Gaussian deployment gives wider mainlobe and has lower chance of large sidelobes. The results suggest that CB is feasible for sensor nodes located randomly with any spatial distribution. The CB average beampattern shows a deterministic behavior and the mainlobe of the CB sample beampattern is independent of particular node locations.

The CB for a cluster of a finite number of collaborative nodes results in a sample beampattern with sidelobes that depend on particular node locations. High level sidelobes can cause unacceptable interference when they occur at directions of unintended BSs/APs. Therefore, sidelobe control in CB has a potential to decrease the interference at unintended BSs/APs and increase the network transmission rate by enabling simultaneous multilink CB. Traditional sidelobe control techniques are proposed for centralized antenna arrays and are not suitable for WSNs. We show that scalable and low-complexity sidelobe control techniques suitable for CB in WSNs can be developed based on node selection technique which makes use of the randomness of sensor node locations. A node selection algorithm with low-rate feedback is developed to search over different node combinations. The performance of the proposed algorithm is analyzed in terms of the average number of search trials required for selecting the collaborative nodes, the resulting interference, and the corresponding transmission rate improvements. It is shown that the interference can be significantly reduced and the transmission rate can be significantly increased when node selection is implemented with CB.

We consider the effect of CB weights power assignment on the energy consumption of WSNs. CB weight power assignment algorithm is proposed to balance the energy consumption in sensor nodes and achieve the required average SNR at the destination(s). The effect of the proposed CB weight design on the WSN lifetime is illustrated by simulations.

1.8 Outline of Thesis

The rest of the thesis is organized as follows. Chapter 2 starts with presenting the main results of the theory of random arrays. Then, the geometrical model for a cluster of sensor nodes is introduced and the corresponding CB beampattern is

defined. Different channel models used for CB are described. Afterwards, the current research directions for CB are presented. Phase synchronization methods, coherent and quasi-coherent CB, information sharing, null-steering for CB, opportunistic CB are discussed briefly. The CB beampattern characteristics in presence of noise and interference, local scattering, mobile nodes, and protocol defects is presented. In Chapter 3, Gaussian pdf is used to model the spatial sensor node distribution in a cluster of WSN. The average beampattern and its characteristics are derived. The distribution of the beampattern level in the sidelobe region and the distribution of the maximum sidelobe peak are also found. The beampattern characteristics derived in the case of Gaussian pdf are compared to the corresponding characteristics in the case of uniform spatial sensor node distribution. In Chapter 4, system and signal models are introduced for the case of multi source multi BSs/APs WSN. Sidelobe control technique for CB in WSNs based on node selection is presented. The performance of the proposed technique is studied and simulation results are reported. Chapter 5 shows the effect of CB weights with different powers on the energy consumption of sensor nodes. First, a simple CB weight power assignment method is proposed. Then, simulations are presented to show the effectiveness of the CB weights power assignment on the WSN lifetime. Chapter 6 concludes the thesis and proposes some possible future work.

Chapter 2

Collaborative Beamforming for Wireless Sensor Networks

Recently, CB for data communication in WSNs has received significant interest. It is an effective technique to exploit the distributed low-power source nodes and achieve long distance transmissions toward far away BS/AP. CB scheme is a good match to the requirements and constraints of data communication with low-power and distributed sensor nodes. It also scalable and can be applied to very large scale WSNs effectively.

The effect of the number of sensor nodes on CB performance is totally different than the case of multi-hop transmission. While, in the later case, increasing the number of sensor nodes introduces more problems to the design [139]–[141]. Increasing the number of sensor nodes improves the CB performance, where the sample beampattern approaches the average beampattern, and the energy consumption spreads over more sensor nodes [14].

While beamforming is well studied technique in antenna arrays. Implementing CB in WSNs has different challenges, as compared to the traditional centralized beamforming, because it is applied in a distributed fashion. Recently, different research groups have studied the challenges and practical problems in CB for WSNs and proposed some potential solutions.

In this chapter, we briefly cover major research directions aimed at CB and conclude some general results. First, the main results of the theory of random arrays are introduced to give the mathematical fundamentals for the following analysis. Then, we introduce a geometrical model of a cluster of the WSN and channel models used in the analysis. Two important requirements need to be satisfied in order to be able to implement CB, namely, phase synchronization and information sharing

between sensor nodes in a cluster of WSN. Thus, the exciting methods for phase synchronization and information sharing are discussed afterwards in which some schemes are specifically designed to target CB in WSNs. Finally, the performance of CB with realistic conditions such as the presence of noise and interference, local scattering, mobile nodes, or protocol defects is analyzed.

2.1 Theory of Random Arrays

Randomly located sensor nodes over a sensing field can be modeled as a random antenna array. Thus, the CB beampattern can also be analyzed based on the theory of random arrays [94], [98], [101], [137].

Consider the linear antenna array configuration shown in Fig. 2.1, where N isotropic antenna elements are randomly located along a line of length a. Assume all lengths are normalized to the signal wavelength λ. Let us use the rectangular coordinates and assume that the antenna array lies along the x-axis from $-a/2$ to $a/2$. Let x_r be the rectangular coordinates for the rth element normalized to $a/2$, i.e., $|x| \leq 1$. The normalized coordinates x_r are modeled as Independent Identically Distributed (iid) random variables with arbitrary spatial pdf $f(x)$ defined for $|x| \leq 1$.

Antenna arrays are characterized by the array factor which is the summation of the transmitted signals from the antenna elements. Thus, the antenna element locations and the transmission power of each antenna element determine the array factor. If the antenna elements transmit sinusoidal signals with equal power, then the complex amplitude of the signal received from the rth antenna element at angle θ is $\exp\{-\frac{2\pi}{\lambda} j \sin(\theta) x_r\}$ where all angles are measured from the normal to the array axis. The complex weight of the rth array is set to $\exp\{\frac{2\pi}{\lambda} j \sin(\vartheta) x_r\}$ so that signals from different array elements add coherently at the observation angle ϑ. Then the complex array factor can be written as

$$\begin{aligned} \mathbb{F}(u) &= \frac{1}{N} \sum_{r=1}^{N} e^{\frac{2\pi}{\lambda} j \sin(\vartheta) x_r} e^{-\frac{2\pi}{\lambda} j \sin(\theta) x_r} \\ &= \frac{1}{N} \sum_{r=1}^{N} e^{\frac{2\pi}{\lambda} j [\sin(\vartheta) - \sin(\theta)] x_r} \end{aligned} \tag{2.1}$$

where $1/N$ is a normalization factor for total of N antenna elements. Let us define $u = \sin(\vartheta) - \sin(\theta)$ as the angle parameter, then the array factor can be equivalently

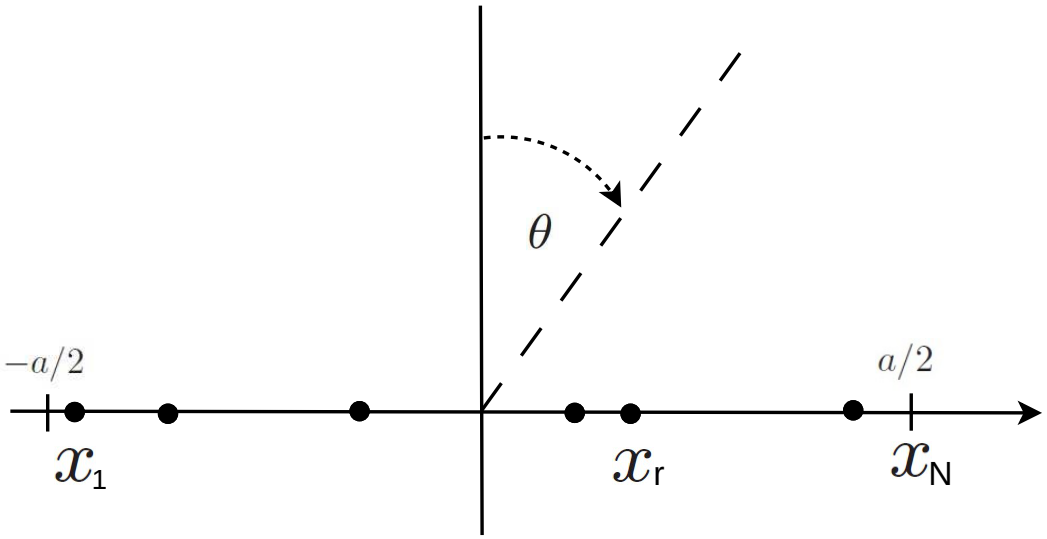

Figure 2.1. Linear random antenna array.

expressed as

$$\mathbb{F}(u) \quad = \quad \frac{1}{N}\sum_{r=1}^{N} e^{\frac{2\pi}{\lambda}jux_r}. \tag{2.2}$$

The beampattern is the spatial distribution of the radiated power and, assuming no mutual coupling between the elements, can be found from the array factor as

$$\mathbb{P}(u) \quad = \quad |\mathbb{F}(u)|^2 \tag{2.3}$$

Because of the random placement of the array elements, the corresponding beampattern is also random. Thus, the characteristics of beampattern have to be studied in statistical terms. Theory of random antenna arrays describes the characteristics of the average beampattern and the distribution of the sample beampattern [94], [98]. The main results are summarized as follows [116]:

- The average beampattern is determined by the spatial distribution of the antenna array elements.
- The average of the sidelobe level inversely proportional to the number of elements.
- The ratio of the mainlobe maximum to the average level of the sidelobes is equal to the number of array elements.
- Away from the mainlobe, the probability of having certain sidelobe level is the same over all the range.

The aforementioned results provide the average characteristics and distribution of the CB beampattern for a randomly located sensor nodes. However, application of theory of random antenna arrays to CB in the WSN context possess some fundamental problems in practical implementation because of the distributed nature of the sensor nodes. Specifically, two important requirements should be guaranteed before applying CB, which are

- **Phase synchronization.** Since sensor nodes are distributed over the sensing field, there is no central oscillator to generate the carriers for all sensor nodes as compared to the case of the centralized antenna arrays. Each sensor node has its own oscillator, therefore, local carrier frequency and phase synchronization are required among the distributed sensor nodes. Frequency synchronization is

achievable if the BS/AP transmits a beacon mono-tone signal and each sensor node's oscillator locks its Phase Locked Loop (PLL) to the received signal. However, phase synchronization is more challenging to achieve because of the lack of unique reference for all oscillators.

- **Information sharing.** Data collected at different source sensor nodes should be shared with all other collaborative sensor nodes before CB. To avoid collisions between different source sensor nodes in the same cluster, information sharing can be achieved over orthogonal channels or using random access protocols. Also, collision resolution protocols can be used to extract different sources of information from the collided transmitted signals.

2.2 Phase Synchronization

Phase synchronization is the most critical requirement to implement CB in WSNs [142], [143]. Individual carrier signals from different sensor nodes should be synchronized in phase and frequency to achieve coherent transmission. While a centralized antenna array can easily achieve this, the case of a cluster of sensor nodes in WSN is different because of the distributed setting of the WSN. Each sensor node has separate RF carrier supplied by its local oscillator, therefore, carrier frequency and phase synchronization algorithms are required for WSNs. Frequency synchronization can be implemented by broadcasting a beacon signal from the BS/AP to the sensor nodes. Then, the internal oscillator's PLL at each sensor node locks to the received signal frequency.

The situation is different for phase synchronization, local carriers do not have a common reference to set the same initial phase. Phase difference comes from propagation delay and the phase due to channel variations which is different from one sensor node to another. Synchronization algorithms targeting WSNs should be distributed and scalable with increasing the number of sensor nodes. Moreover, techniques for phase synchronization should have minimal information exchange with the BS/AP. A variety of distributed and scalable phase synchronization schemes are proposed for WSNs and can be classified into:

- **Random search synchronization:** Each sensor node changes its phase randomly and keep/reject the phase changes according to the quality of the received signal at the receiver.

- **Master-slave synchronization:** Sensor nodes synchronize their carrier signals to a bacon signal from a master sensor node or BS/AP.

- **Round-trip synchronization:** Sensor nodes synchronize their carrier signals based on the fact that the phase offset in the down link transmissions is the same as the phase offset in the up link transmissions.

2.2.1 Random Search Synchronization

Random search algorithms for phase synchronization are suitable for WSNs, thanks to the distributed nature of WSNs, where each sensor node changes its carrier initial phase independently on the other sensor nodes. The scheme proposed in [144], [145] randomly changes the phase according to the improvement of the received SNR at the BS/AP. This method exploits the fact that different phase alignments result in different received SNRs at the BS/AP. The algorithm starts with arbitrary carrier initial phases at sensor nodes and at each iteration each sensor node make an independent random phase change to its phase. Sensor nodes use CB transmission to send a pilot signal to the BS/AP using the current carrier phases. The BS/AP measures the received SNR and broadcasts one bit of feedback, 1 if the current initial phases increased the received SNR compared to the previous value, and 0 otherwise. The BS/AP keeps a record of the best achieved SNR so far. Sensor nodes keep the current phase values that increase the SNR at the BS/AP, or restore the previous values otherwise.

This method requires minimum data exchange from the BS/AP to sensor nodes where only the SNR improvement state at the BS/AP with the new phase values is broadcasted using single bit of feedback. It is not required that the BS/AP knows the individual phases of sensor nodes as well as sensor nodes do not need to know the exact value of the SNR at the BS/AP. Results from an experimental prototype validate the applicability and efficiency of such a method and are presented in [144]. These experimental results show that CB is practically feasible and most of the theoretical SNR gains can be achieved under practical conditions.

In [146], different factors of the algorithm are explored to improve the algorithm. The effect of the number of sensor nodes participating in synchronization at each iteration and the effect of distribution of the phase change on the performance of the synchronization process are studied. Uniform and Gaussian pdfs are proposed and compared for the distribution of the random changes in the carrier phases. Uniform

distribution gives equally probable phase changes, while the Gaussian distribution results in more probable smaller changes. The variance of the normal distribution is used to control the range of the changes. It is shown that at the beginning of the algorithm, all sensor nodes have random phases which are typically far away from alignment. To achieve the synchronization faster, it is suggested that a larger number of nodes should participate in the phase synchronization and phase change values should be large at the beginning. With the progress in synchronization, the carrier phases of different sensor nodes come closer to alignment and the phase changes become smaller. Overall, the performances for the normal and uniform distributed phase changes are similar and an acceptable synchronization within several milliseconds is guaranteed.

Improvement to the algorithm of [144] are proposed in [147] and [148]. The original algorithm uses only the phase changes that lead to SNR improvement at the BS/AP and discards any other phase changes. However, the phase changes that lead to the reduction of received SNR can also be used to improve the following phase changes. Thus, the modified algorithm uses the rejected phase changes to improve the convergence speed by allowing both the accepted and rejected phase changes to contribute to the convergence speed.

2.2.2 Master-Slave Synchronization

In master-slave synchronization schemes, one central point or sensor node in the cluster serves as a master node [142]. This node broadcasts a beacon signal with carrier, timing, and location information content to all slave nodes in the cluster. The local oscillator's PLL locks to beacon carrier sent by the master and achieve frequency synchronization. Each slave node in the cluster estimates the distance to the master node and compensate for the phase delay to achieve phase synchronization. The accuracy of such synchronization depends on the received SNR and the accuracy of the frequency and phase estimators [15].

Another master-slave scheme for phase synchronization in WSNs, which does not require location information, is presented in [149]. According to this scheme, the BS/AP continuously broadcasts a common beacon signal to all sensor nodes. Each sensor node synthesizes the local carrier to this beacon signal and then transmits a Direct Sequence Code Division Multiple Access (DS-CDMA) signal with a unique code back to the BS/AP. The BS/AP separates the received signals, esti-

mates the overall phase offset of each sensor node and then transmits phase/timing synchronization messages to the sensor nodes via DS-CDMA. While this scheme has low-complexity, it results in significant overhead especially for WSNs with large number of sensor nodes.

2.2.3 Round-Trip Synchronization

Round-trip synchronization techniques utilize the fact that the phase delay between the BS/AP and any arbitrary sensor node is the same for uplink and downlink directions [143], [150]. Phase synchronization protocol based on round-trip principle was first described in [151] for two nodes communicating to a BS/AP. Three beacon signals at different frequencies and pair of PLLs at each node are used to achieve synchronization. The BS/AP continuously broadcasts a master beacon signal so that the two nodes master PLLs lock to it and generate secondary beacon signals at different frequency. Nodes broadcast the secondary beacon signals to each other and the secondary PLL in each node locks to it in order to generate a carrier signal at third frequency. The carrier signals from both nodes are then synchronized with each other and can be used for transmission to the BS/AP. While the protocol is shown to be efficient in time-invariant and time-varying single-path channels, its performance degrades in multipath channels because of the use of three different frequencies.

Another round-trip scheme was proposed in [150] It employs a single frequency beacon signals and Time-Division Duplexing (TDD). Due to the channel reciprocity, single frequency beacons are used in a half-duplex time-slotted fashion to maintain the performance in multipath conditions. Transmitted beacon from the BS/AP is used to generate local version of the carrier at one sensor node and then copies of this carrier are passed to different sensor nodes [150], [152]. The scheme can be applied to more than two sensor nodes in multipath channel and mobility scenarios, however, it generally requires significant coordination with the BS/AP.

2.3 Information Sharing

Information to be transmitted should be available at all sensor nodes before the CB step for enabling simultaneous transmission of the same data symbol. Information sharing can be done straightforward via broadcasting if the WSN has only one source node. However, protocols or schemes are required if more than one source

node exists in the WSN.

2.3.1 Orthogonal Channels

The simplest way for information sharing in WSNs with multiple source nodes is transmitting their data over orthogonal channels. Orthogonality can be achieved using different multiple access schemes to avoid collision during simultaneous transmissions. Multiple access techniques are Time-Division Multiple Access (TDMA), Frequency-Division Multiple Access (FDMA)/Orthogonal Frequency-Division Multiple Access (OFDMA), and Code Division Multiple Access (CDMA). However, using orthogonal channels for simultaneous transmissions is not efficient for WSNs with increased number of source nodes. Alternative methods is required to reduce resources consumed for information sharing.

2.3.2 Random Access

Source nodes can use random access protocols to organize transmissions over one channel. The simplest random access protocol to implement is the slotted ALOHA [153]–[155]. Transmissions are organized in time-slots and when data are to be transmitted, source node transmits at the beginning of the next time-slot. If there is no transmissions from the other sensor nodes at the same time-slot, data will be successfully received at the other sensor nodes. If another source node is simultaneously transmitting, collision occurs and the data will be corrupted. Source nodes involved in the collision re-transmit the data again after random number of time-slots delay. However, ALOHA does not utilize the channel during collisions and the collided signals at the receiving sensor nodes are discarded.

2.3.3 Collision Resolution

Transmission over orthogonal channels or using random access protocols are collision avoidance techniques resulting in loss of resources as compared to collision resolution. Collision resolution protocols are introduced for random access networks to utilize the received signal during collision and separate collided data symbols at the expense of more complex processing. We present here two of collision resolution protocols proposed for general wireless networks.

Network-Assisted Diversity Multiple Access (NDMA) is a collision resolution protocol introduced for time-slotted transmissions [156]. In case of collision at given

time-slot, the received collided signal is saved at each receiving node and the transmitting nodes retransmit the same signals during the following time-slots. The total number of the original transmission and the re-transmissions is equal to the number of transmitting nodes. The receiving nodes use the saved collided and retransmitted signals to recover each individual collided data based on a Multiple-Input Multiple-Output (MIMO) model. The scheme requires only one time-slot for each collided signal.

Another collision resolution protocol is the ALLow Improved Access in the Network via Cooperation and Energy Savings (ALLIANCES) protocol [157]. In case of collision, a designated set of nodes re-transmit the collided signal, which they received, to the destination, each relaying node transmits in a different time-slot. The destination process the originally received collided signal and the signals received from the relaying nodes and recover the original signal. A multichannel extension of ALLIANCES is proposed to exploit the multipath diversity [158]. Since the previous collision resolution protocols are generally introduced for wireless networks, the required processing for these protocols is not optimized to match the WSNs limitations.

2.3.4 Cross-Layer Information Sharing

Besides random access and collision resolution schemes that are designed for general wireless networks, some schemes are designed to target certain wireless networks and exploit their characteristics. One example of such schemes is the Medium Access Control - PHYsical (MAC-PHY) scheme proposed in [159] to achieve information sharing for CB in WSNs. In this scheme, source nodes broadcast their information simultaneously, and thus, information sharing takes only one time-slot in a random access fashion. Collaborative nodes receive combinations of all simultaneous transmitted symbols from multiple source nodes. For each collaborative node, the CB weight is the multiplication of two term, an initial phase corresponding to the propagation delay to the BS/AP and the conjugate of the channel gain between the collaborative node and the source node.

The initial phase in the CB weight allows the transmitted signals from collaborative nodes to add coherently at the intended BSs/APs. It is assumed that the channel coefficients between collaborative nodes are independent. This assumption is needed to be able to cancel out the cross-interference between different source

nodes. CB transmissions target one BS/AP at each time-slot, or multiple beams can be formed simultaneously if multiple BSs/APs at distinct directions exist. The resulting average beampattern is similar to the conventional CB, but it is characterized by increased sidelobe power levels. Therefore, the scheme of [159] reduces the information sharing time at the cost of lower Signal-to-Interference-plus-Noise Ratio (SINR). Moreover, this scheme does not work well if the channel coefficients are not zero-mean.

Optimal CB weights are designed in [160] and compared with traditional CB with TDMA or any orthogonal channel multiple access based information sharing. CB weights are designed to maximize the received SNR in the case of the traditional CB or SINR in the case of the cross-layer CB. Optimal CB weights for the cross-layer CB requires global Channel State Information (CSI), thus resulting at high overhead and complex processing. Moreover, cross-layer CB achieves higher sidelobe levels than traditional CB due to the multiuser interference. Traditional CB is simpler to implement since it requires only the knowledge of sensor node locations. Moreover, it is more robust to channel/phase errors.

2.4 CB with Deviations from Ideal Model

Many ideal assumptions are used to analyze the CB fundamental results, however, any practical analysis or implementation should consider different real factors. Some deviations from the ideal assumptions are presented here. The effects of such mismatches to the ideal assumptions on CB are analyzed as well.

2.4.1 Imperfect Phase Synchronization

Phase synchronization algorithms should be robust under practical conditions and the channel effects should be considered. The channel variations change the phase responses of the channel gains and the overall phase offset changes. Moreover, imperfect phase synchronization among sensor nodes can result from phase errors, oscillator drift, or localization errors. Received signals at the BS/AP lose coherence over time and the phase synchronization should be repeated periodically or whenever the BS/AP detects loss in the SNR.

The accuracy of phase synchronization algorithms is limited by the half-duplex transmission of the sensor nodes. Analyzing the performance of CB with imperfect phase synchronization shows a tradeoff between synchronization overhead and

achieved gains [15]. Large fraction of the CB gains can be achieved even with phase errors with moderately large variance [161]. The effect of the channel on the estimation of the channel phase by the sensor nodes is analyzed in [162]. The distribution of the phase estimation error and the probability of signal corruption at the BS/AP due to imperfect phase estimation is found as well.

2.4.2 Noise and Interference

An adaptive filter is proposed [163] to achieve phase synchronization for CB in the presence of noise and interference in WSNs. The CB gain approaches the ideal value and the noise power at the BS/AP decreases with increasing the number of sensor nodes. The interference effect is determined by the ratio between the number of sensor nodes and the number of interference sources. While the designed filter is computationally efficient, it is not practical because the position of sensor nodes are assumed to be known in advance.

2.4.3 Local Scattering

Multipath-free conditions are assumed in the original analysis of the CB beampattern where the transmitted signal suffers no reflection or scattering. However, multipath propagation is more realistic model and scattering affects the beampattern even with perfect synchronization. The CB beampattern is studied in the case of multipath propagation where the signal suffers angular spreading due to local scattering [164]. The received signal is modeled as a superposition of a large number of scattered paths with angles of incidence which are uniformly distributed around the destination nominal direction. The CB average beampattern and the corresponding maximum gain and beamwidth are derived as functions of the number of nodes, the cluster size, and the scattering parameters. Analysis shows that CB gives acceptable performance in multipath channels.

2.4.4 Mobile Sensor Nodes

Wireless communication between sensor nodes allows for implementing WSN with mobile sensor nodes if the sensor mobility does not break the network connectivity. In the case of mobile sensor nodes, CB weight design should consider the motion of the sensor nodes and compensate for it [165]. The relationship between array factor and random sensor nodes' motion is developed. The average beampattern

characteristics are derived in [166] where the mobility of sensor nodes is modeled as 2 Dimensional (2D) Brownian motion. Beampattern with both small mainlobe width as well as large 3dB sidelobe region is derived and a low complexity algorithm is designed to arrange distribution of sensor nodes to produce such beampattern.

2.4.5 Protocols Defects

The performance of CB is not independent on the performance of the other protocols in the network. Defects in the network protocols can cause pointing errors, mainlobe gain loss, or increase of the average sidelobe level [167]–[169]. A frame work for studying the effect of errors in different protocols is proposed in [170]. Effects of errors in localization protocol, synchronization protocol, and data dissemination protocol on the performance of CB are studied. Comparing the effect of synchronization and location errors, it is found that the impact of location errors is much more significant.

As shown in this section, CB can provide most of the theoretical gains under non-ideal conditions.

2.5 Other CB Research Trends

2.5.1 Opportunistic CB

In the conventional CB scheme, each sensor node sets its local carrier initial phase to cancel out the phase offset due to the channel phase and propagation delay. However, since the CB is robust against moderate phase offsets, beamforming gain can be achieved even with imperfect phase synchronization. Quasi-coherent CB is introduced based on this fact. It is motivated by the need to use less coordination between sensor nodes while achieving acceptable loss in the received signal power [171], [172]. It provides a compromise between the CB gain and the amount of the overhead in the CB scheme.

Opportunistic CB is another way of achieving quasi-coherent transmission without any phase synchronization. Sensor nodes transmit to the BS/AP using unsynchronized carriers with random initial phases. The BS/AP measures the received signal from each sensor node and finds the overall effect of the channel phase and the propagation delay. The destination selects a subset of sensor nodes with close total phase and broadcasts a selection vector. The received signal from the selected

sensor nodes combine in a quasi-coherent manner at the destination. The advantage of this method is that there are no calculations need to be performed at sensor nodes where the amplitude and phase for each sensor node is used to compute the selection vector at the BS/AP. The channel estimation and selection computations are done at the destination, only the selection vector is required to be transmitted to the sensor nodes. The selection vector has one bit corresponding to each sensor node in the cluster to turn on or off the sensor nodes to participate in the CB.

Opportunistic CB scheme is similar to the conventional one in the sense that the gain at the BS/AP increases with the number of collaborative nodes. However, even if the calculation of the the selection vector is performed at the BS/AP, the use of full search for finding optimum sensor nodes is impractical for WSNs with large number of sensor nodes. Low-complexity sub-optimal node selection algorithms can be used to maximize the power gain, namely, sector-based, iterative greedy, and iterative pruning. For iterative greedy and iterative pruning, in each iteration, one sensor node is added or removed to/from the selected subset according to the gain changes until no acceptable beamforming gain change can be achieved through further iterations.

2.5.2 Beampattern Control

Achieving CB beampattern with desirable characteristics is an important factor in improving the transmission performance with CB. High directivity and lower interference levels are both desired characteristics for the CB beampattern.

One way to increase the directivity of the conventional CB beampattern is to use only the sensor nodes placed in a ring instead of using all the nodes in the disk of the same radius [173]. A larger and narrower ring results in average beampattern with smaller mainlobe width. However, the outer radius of the ring has to be kept small to save transmission energy between nodes. One advantage of using smaller number of sensor nodes distributed over a ring instead of a disk is the ability to increase the overall energy saving and network connectivity. However, the use of nodes in a ring with a small width limits the number of candidate nodes available for CB. The resulting average beampattern under this choice of sensor node locations has larger sidelobe peak levels than the conventional CB. To reduce the sidelobe peak levels, multiple concentric rings can be used [173].

To reduce interference caused by the CB beampattern, nulls in the beampattern

can be placed in the directions of unintended BSs/APs. A distributed null-steering scheme for WSNs is introduced in [174]. The average beampattern is approximately equal to that of the conventional CB in the directions far enough from the direction of unintended BS/AP. Also, the proposed scheme is used to minimize the maximum sidelobe of the average beampattern. However, this scheme results in decreased received power at the targeted direction. To keep the decrease in the received power at the intended BS/AP very small, the unintended BS/AP should be far away from the intended BSs/APs and the cluster area should be large enough. However, only the average beampattern behavior is studied in [174], while the sample beampattern behavior is of real interest.

2.5.3 Power Control for CB

Sensor nodes perform different tasks in the WSN and each sensor node can have different energy budget. Considering this, CB weights with different transmit powers are likely to be more efficient for extending the sensor nodes lifetime. Optimal CB weight powers have been found in [91] under different metrics with the assumption of infinite number of sensor nodes. Achieved SINR with optimal CB weights power control is studied through simulations for finite number of sensor nodes.

When multiple clusters are simultaneously transmitting using CB, each cluster can optimize the average transmit power, and thus, optimize its throughput-to-average transmit power ratio. A game-theoretic model for power control of CB transmission in WSN clusters is proposed in [175]. Better results are achieved through cooperation but at the expense of significantly large data overhead for centralized control.

2.5.4 Performance Analysis of CB Random Search Algorithms

Random search algorithms are used in WSNs for CB phase synchronization to increase coherence between transmitted signals at the BS/AP. The distributed nature, scalability, and low-complexity of such algorithms make them tempting techniques for implementing in WSNs context. Convergence time of random search algorithms is very important performance measure and mathematical analysis is required to guarantee convergence in acceptable time. Performance analysis framework is introduced in [176] for general random search algorithms targeting distributed CB schemes. Conclusions obtained from the analysis help to modify random search al-

gorithms and reduce their convergence time. The framework is applied to the phase synchronization scheme developed in [144] and the convergence of this scheme is proved. Furthermore, it is shown that the convergence time scales linearly with the number of sensor nodes. An asymptotic bounds on the convergence time for the random search phase synchronization are provided in [146].

Another model is introduced in [177] to study the performance limits of the CB random search algorithms. To simplify analysis, sensor nodes are assumed to transmit carriers with binary phases instead of continuous valued phases and the channels between sensor nodes and the BS/AP are assumed to be binary as well. Upper and lower bounds on the convergence time are derived using combinatorial techniques. Numerical approximations to the convergence time are derived and improvement on the the running time is achieved with modifications of the basic algorithm.

2.5.5 Receive CB

While CB is introduced originally for long-distance energy-efficient transmission in WSNs, alternatively, a cluster of sensor nodes can use CB to receive a signal from the BS/AP [178], [179]. In antenna arrays, transmit and receive beampatterns are identical for the same antenna array because of the reciprocity principle [180]. Due to directivity of the beampattern, receive CB introduces gain to the signal received from direction of the mainlobe and suppresses the other interfering signals from other directions. Receive CB weights are designed to maximize the signals SINR at the receiver. However, SINR-optimal weights depend on the global CSI and location information. This information is, however, not feasible in WSNs. Based on the large number of sensor nodes, an approximation to the SINR-optimal weights that depends only on the local information at each sensor node, is proposed. CB average beampattern expression is obtained to validate the corresponding achieved gain. The ability to suppress the interferences from unintended BS/AP is also shown.

Using receive CB for reception overcomes the broadcasting nature of the BS/AP and a cluster of sensor nodes are able to ignore multiple BSs/APs simultaneous transmissions and receive only signals from the BS/AP of interest. Implementing receive and transmit CB in WSNs allows clusters of sensor nodes to work collaboratively as relays to receive/transmit signals from/to different BSs/APs or other clusters.

Chapter 3

Effect of Sensor Nodes Spatial Distribution on the Beampattern

3.1 Introduction

Theory of random arrays has established the performance baseline of CB in the WSNs [94], [97]. It shows that, using phase synchronization, randomly located sensor nodes result in beampatterns that are able to focus the radiated power at predetermined direction. However, building a transmission scheme based on CB additionally depends on beampattern characteristics such as the beamwidth and sidelobe levels. The beamwidth defines the usable range of beampattern where the transmitted power does not go below an acceptable level. The sidelobe levels determine the anticipated interference at unintended BSs/APs located away from the targeted directions. Moreover, the beampattern and its characteristics have to be found for practical WSN setting. Unlike calibrated antenna arrays, ad hoc deployment of sensor nodes does not give much freedom on choosing the sensor node locations or even its spatial distribution probability. The beampattern is deferent for each deployment of sensor nodes and, thus, it is analyzed statistically and its characteristics are averaged over all realizations of sensor node locations. Furthermore, it is important to find the effect of the sensor node spatial distribution on the CB beampattern and justify that it has acceptable characteristics with any spatial distributions.

The beampattern characteristics of CB have been recently derived in [14] assuming that sensor nodes in one cluster of WSN are uniformly distributed. However, the actual sensor node distribution depends on the deployment method. Indeed, to

cover a wide area, large numbers of sensor nodes must be deployed simultaneously in an ad hoc way which cannot guarantee uniform distribution over the area [181]. An example of such scenario is rural areas monitoring when the deployment is done by dropping a group of sensor nodes from an airplane Fig. 3.1. The spatial distribution of sensor nodes in this case is argued to be Gaussian [138], [182], [183]. Indeed, the sensor nodes actual locations are affected by different factors such as wind, the releasing mechanism, speed, height, etc. The displacement from the targeted location due to each of these multiple factors can be modeled as a random variable and the effective displacement is the sum of these random variables. Therefore, according to the central limit theorem, the actual location will follow Gaussian distribution [184].

In this chapter, Gaussian pdf is used to model the spatial sensor node distribution in a cluster of WSN. The average beampattern and its characteristics are derived under this assumption. The distribution of the beampattern level in the sidelobe region and the distribution of the maximum sidelobe peak are also found. The beampattern characteristics derived here in the case of Gaussian pdf are compared to the corresponding characteristics in the case of uniform spatial sensor node distribution of [14]. We explore the changes in the beampattern characteristics due to the spatial distribution of sensor nodes.

3.2 System Model and Beampattern

The mathematical framework of the theory of random arrays is used to analyze the performance of CB in the context of WSNs. A cluster of sensor nodes is modeled as a 2D antenna array and the corresponding CB beampattern is derived. The initial phase of each sensor node carrier is set so that signals add coherently at the targeted direction.

3.2.1 Geometric Model

We consider a cluster of sensor nodes in which one sensor node represents a data source and other sensor nodes serve as collaborative nodes to transmit data to a remote BS/AP. Each sensor nodes is aware of its location and is able to communicate to other sensor nodes in the cluster using links with low power consumption for information sharing and synchronization. It is also assumed that each sensor node transmits the same power and the synchronization error and frequency drift effects are negligible. Fig. 3.2 shows the geometric model of a cluster which consists of

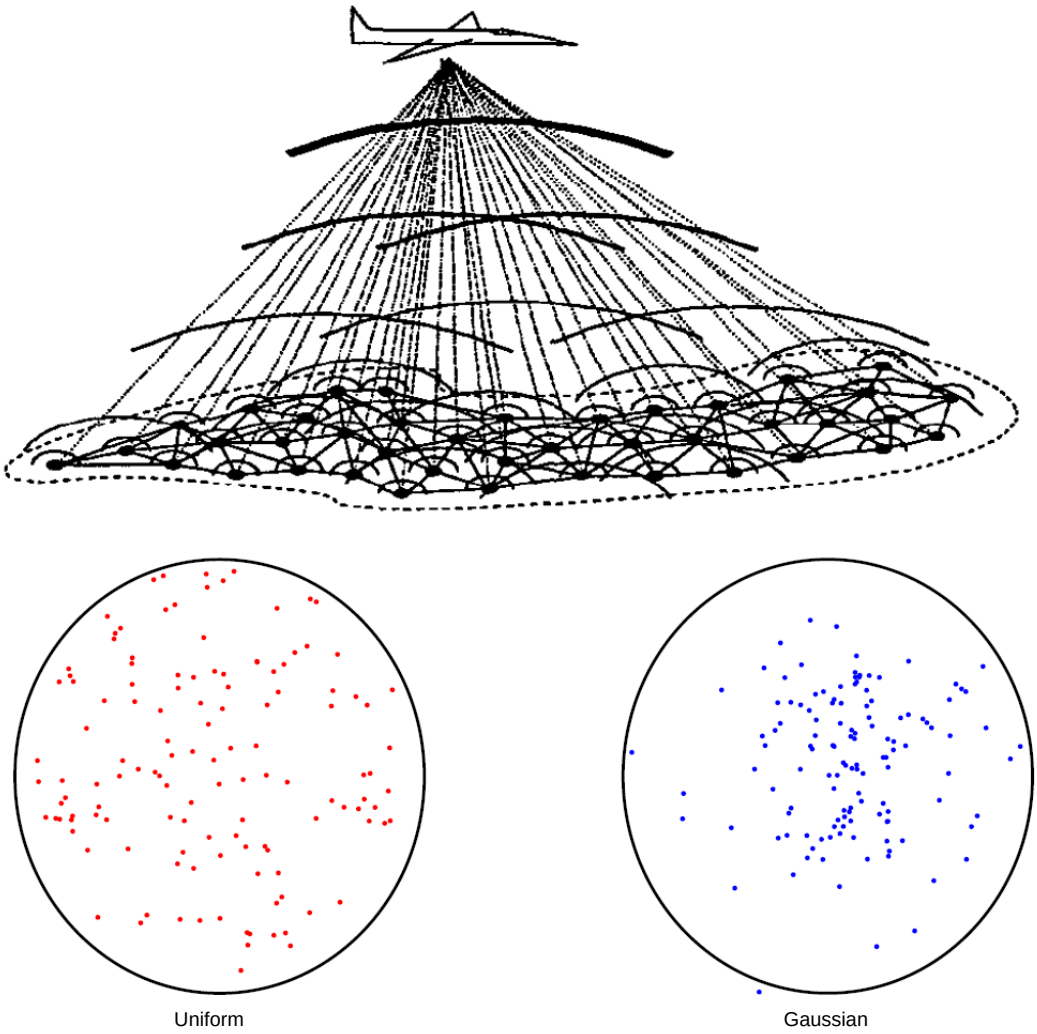

Figure 3.1. Deployment of sensor nodes by dropping from an airplane.

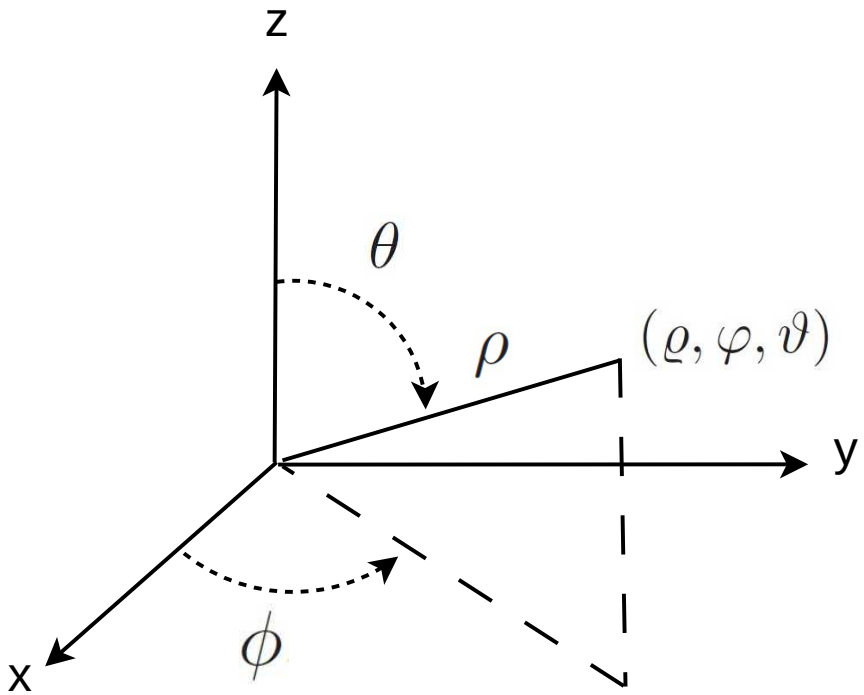

Figure 3.2. Geometric model.

N sensor nodes. For the spherical coordinates (ρ, ϕ, θ), the angle θ denotes the elevation direction, ϕ represents the azimuth direction, and ρ is the distance from the origin to a given point. Assume that the destination BS/AP is located at $(\varrho, \varphi, \vartheta)$ and sensor nodes are co-located in (x, y) plane. The rectangular sensor node coordinates are (x_r, y_r), $r = 1, \ldots, N$, and they are chosen randomly according to Gaussian distribution with zero mean and variance σ_0^2. The corresponding spherical coordinates are

$$\begin{aligned} \rho_r &= \sqrt{x_r^2 + y_r^2} \\ \phi_r &= \tan^{-1}(\frac{y_r}{x_r}) \\ \theta_r &= \frac{\pi}{2} \qquad\qquad r = 1, \ldots, N, \end{aligned} \tag{3.1}$$

where ρ_r and ϕ_r have Rayleigh and uniform distributions, respectively, i.e.,

$$\begin{aligned} f_{\rho_r}(\rho) &= \frac{\rho}{\sigma_0^2} \exp^{-\frac{\rho^2}{2\sigma_0^2}} \qquad 0 \leq \rho < \infty \\ f_{\phi_r}(\phi) &= \frac{1}{2\pi} \qquad\qquad -\pi \leq \phi < \pi. \end{aligned} \tag{3.2}$$

3.2.2 Channel Model

Different channel models are used in communication literature to account for various propagation scenarios and attenuation conditions of the transmitted signals [185], [186]. In this chapter, wireless communication channel conditions between the sensor nodes and the BS/AP are assumed to be ideal. In such channel model, transmitted signal is assumed to propagate in single-path line-of-sight (LOS) track according to free-space propagation model. The environment between the transmitter and the receiver does not have any obstacles so that reflection, scattering, or shadowing of the signal are neglected. Distances between different sensor nodes in the WSN are assumed to be large enough to neglect the mutual coupling effects between antenna elements. While the ideal channel model is not realistic, it is used in the analysis to find the fundamental results of the communication systems before generalizing the analysis to more realistic channel models. In CB analysis, the ideal channel model is used to explore the basic relationship between the spatial distribution of sensor nodes and the corresponding beampattern [14], [187].

3.2.3 Beampattern

Based on the aforementioned geometric and channel models, the beampattern corresponding to a cluster of sensor nodes can be derived as follows. Let us denote the Euclidean distance between the rth sensor node and a point (ϱ, ϕ, θ) in a sphere of radius $\rho = \varrho$ as $\delta_r(\phi, \theta)$, then

$$\delta_r(\phi, \theta) \triangleq \sqrt{\varrho^2 + \rho_r^2 - 2\rho_r \varrho \sin(\theta)\cos(\phi - \phi_r)}. \tag{3.3}$$

Introducing the vectors $\boldsymbol{\rho} = [\rho_1, \rho_2, \ldots, \rho_N] \in [0, \infty)^N$ and $\boldsymbol{\phi} = [\phi_1, \phi_2, \ldots, \phi_N] \in [-\pi, \pi)^N$, the array factor for a cluster of randomly located sensor nodes can be defined as

$$\mathbb{F}(\phi, \theta|\boldsymbol{\rho}, \boldsymbol{\phi}) = \frac{1}{N}\sum_{k=1}^{N} e^{j\psi_r} e^{j\frac{2\pi}{\lambda}\delta_r(\phi,\theta)} \tag{3.4}$$

where λ is the wavelength and ψ_r is initial phase of the rth sensor node's carrier. The factor $1/N$ is used to insure that $\max\{\mathbb{F}(\phi, \theta|\boldsymbol{\rho}, \boldsymbol{\phi})\}$=1. Synchronizing the carriers of the sensor nodes with initial phase $\psi_r = -\frac{2\pi}{\lambda}\delta_r(\varphi, \vartheta)$ to target the BS/AP at $(\varrho, \varphi, \vartheta)$, we can write the array factor as

$$\mathbb{F}(\phi, \theta|\boldsymbol{\rho}, \boldsymbol{\phi}) = \frac{1}{N}\sum_{k=1}^{N} e^{j\frac{2\pi}{\lambda}[\delta_r(\phi,\theta) - \delta_r(\varphi,\vartheta)]}. \tag{3.5}$$

Moreover, using the following approximation

$$\delta_r(\phi, \theta) \approx \varrho - \rho_r \sin(\theta)\cos(\phi - \phi_r) \tag{3.6}$$

which is valid for the far-field region with $\varrho \gg \rho_r$, we obtain that

$$\mathbb{F}(\phi, \theta|\boldsymbol{\rho}, \boldsymbol{\phi}) \approx \frac{1}{N}\sum_{k=1}^{N} \exp\left\{ j\frac{2\pi}{\lambda}\rho_r[\sin(\vartheta)\cos(\varphi - \phi_r) - \sin(\theta)\cos(\phi - \phi_r)] \right\}. \tag{3.7}$$

Note that (3.7) is symmetric with respect to the azimuth direction ϕ. Therefore, without any loss of generality, we can set $\varphi = 0$. For notation simplicity, we also assume that the destination BS/AP is located in the (x, y)-plane, i.e., $\vartheta = 0$, and we are interested in the beampattern at this plane only. Then, (3.7) simplifies to

$$\mathbb{F}(\phi|\boldsymbol{\rho}, \boldsymbol{\phi}) = \frac{1}{N}\sum_{k=1}^{N} e^{-j4\pi\tilde{\rho}_r \sin(\frac{\phi}{2})\sin(\tilde{\phi}_r)} \tag{3.8}$$

where $\tilde{\rho}_r = \frac{\rho_r}{\lambda}$ and $\tilde{\phi}_r = (\phi_r - \frac{\phi}{2})$. Equivalently, we can write that

$$\mathbb{F}(\phi|\mathbf{z}) = \frac{1}{N}\sum_{r=1}^{N} e^{-j\alpha z_r} \tag{3.9}$$

where $\alpha = \alpha(\phi) = 4\pi \sin(\frac{\phi}{2})$ is the azimuth direction parameter, $\mathbf{z} = [z_1, z_2, \ldots, z_N] \in (-\infty, \infty)^N$, and $z_r \triangleq \tilde{\rho}_r \sin(\tilde{\phi}_r)$ represents the sensor node location parameter. Note that z_r is Gaussian distributed random variable with zero mean and variance $\sigma^2 = \sigma_0^2/\lambda^2$, i.e.,

$$f_z(z) = \frac{1}{\sqrt{2\pi}\sigma} e^{-\frac{z^2}{2\sigma^2}}, \ -\infty < z < \infty. \tag{3.10}$$

For each realization of $\mathbf{z}$, the far-field beampattern can be found as

$$\begin{aligned} \mathbb{P}(\phi|\mathbf{z}) &= |\mathbb{F}(\phi|\mathbf{z})|^2 \\ &= \frac{1}{N} + \frac{1}{N^2} \sum_{r=1}^{N} e^{-j\alpha z_r} \sum_{l=1, l\neq r}^{N} e^{j\alpha z_l}. \end{aligned} \tag{3.11}$$

From (3.11), we conclude that with ideal channel conditions and perfect synchronization, the CB beampattern is completely defined by sensor node locations. The beampattern at any arbitrary direction $\phi \neq \varphi$ is the summation of the out-of-phase signals and, thus, it is random. However, the beampattern value at the BS/AP direction $\varphi = 0$ is deterministic and equals unity for any sensor node locations.

3.3 Average Beampattern and Its Characteristics

The sample beampattern of (3.11) does not give an insight about the effect of the spatial distribution of sensor nodes on the CB beampattern. To investigate the effects of the spatial distribution on the CB beampattern, the average of the beampattern is taken over all realizations of sensor node locations given by this spatial distribution. Then, the average CB beampattern characteristics are compared with characteristics corresponding to uniform spatial distribution of [14].

3.3.1 Average Beampattern

The average beampattern is defined as

$$\mathbb{P}_{\text{av}}(\phi) = E\{\mathbb{P}(\phi|\mathbf{z})\} \tag{3.12}$$

where $E\{\cdot\}$ denotes the statistical expectation and the average is found over all realizations of $\mathbf{z}$. In the case of Gaussian sensor node distribution, the average beampattern can be derived by substituting (3.10) and (3.11) in (3.12). Then we

have

$$\begin{aligned}
\mathbb{P}_{\text{av}}(\phi) &= E\left\{\mathbb{P}(\phi|\mathbf{z})\right\} \\
&= \int_{-\infty}^{\infty}\int_{-\infty}^{\infty} \left|\mathbb{F}(\phi|\mathbf{z})\right|^2 f_z(z_r)\ f_z(z_l)\ dz_r\ dz_l \\
&= \int_{-\infty}^{\infty}\int_{-\infty}^{\infty} \left\{\frac{1}{N} + \frac{1}{N^2}\sum_{r=1}^{N} e^{-j\alpha z_r} f_z(z_r) \sum_{l=1,l\neq r}^{N} e^{j\alpha z_l} f_z(z_l)\right\} dz_r\ dz_l \\
&= \frac{1}{N} + \frac{1}{N^2}\left[\sum_{r=1}^{N}\left\{\int_{-\infty}^{\infty} e^{-j\alpha z_r}\frac{1}{\sqrt{2\pi}\sigma}e^{-\frac{z_r^2}{2\sigma^2}}dz_r\right\}\right. \\
&\times \left.\sum_{l=1,l\neq r}^{N}\left\{\int_{-\infty}^{\infty} e^{-j\alpha z_l}\frac{1}{\sqrt{2\pi}\sigma}e^{-\frac{z_l^2}{2\sigma^2}}dz_l\right\}\right] \qquad (3.13)
\end{aligned}$$

The integrals between the figure brackets in (3.13) can be simplified as

$$\begin{aligned}
\int_{-\infty}^{\infty} e^{-j\alpha z}\frac{1}{\sqrt{2\pi}\sigma}e^{-\frac{z^2}{2\sigma^2}}dz &= e^{\frac{-\alpha^2\sigma^2}{2}}\left\{\frac{1}{\sqrt{2\pi}\sigma}\int_{-\infty}^{\infty} e^{-\frac{(z+j\alpha\sigma^2)^2}{2\sigma^2}}dz\right\} \\
&= e^{\frac{-\alpha^2\sigma^2}{2}}\left\{\frac{1}{\sqrt{2\pi}\sigma}\int_{-\infty}^{\infty} e^{-\frac{u^2}{2\sigma^2}}du\right\} \\
&= e^{\frac{-\alpha^2\sigma^2}{2}}. \qquad (3.14)
\end{aligned}$$

where the change of the variable $u = z + j\alpha\sigma^2$ is used while establishing the second equality. Substituting (3.14) in (3.13)

$$\begin{aligned}
\mathbb{P}_{\text{av}}(\phi) &= \frac{1}{N} + \frac{1}{N^2}\left\{\sum_{r=1}^{N} e^{\frac{-\alpha^2\sigma^2}{2}} \sum_{l=1,l\neq r}^{N} e^{\frac{-\alpha^2\sigma^2}{2}}\right\} \\
&= \frac{1}{N} + \frac{1}{N^2}N(N-1)\left|e^{\frac{-\alpha^2\sigma^2}{2}}\right|^2 \qquad (3.15)
\end{aligned}$$

Consequently, the average beampattern can be expressed as

$$\mathbb{P}_{\text{av}}(\phi) = \frac{1}{N} + \left(1 - \frac{1}{N}\right)\left|e^{-\frac{\alpha^2\sigma^2}{2}}\right|^2. \qquad (3.16)$$

The term $1/N$ in (3.16) represents the value of the average beampattern in the sidelobe region. It can be seen that the average beampattern has no nulls and no sidelobes. The mainlobe of the average beampattern is represented by the second term in (3.16), and it decays exponentially with a rate proportional to the variance σ^2. Note that the average beampattern (3.16) is somewhat similar to the one derived for the case of uniformly distributed sensor nodes [14]

$$\mathbb{P}_{\text{av}}(\phi) = \frac{1}{N} + \left(1 - \frac{1}{N}\right) 2\left|\frac{J_1(\alpha)}{\alpha}\right|^2 \qquad (3.17)$$

where $J_1(\alpha)$ is the first order Bessel function of the first kind and $\alpha = \alpha(\phi) = 4\pi\tilde{R}\sin(\frac{\phi}{2})$ in this case. However, in the latter case, the Bessel function of the first kind results also in nulls and sidelobes. The presence of sidelobes in the average beampattern increases the chance of sidelobes with high peaks in a sample beampattern for a specific realization of sensor node locations.

The average beampatterns for both cases of Gaussian and uniform spatial distributions are shown in Fig. 3.3, where $\sigma^2 = 1$ and $N \in \{16, 1024\}$. Hereafter, when comparing the cases of uniform and Gaussian spatial sensor node distributions, we use $\sigma = \tilde{R}/3$ in the case of Gaussian spatial distribution, where the normalized radius of the cluster $\tilde{R} = R/\lambda$ is defined for uniform distribution [14]. This assumption suggests that in the case of Gaussian distribution, 99.73% of all sensor nodes are located in the disk of radius $\tilde{R}$ and, thus, the sensor nodes' coverage areas in both cases are the same.

3.3.2 3dB Beamwidth

The 3dB beamwidth is defined as shown in Fig. 3.4 as the angle $\phi_{3\text{dB}}$ at which the power of the average beampattern drops 3dB below the maximum value at $\phi = \varphi = 0$, i.e.,

$$\mathbb{P}_{\text{av}}(\phi_{3\text{dB}}) = \frac{1}{2}. \tag{3.18}$$

In the case of Gaussian distributed sensor nodes, the 3dB beamwidth of the average beampattern (3.16) can be derived by substituting (3.16) in (3.18) as follows

$$\frac{1}{N} + \left(1 - \frac{1}{N}\right)\left|e^{\frac{-\alpha_{3\text{dB}}^2\sigma^2}{2}}\right|^2 = \frac{1}{2} \tag{3.19}$$

where $\alpha_{3\text{dB}}$ is the azimuth direction parameter corresponding to $\phi_{3\text{dB}}$. Simplifying (3.19), we can write that

$$e^{\frac{-\alpha_{3\text{dB}}^2\sigma^2}{2}} = \sqrt{\left(\frac{1}{2} - \frac{1}{N}\right)\left(\frac{N}{N-1}\right)} = \sqrt{\frac{1}{2}\frac{N-2}{N-1}} \approx \sqrt{\frac{1}{2}} \tag{3.20}$$

where the last approximation is valid for $N \gg 1$. Thus, the value of $\alpha_{3\text{dB}}$ can be expressed as

$$\alpha_{3\text{dB}} = \sqrt{\frac{-2\ln(\sqrt{\frac{1}{2}})}{\sigma^2}} = \sqrt{\frac{\ln(2)}{\sigma^2}}. \tag{3.21}$$

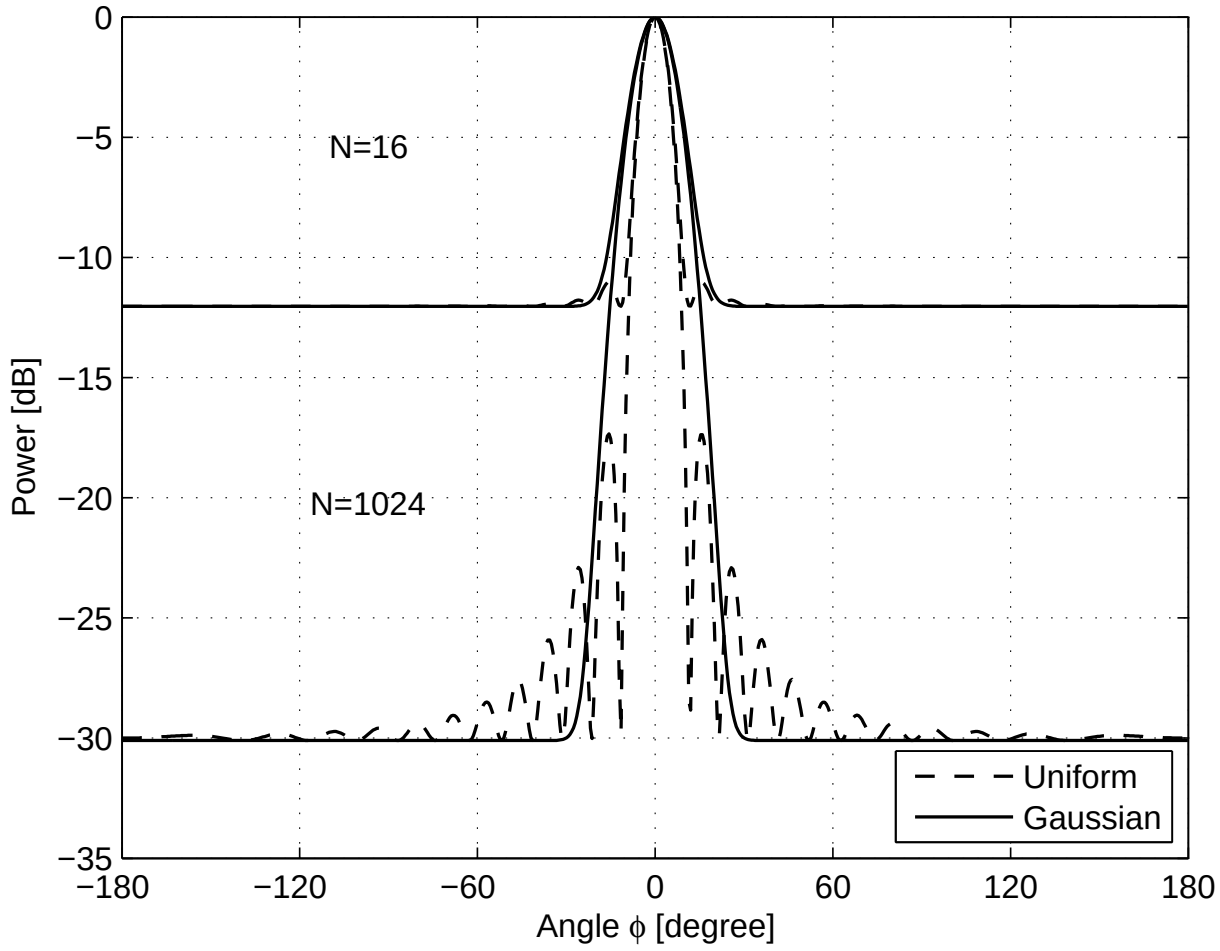

Figure 3.3. The average beampattern for both uniform and Gaussian spatial distributions: $N = 16$ and $1024, \sigma^2 = 1$, $\tilde{R} = 3\sigma$.

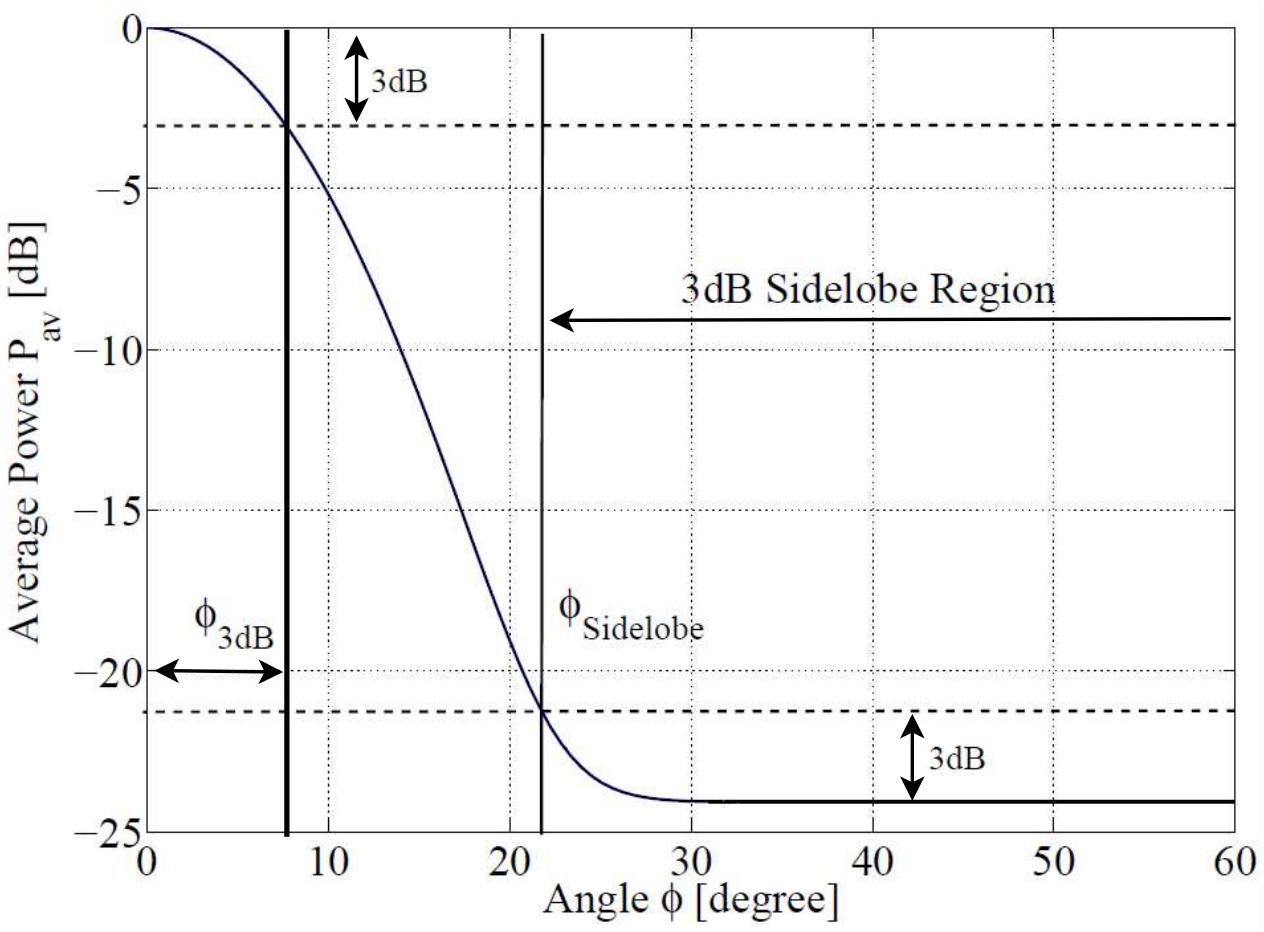

Figure 3.4. Definitions of average beampattern characteristics.

Substituting the value of $\alpha_{3\text{dB}} = 4\pi \sin(\frac{\phi_{3\text{dB}}}{2})$, we can write that

$$\sin\left(\frac{\phi_{3\text{dB}}}{2}\right) = \frac{\sqrt{\ln(2)}}{4\pi\sigma}. \tag{3.22}$$

Finally, the 3dB beamwidth of the average beampattern is given as

$$\phi_{3\text{dB}} = 2\sin^{-1}\left(\frac{0.0663}{\sigma}\right) \approx \frac{0.1326}{\sigma}. \tag{3.23}$$

where the last approximation come from the fact that $\sin^{-1}(a) \approx a$ for small angles.

For the sake of comparison with the case of uniformly distributed sensor nodes, we express (3.23) in terms of $\tilde{R} = 3\sigma$. Then, the expression (3.23) can be rewritten as

$$\phi_{3\text{dB}} \approx \frac{0.4}{\tilde{R}}. \tag{3.24}$$

Similar to the case of uniform distribution [14], the 3dB beamwidth in the case of Gaussian spatial sensor node distribution decreases when the cluster radius increases. However, the 3dB beamwidth in the case of Gaussian distributed sensor nodes is larger than in the case of uniform distributed sensor nodes for the same cluster area. The only factor that affect the 3dB beamwidth is the radius $\tilde{R}$. Note that it can often be adjusted at the deployment stage to the desired value.

3.3.3 3dB Sidelobe Region

The 3dB sidelobe region, shown in Fig. 3.4, is the range between the angle ϕ_{SL} at which the mainlobe of the average beampattern reduces to 3dB above $1/N$ and π, i.e.,

$$\text{Sidelobe Region} = \{\phi \mid \phi_{\text{SL}} \leq |\phi| \leq \pi\}. \tag{3.25}$$

In the case of Gaussian distributed sensor nodes, ϕ_{Sidelobe} can be derived by substituting (3.16) in

$$\mathbb{P}_{\text{av}}(\phi_{\text{SL}}) = \frac{2}{N} \tag{3.26}$$

Then we obtain that

$$\frac{1}{N} + \left(1 - \frac{1}{N}\right)\left|e^{\frac{-\alpha_{\text{SL}}^2\sigma^2}{2}}\right|^2 = \frac{2}{N}. \tag{3.27}$$

where α_{SL} is the azimuth direction parameter corresponding to ϕ_{SL} and can be substituted by $4\pi \sin(\frac{\phi_{\text{SL}}}{2})$ and, thus, (3.27) becomes

$$4\pi \sin\left(\frac{\phi_{\text{SL}}}{2}\right) = \frac{\sqrt{\ln(N-1)}}{\sigma}. \tag{3.28}$$

After some straightforward manipulations, ϕ_{SL} can be founded as

$$\phi_{\mathrm{SL}} = 2\sin^{-1}\left(\frac{\sqrt{\ln(N-1)}}{4\pi\sigma}\right). \tag{3.29}$$

It can be seen that the sidelobe region depends on the cluster area and the number of sensor nodes N. However, the effect of N is small due to the logarithm and square root operations. Hence, increasing the number of sensor nodes in the case of Gaussian spatial sensor node distribution is not as critical for the sidelobe region as it is in the case of uniform spatial sensor node distribution [14]. Comparing it to the case of uniform distribution, we see that Gaussian distribution produces average beampattern with larger sidelobe region, i.e., the mean of the beampattern is close to $1/N$ over a larger area and, therefore, the sidelobes with high peaks are less probable.

Fig. 3.5 shows the 3dB beamwidth ϕ_{3dB} and 3dB sidelobe region starting angle ϕ_{SL} versus normalized radius $\tilde{R} = 3\sigma$ for both uniform and Gaussian spatial distributions. The angle ϕ_{SL} is calculated for $N = 16$ and $N = 1024$. For cluster radius $\tilde{R} > 10$, we find that ϕ_{3dB} and ϕ_{SL} are less than 20^o for all considered cases. Large cluster radius $\tilde{R}$ results in sparsely distributed nodes and the effect of the spacial distribution becomes less obvious.

3.3.4 Average Directivity

The directivity, in the context of WSNs, is changing from one realization of sensor node locations to another. Given a realization of sensor node locations $\mathbf{z}$, the directivity can be expressed as [14]

$$\begin{aligned} D(\mathbf{z}) &= \frac{\int_{-\pi}^{\pi}\mathbb{P}(0)d\phi}{\int_{-\pi}^{\pi}\mathbb{P}(\phi/\mathbf{z})d\phi} \\ &= \frac{2\pi}{\int_{-\pi}^{\pi}\mathbb{P}(\phi/\mathbf{z})d\phi} \end{aligned} \tag{3.30}$$

where $\mathbb{P}(0) = \mathbb{P}(0|\mathbf{z}) = 1$. Then, the average directivity is defined as

$$D_{\mathrm{av}} = E\left\{D(\mathbf{z})\right\}. \tag{3.31}$$

The following lower bound on the average directivity is typically considered

$$D^*_{\mathrm{av}} = \frac{2\pi}{\int_{-\pi}^{\pi}\mathbb{P}_{\mathrm{av}}(\phi)d\phi}. \tag{3.32}$$

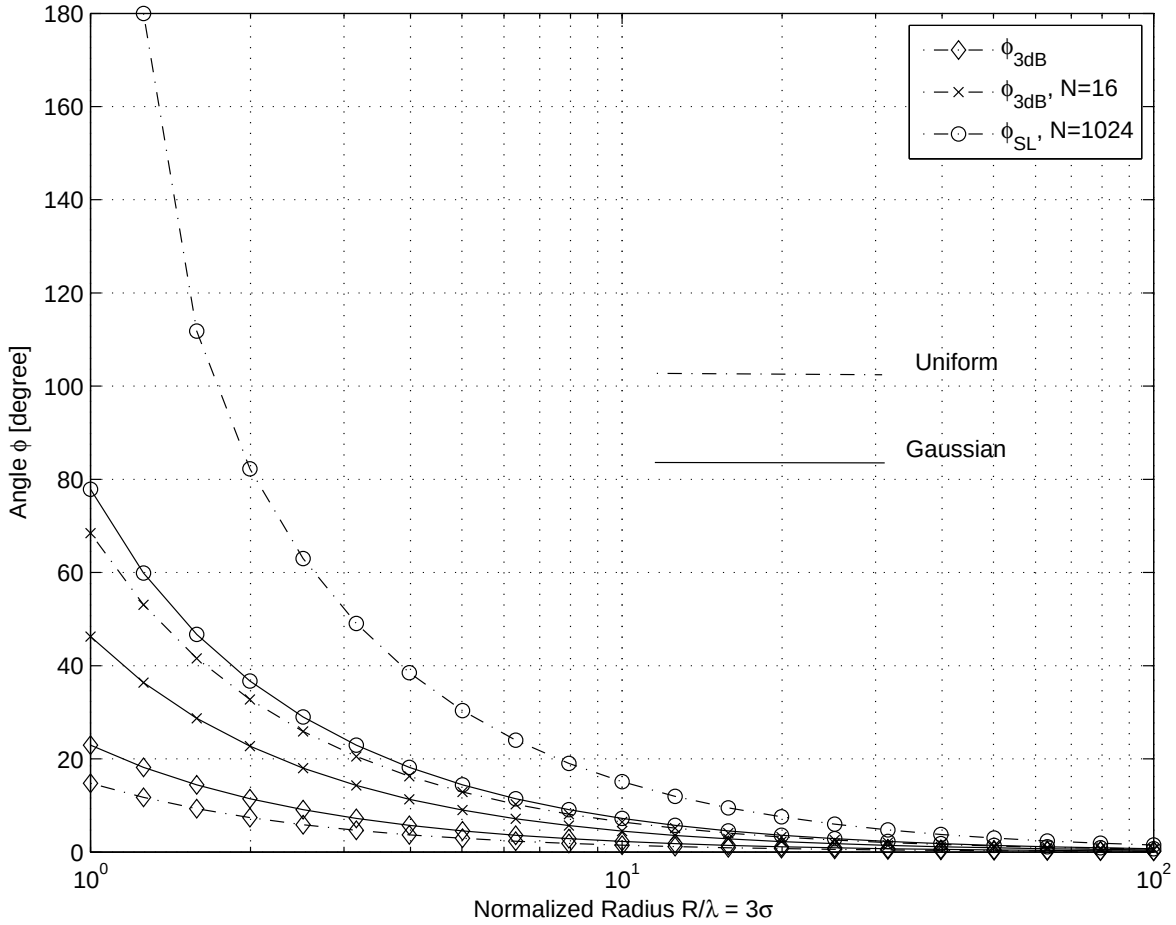

Figure 3.5. The 3dB beamwidth ϕ_{3dB} and 3dB sidelobe region start angle ϕ_{SL} for both uniform and Gaussian spatial distributions: $N = 16$ and 1024.

We can find the lower bound on the average directivity in the case of Gaussian distributed sensor nodes as follows.

Substituting (3.16) in (3.32), we can write that

$$\begin{aligned}\tilde{D}_{\text{av}} &= \frac{2\ \pi}{\int_{-\pi}^{\pi} \frac{1}{N} + (1-\frac{1}{N})\left|e^{\frac{-\alpha(\phi)^2\sigma^2}{2}}\right|^2 d\phi} \\ &= \frac{2\ \pi\ N}{2\ \pi + (N-1)\int_{-\pi}^{\pi}\left|e^{\frac{-\alpha(\phi)^2\sigma^2}{2}}\right|^2 d\phi}. \end{aligned} \tag{3.33}$$

The integral in (3.33) can be found as

$$\int_{-\pi}^{\pi}\left|e^{\frac{-\alpha(\phi)^2\sigma^2}{2}}\right|^2 d\phi = \int_{-\pi}^{\pi} e^{-(4\ \pi\sin(\phi/2))^2\sigma^2} d\phi. \tag{3.34}$$

Introducing a new notation $c = (4\pi\sigma)^2$ and by using the change of variable integration method for $u = \sin(\phi/2)$ and $du/d\phi = 1/2\cos(\phi/2)$, we can rewrite (3.34) as

$$\begin{aligned}\int_{-1}^{1} e^{-cu^2}\frac{2}{\cos(\frac{\phi}{2})}du &= \int_{-1}^{1} e^{-cu^2}\frac{2}{\sqrt{1-\sin(\frac{\phi}{2})^2}}du \\ &= \int_{-1}^{1} e^{-cu^2}\frac{2}{\sqrt{1-u^2}}du. \end{aligned} \tag{3.35}$$

Changing the variable again as $x = u^2$, $dx/du = 2u$, the integral (3.35) becomes

$$\begin{aligned}2\int_0^1 e^{-cx}\frac{2}{\sqrt{1-x}}\frac{1}{2\sqrt{x}}dx &= 2\int_0^1 e^{-cx}(1-x)^{-\frac{1}{2}}x^{-\frac{1}{2}}dx \\ &= 2\ \pi\ {}_1F_1(\frac{1}{2};1;-(4\ \pi\sigma)^2). \end{aligned} \tag{3.36}$$

where

$$\int_0^1 e^{-cx}(1-x)^{b-a-1}x^{a-1}dx = \frac{\Gamma(b-a)\ \Gamma(a)}{\Gamma(b)}\ {}_1F_1(a;b;c). \tag{3.37}$$

Finally, substituting (3.36) in (3.33), we obtain

$$D^*_{\text{av}} = \frac{N}{1+(N-1)\ {}_1F_1(\frac{1}{2};1;-(4\pi\sigma)^2)} \tag{3.38}$$

where ${}_1F_1(\frac{1}{2};1;-(4\pi\sigma)^2)$ is the hypergeometric function of the first kind. Note that in the case of uniform spatial distribution, the average directivity is represented in terms of the generalized hypergeometric function ${}_2F_3(\frac{1}{2},\frac{3}{2};1,2,3;-(4\pi\tilde{R})^2)$ instead of ${}_1F_1(\frac{1}{2};1;-(4\pi\sigma)^2)$.

As compared to the case of uniform spatial distribution [14],

$$D^*_{\text{av}} = \frac{N}{1 + (N-1)\,{}_2F_3(\frac{1}{2}, \frac{3}{2}; 1, 2, 3; -(4\pi\tilde{R})^2)} \tag{3.39}$$

the hypergeometric function of the first kind in (3.39) has larger value than the generalized hypergeometric function ${}_2F_3(\frac{1}{2}, \frac{3}{2}; 1, 2, 3; -(4\pi\tilde{R})^2)$. Therefore, the average directivity is lower in the case of Gaussian sensor node distribution as compared to the case of uniform distribution for the same cluster area.

Fig. 3.6 shows the normalized average directivity D_{av}/N and its normalized lower bound D^*_{av}/N for both uniform and Gaussian spatial distributions. It can be seen that the directivity approaches N asymptotically with increasing the normalized radius $\tilde{R} = 3\sigma$ in both aforementioned cases. Therefore, for a given number of sensor nodes, we can increase the directivity by spreading the sensor nodes over a larger area.

3.4 Random Behavior of the Beampattern

In this section, we first model the array factor as a complex random variable and find the corresponding mean and variance. In order to guarantee that the interference to the neighboring clusters is limited, the Complementary Cumulative Distribution Function (CCDF) of the beampattern level in the sidelobe region should be small enough for any specific realization of sensor node locations. The CCDF of the beampattern level and the distribution of the maximum sidelobe peak which both characterize the random behavior of a sample beampattern, are derived for the case of Gaussian sensor node distribution. The derived expressions are compared with the corresponding ones in the case of uniform distributed sensor nodes.

3.4.1 Array Factor Approximation

The distribution function can be derived by approximating the array factor level at a given angle ϕ using an uncorrelated complex Gaussian random variable with a real part X and an imaginary part Y [137], [188], that is,

$$\mathbb{F}(\phi|\mathbf{z}) = \frac{1}{N}\sum_{r=1}^{N} e^{-j\alpha z_r} = \frac{1}{\sqrt{N}}(\mathsf{X} - j\mathsf{Y}). \tag{3.40}$$

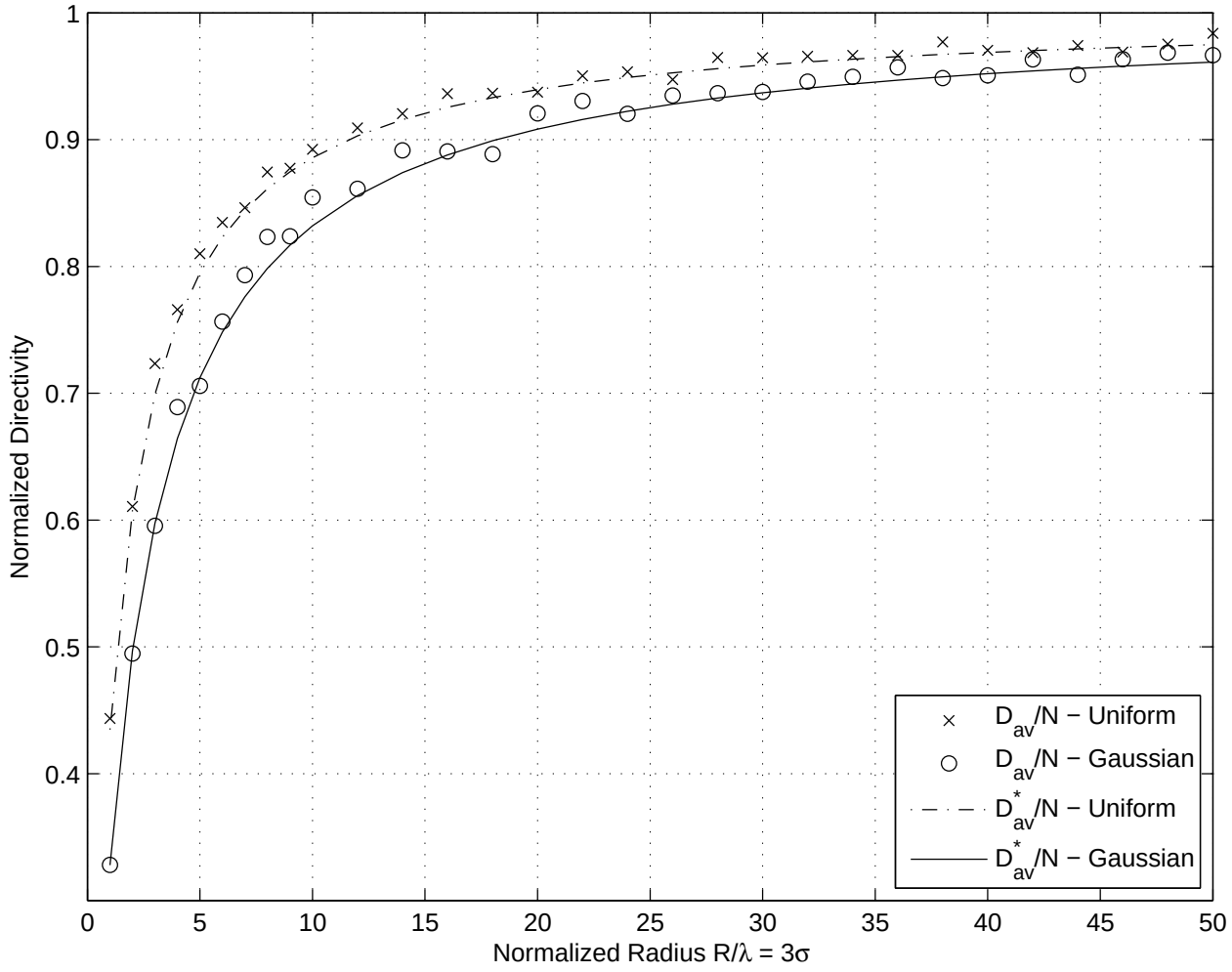

Figure 3.6. The normalized directivity D_{av}/N and the upper bound on the normalized directivity D^*_{av}/N for both uniform and Gaussian spatial distributions: $N = 16$.

where

$$\mathsf{X} = \mathcal{R}\left\{\frac{1}{\sqrt{N}}\sum_{r=1}^{N} e^{-j\alpha z_r}\right\} = \frac{1}{\sqrt{N}}\sum_{r=1}^{N}\cos\left(\alpha z_r\right) \tag{3.41}$$

$$\mathsf{Y} = \mathcal{I}\left\{\frac{1}{\sqrt{N}}\sum_{r=1}^{N} e^{-j\alpha z_r}\right\} = \frac{1}{\sqrt{N}}\sum_{r=1}^{N}\sin\left(\alpha z_r\right) \tag{3.42}$$

and $\mathcal{R}\{\cdot\}$ and $\mathcal{I}\{\cdot\}$ represent the real and the imaginary parts of a complex number, respectively.

The joint pdf of X and Y can be written as

$$f_{\mathsf{X},\mathsf{Y}}(\mathsf{x},\mathsf{y}) = \frac{1}{2\pi\sigma_{\mathsf{X}}\sigma_{\mathsf{Y}}}\ \exp\left(-\frac{|\mathsf{x}-m_{\mathsf{X}}|^2}{2\sigma_{\mathsf{X}}^2} - \frac{\mathsf{y}^2}{2\sigma_{\mathsf{Y}}^2}\right) \tag{3.43}$$

where the means m_{X}, m_{Y} and variances σ_{X}^2, σ_{Y}^2 in the case of Gaussian distributed sensor nodes are given as [188]

$$m_{\mathsf{X}} = \sqrt{N}\Omega(\alpha) = \sqrt{N}e^{-\frac{\alpha^2\sigma^2}{2}} \tag{3.44}$$

$$\sigma_{\mathsf{X}}^2 = \frac{1}{2}\left(1+\Omega(2\alpha)\right) - \frac{1}{N}\Omega(\alpha)^2 = \frac{1}{2}\left(1+e^{-2\alpha^2\sigma^2}\right) - e^{-\alpha^2\sigma^2} \tag{3.45}$$

$$m_{\mathsf{Y}} = 0 \tag{3.46}$$

$$\sigma_{\mathsf{Y}}^2 = \frac{1}{2}\left(1-\Omega(2\alpha)\right) = \frac{1}{2}\left(1-e^{-2\alpha^2\sigma^2}\right) \tag{3.47}$$

where $\Omega(\alpha)$ is the characteristic function of the Gaussian distributed random variable z that is given by

$$\Omega(\alpha) = e^{-\frac{\alpha^2\sigma^2}{2}}. \tag{3.48}$$

Note that the corresponding values of the means m_{X}, m_{Y} and variances σ_{X}^2, σ_{Y}^2 in the case of uniform distributed sensor nodes are given as [14]

$$m_{\mathsf{X}} = 2\sqrt{N}\ \frac{J_1(\alpha)}{\alpha} \tag{3.49}$$

$$\sigma_{\mathsf{X}}^2 = \frac{1}{2}\left(1+\frac{J_1(2\alpha)}{\alpha}\right) - \left(2\frac{J_1(\alpha)}{\alpha}\right)^2 \tag{3.50}$$

$$m_{\mathsf{Y}} = 0 \tag{3.51}$$

$$\sigma_{\mathsf{Y}}^2 = \frac{1}{2}\left(1-\frac{J_1(2\alpha)}{\alpha}\right) \tag{3.52}$$

Figs. 3.7 and 3.8 show, respectively, the means and the variances of array factor for both uniform and Gaussian spatial distributions. It can be seen that for fixed N the array factor in the case of Gaussian spatial distribution has large mean at the

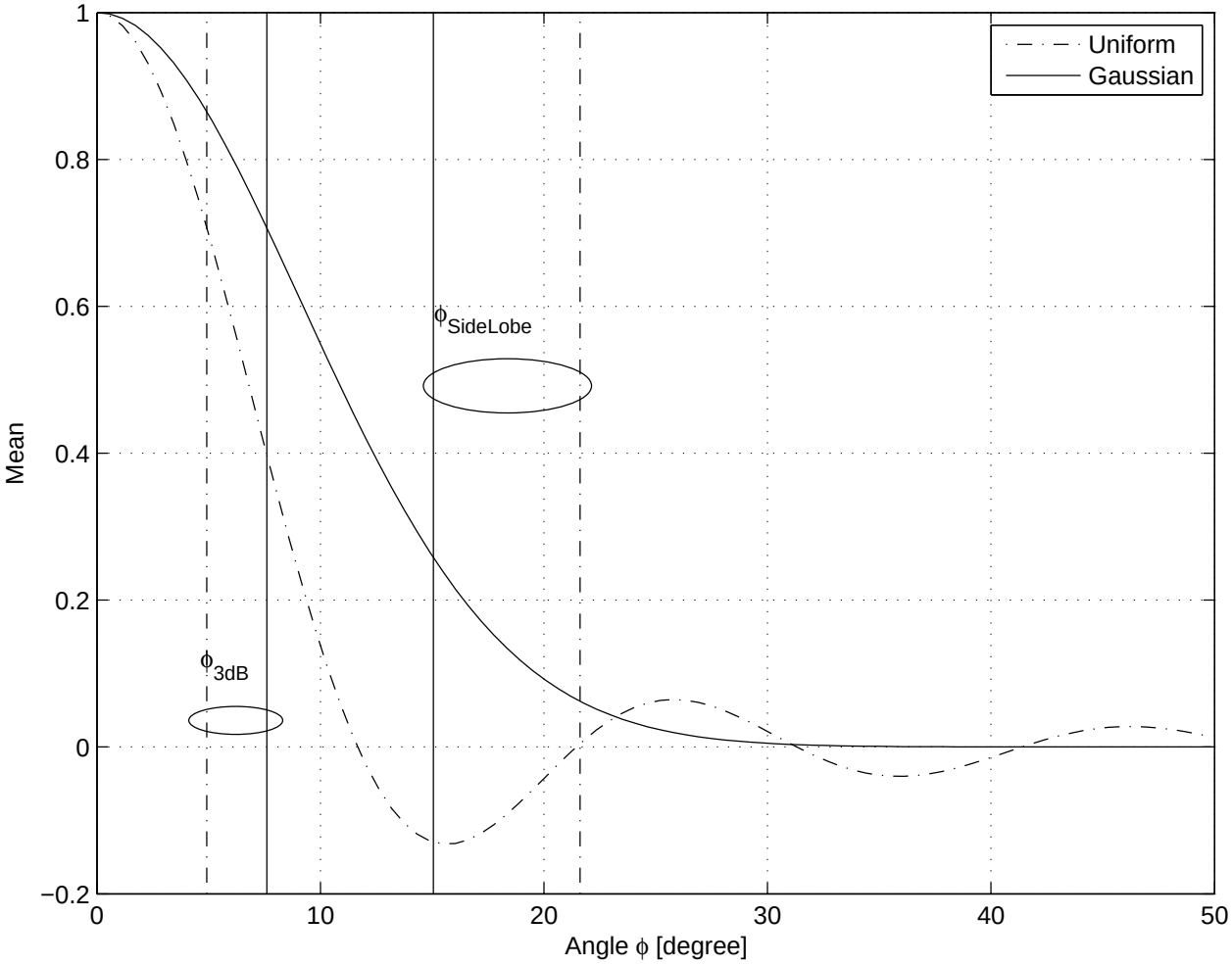

Figure 3.7. The mean of the array factor for both uniform and Gaussian spatial distributions: $N = 16, \sigma^2 = 1, \tilde{R} = 3\sigma$.

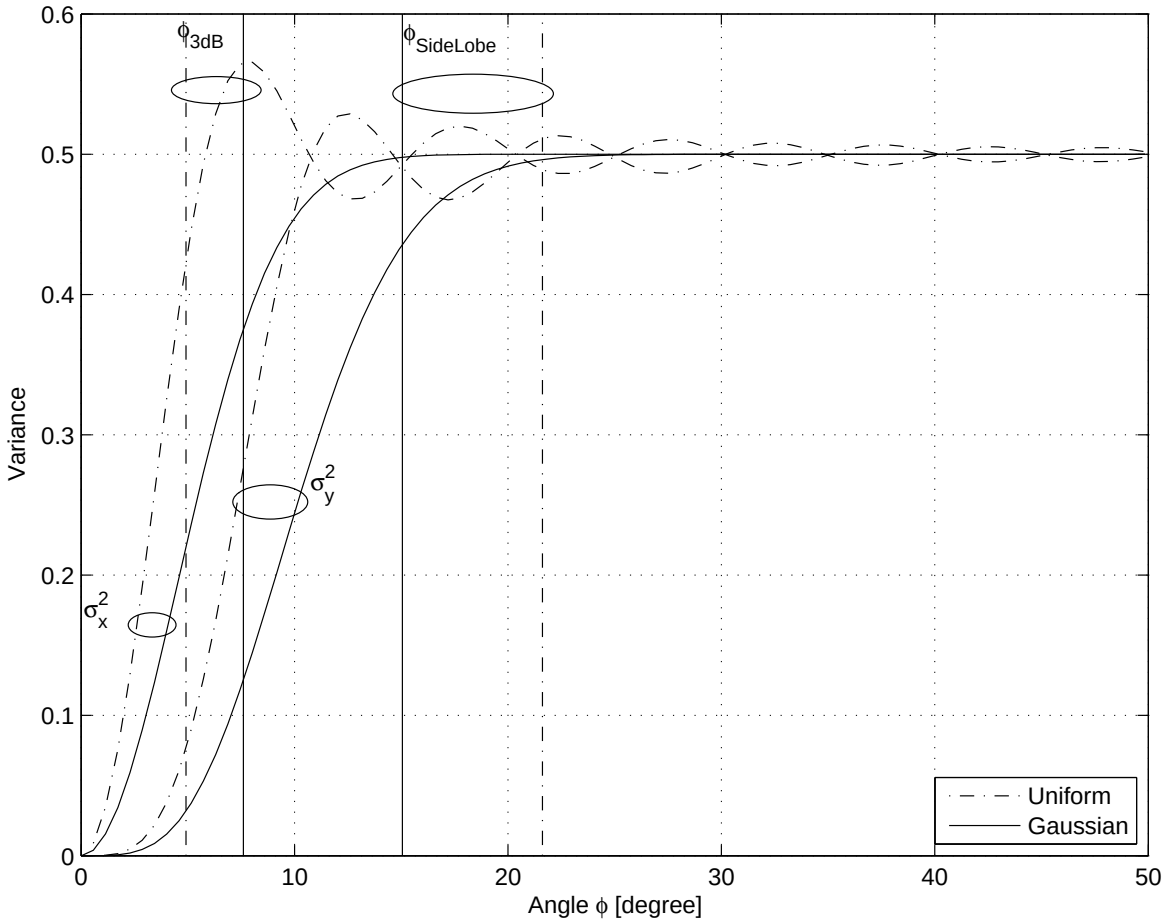

Figure 3.8. The variance of X and Y for both uniform and Gaussian spatial distributions: $N = 16, \sigma^2 = 1, \tilde{R} = 3\sigma$.

region near to the target direction ($\phi = 0$), and it approaches zero with increasing ϕ. Thus, sidelobes of equal level occur with equal probability over whole sidelobe region. In the case of uniform distribution, the mean is oscillating in the sidelobe region and, thus, the probability of high level sidelobes in the beampattern is larger at the angles which correspond to the mean peaks. The variance for both distributions is equal to zero at $\phi = 0$ and increases with the directions far from the targeted direction. Therefore, the mainlobe of the sample beampattern matches precisely the mainlobe of the average beampattern, and its behavior can be considered as deterministic. This suggests that the 3dB beamwidth and directivity do not deviated much from the average values, and thus, the average beampattern is suitable for characterizing the mainlobe of a sample beampattern. Moreover, the variance in the case of Gaussian distribution has lower value than the corresponding value in the case of uniform distribution [14], and thus, the mainlobe is more stable in the Gaussian case.

3.4.2 Distribution of the Beampattern Level in the Sidelobe Region

Synchronizing the carriers of sensor nodes guarantees a deterministic power level at the targeted direction and the mainlobe can be determined for any spatial distribution. However, the ad hoc locations of sensor nodes result in random beampattern in the sidelobe region. Therefore, it is important to predict the interference to neighboring clusters for any sample beampattern. Because of the high value of the variance in the sidelobe region for both Gaussian and uniform pdfs, the shape of a sample beampattern in the sidelobe region can completely deviate from the shape of the average beampattern. Hence, the average beampattern does not reflect the behavior of a sample beampattern in the sidelobe region, and its characteristics should be expressed in a statistical form. The CCDF of the beampattern level in the sidelobe region is given as

$$\begin{aligned}
\Pr\left\{\mathbb{P}(\phi|\mathbf{z}) > P_0\right\} &= \Pr\left\{\left|\mathbb{F}(\phi|\mathbf{z})\right|^2 > P_0\right\} \\
&= \Pr\left\{\left|\frac{1}{\sqrt{N}}(\mathsf{X} - j\mathsf{Y})\right|^2 > P_0\right\} \\
&= \Pr\left\{\mathsf{X}^2 + \mathsf{Y}^2 > N\ P_0\right\}. \qquad (3.53)
\end{aligned}$$

Therefore, the distribution of the beampattern level is the same as the distribution of the summation $\mathsf{X}^2 + \mathsf{Y}^2$. From (3.47), we observe that the variances σ^2_{X} and σ^2_{Y}

approach 0.5 in the sidelobe region, and thus, the value of the summation $\mathsf{X}^2 + \mathsf{Y}^2$ has non-central chi-square distribution with 2 degrees of freedom [186], i.e.,

$$f_{\mathsf{X}^2+\mathsf{Y}^2}(u) = \frac{1}{2\sigma^2} e^{-\frac{u+s^2}{2\sigma^2}} I_0\left(\frac{s}{\sigma^2}\sqrt{u}\right), \quad u \geq 0 \tag{3.54}$$

where $s^2 = m_{\mathsf{X}}^2 + m_{\mathsf{Y}}^2$ and $I_n(\cdot)$ is the nth-order modified Bessel function of the first kind. In the case of non-central chi-square distribution with even number of degrees of freedom, the CCDF can be expressed in terms of the generalized Marcum-Q function $Q_M(\cdot)$ as

$$Q_M(a,b) = \int_b^\infty u \left(\frac{u}{a}\right)^{M-1} e^{-\frac{u^2+a^2}{2}} I_{M-1}(au)\, du. \tag{3.55}$$

Using the latter expression, the CCDF (3.53) can be simplified as

$$\begin{aligned} \Pr\{\mathbb{P}(\phi) > P_0\} &= Q_M\left(\frac{s}{\sigma}, \frac{\sqrt{u}}{\sigma}\right) \\ &= Q_M\left(\frac{m_{\mathsf{X}}}{\sigma_{\mathsf{X}}}, \frac{\sqrt{NP_0}}{\sigma_{\mathsf{Y}}}\right) \\ &= Q_M\left(\sqrt{2}m_{\mathsf{X}}, \sqrt{2NP_0}\right). \end{aligned} \tag{3.56}$$

Moreover, the CCDF of the beampattern level can also be expressed as

$$\Pr\{\mathbb{P}(\phi|\mathbf{z}) > P_0\} = \Pr\left\{\sqrt{\mathsf{X}^2 + \mathsf{Y}^2} > \sqrt{N\ P_0}\right\}. \tag{3.57}$$

Therefore, the beampattern distribution is the same as the distribution of the random variable $\sqrt{\mathsf{X}^2 + \mathsf{Y}^2}$. Using the fact that the variances approach equal values, and the mean m_{X} approaches zero, we can conclude that the beampattern level has Rayleigh distribution, i.e.,

$$f(u) = \frac{u}{\sigma^2} e^{-\frac{u^2}{2\sigma^2}}, \quad u \geq 0 \tag{3.58}$$

Consequently, the CCDF can be expressed as

$$\Pr\{\mathbb{P}(\phi) > P_0\} = e^{-NP_0}. \tag{3.59}$$

This approximation is very accurate in the case of Gaussian distribution for the whole sidelobe region where the array factor has zero mean and the variances are equal to 0.5 as shown in Figs. 3.7 and 3.8. However, in the case of uniform distribution, the mean values and the variances have the same oscillatory nature as the Bessel function $J_1(\alpha)$ and, thus, the approximation is valid only for the beampattern nulls and large values of ϕ.

The CCDFs (3.56) for both uniform and Gaussian sensor node distributions and the Rayleigh approximation to CCDFs (3.59) are shown in Fig. 3.9 for N=16, 256, and 1024. It can be seen from the figure that the chance of a high beampattern level in the sidelobe region reduces with increasing the number of sensor nodes N, while this chance is almost independent on the cluster area. The CCDFs for both distributions are the same for low values of N. However, the CCDF in the case of Gaussian distribution is lower than the CCDF in the case of uniform distribution if N is large. The Rayleigh approximation is valid in the case of uniform distribution only if N is small, while it is accurate in the case of Gaussian distribution for any value of N.

Fig. 3.10 shows the CCDF as a function of N for given values of power level P_0. This figure can be used to estimate the number of sensor nodes N required for achieving a certain beampattern level with high probability. It can be seen that for high beampattern levels, both Gaussian and uniform spatial distributions give the same results. However, for low beampattern levels, Gaussian spatial distribution requires less sensor nodes then uniform distribution.

3.4.3 Distribution of the Maximum Sidelobe Peak

The probability that the sidelobe with a maximum peak exceeds a given power level P_0 is referred hereafter as the outage probability $\mathrm{Pr}_{\mathrm{out}}$ [14], i.e.,

$$\mathrm{Pr}_{\mathrm{out}} \triangleq \mathrm{Pr}\left\{\max_{\phi\in\text{Sidelobe Region}} \mathbb{P}(\phi) > P_0\right\} \tag{3.60}$$

The outage probability can be used to estimate the maximum possible interference to other clusters in the neighborhood or to estimate the probability of a given interference level to these clusters.

To find the outage probability, the array factor in the sidelobe region $\mathbb{F}(u|\mathbf{z})$ is modeled as a random process, where $u = \sin(\phi/2), \phi \in$ Sidelobe Region. In this case, the real and imaginary parts of $\mathbb{F}(u|\mathbf{z})$, denoted as $\mathsf{X}(u)$ and $\mathsf{Y}(u)$, are found to be wide sense stationary normal random processes with zero-mean and variances $\sigma^2_{\mathsf{X}} = \sigma^2_{\mathsf{Y}} = 1/2$ [137]. An upper bound on the outage probability $\mathrm{Pr}_{\mathrm{out}}$ can be derived by finding the distribution of the local maxima of the square root [14]

$$\mathsf{R}(u) \triangleq \sqrt{\mathsf{X}^2(u) + \mathsf{Y}^2(u)} = \sqrt{N}|\mathbb{F}(\phi|\mathbf{z})| = \sqrt{N\mathbb{P}(\phi|\mathbf{z})}. \tag{3.61}$$

The probability of a local maxima of R exceeding level a in the sidelobe region

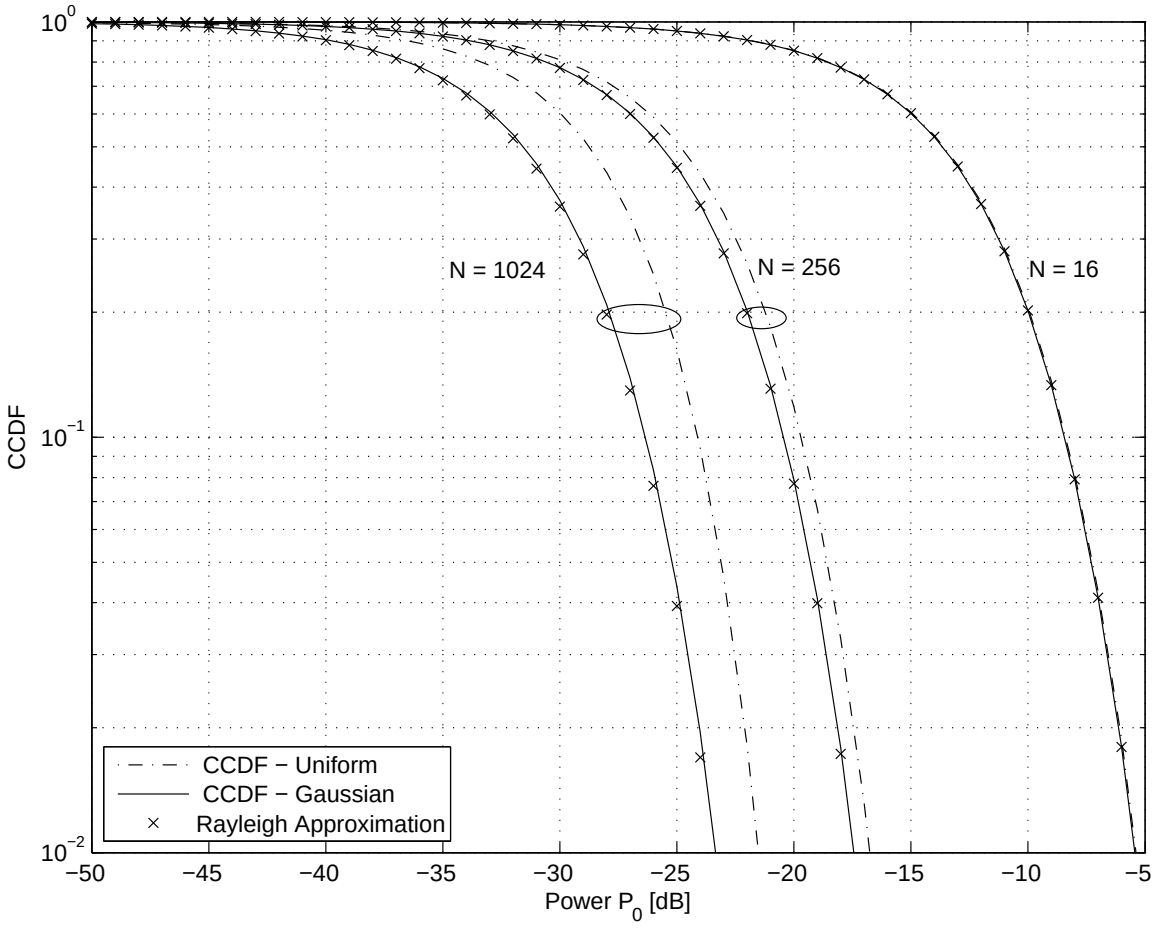

Figure 3.9. The CCDF of a sample beampattern for both uniform and Gaussian spatial distributions: $\phi = \pi/4$ and $\tilde{R} = 3\sigma = 2$.

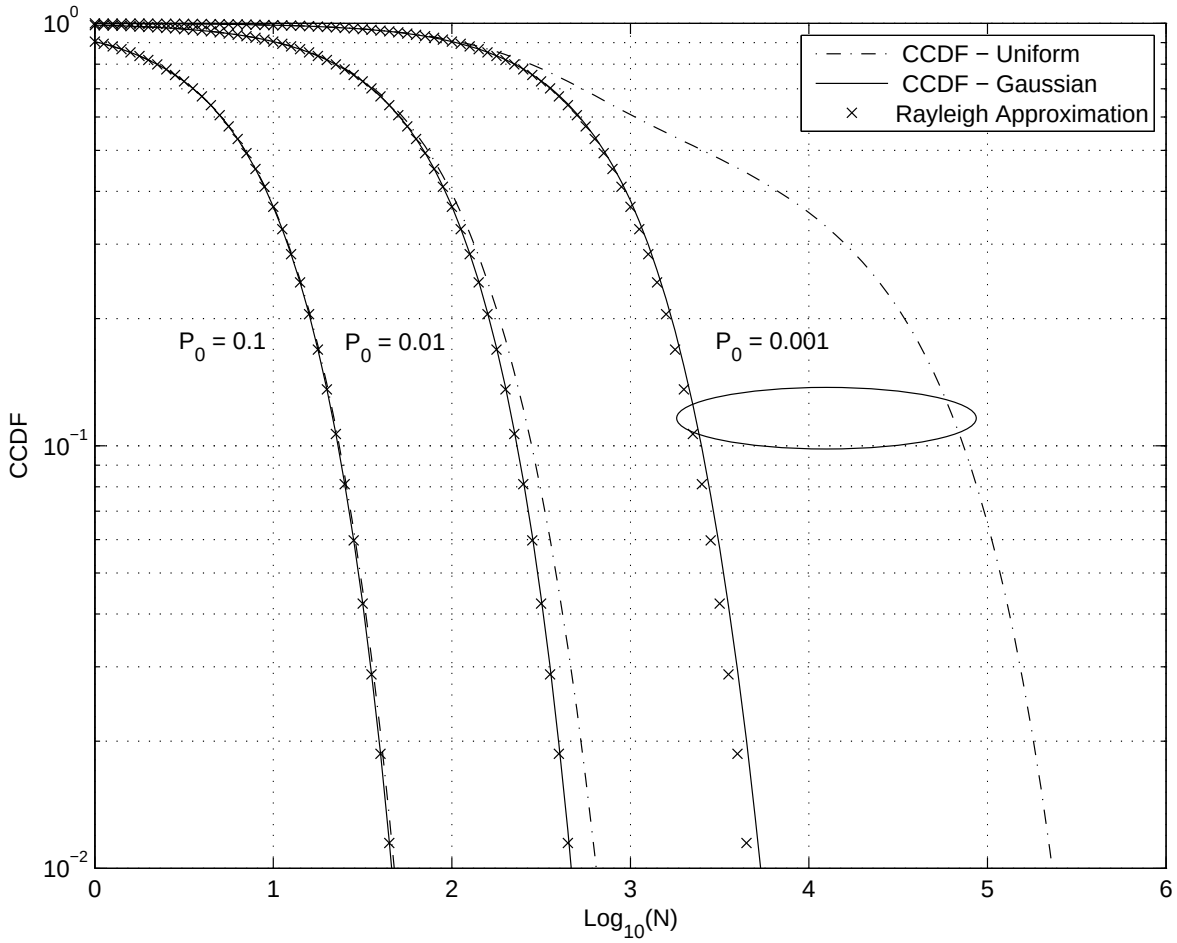

Figure 3.10. The CCDF of a sample beampattern as a function of N for both uniform and Gaussian spatial distributions: $\phi = \pi/4$ and $\tilde{R} = 3\sigma = 2$.

is equivalent to the probability of R crossing the level a in upward direction, for $a > E\{\mathsf{R}(u)\}$ [137]. There are at least as many local maxima above a as there are upward crossings of a. Therefore, the average number of local maxima above a approaches the average number of upward crossings of a. Let $U(a)$ denote the number of upward crossings by R of a given level a per unit length in the sidelobe region. Then the average number $E\{U(a)\}$ is given by [189]

$$\frac{E\{U(a)\}}{du} = \int_0^\infty \mathsf{R}' f_{\mathsf{R},\mathsf{R}'}\left(a, \mathsf{R}'\right) d\mathsf{R}' \tag{3.62}$$

where R' is the derivative of R and $f_{\mathsf{R},\mathsf{R}'}(\mathsf{R}, \mathsf{R}')$ is the joint pdf of R and R' given by [137]

$$f_{\mathsf{R},\mathsf{R}'}\left(\mathsf{R}, \mathsf{R}'\right) = \frac{\mathsf{R}}{\sqrt{2\pi\sigma_{\mathsf{X}'}^2\sigma_{\mathsf{X}}^2}} \exp\left(-\frac{\mathsf{R}^2}{2\sigma_{\mathsf{X}}^2} - \frac{\mathsf{R}'^2}{2\sigma_{\mathsf{X}'}^2}\right) \tag{3.63}$$

where $\sigma_{\mathsf{X}'}^2 = \sigma_{\mathsf{Y}'}^2$ are the variances of the derivatives of X and Y with respect to u. In order to calculate the variance $\sigma_{\mathsf{X}'}^2$, consider the autocorrelation function of X at u_1 and u_2 given by

$$\begin{aligned}
\mathbf{R}_{\mathsf{XX}}(u_1, u_2) &= E\{\mathsf{X}(u_1)\,\mathsf{X}(u_2)\} \\
&= E\{\cos(4\pi u_1 z)\cos(4\pi u_2 z)\} \\
&= \frac{1}{2}E\{\cos(4\pi(u_1+u_2)z)\} + \frac{1}{2}E\{\cos(4\pi(u_1-u_2)z)\} \\
&\approx \frac{1}{2}E\{\cos(4\pi(u_1-u_2)z)\}
\end{aligned} \tag{3.64}$$

where the first term approaches zero in the sidelobe region [14]. Let $v = u_1 - u_2$. Then we can write that

$$\mathbf{R}_{\mathsf{XX}}(v) \approx \frac{1}{2}E\{\cos(4\pi v z)\}. \tag{3.65}$$

Differentiating (3.65) with respect to v twice, we obtain

$$\begin{aligned}
\mathbf{R}''_{\mathsf{XX}}(v) &= \frac{1}{2}E\left\{-\cos(4\pi v z)(4\pi z)^2\right\} \\
&= -8\pi^2 E\left\{-\cos(4\pi v z)(4\pi z)^2\right\}
\end{aligned} \tag{3.66}$$

Setting $v = 0$, the variance $\sigma_{\mathsf{X}'}^2$ or $\sigma_{\mathsf{Y}'}^2$ can be expressed as [190]

$$\sigma_{\mathsf{X}'}^2 = \sigma_{\mathsf{Y}'}^2 = -\mathbf{R}''_{\mathsf{XX}}(0) = 8\pi^2 E\left\{z^2\right\} = 8\pi^2\sigma^2 \tag{3.67}$$

where $E\left\{z^2\right\} = \sigma^2$. Substituting $\sigma_{\mathsf{X}}^2 = 0.5$ and $\sigma_{\mathsf{X}'}^2 = 8\pi^2\sigma^2$ in (3.63), we find

$$f_{\mathsf{R},\mathsf{R}'}\left(a, \mathsf{R}'\right) = \frac{a}{2\pi\sqrt{\pi}\sigma^2} \exp\left(-a^2 - \frac{\mathsf{R}'^2}{16\pi^2\sigma^2}\right) \tag{3.68}$$

Moreover, substituting (3.68) in (3.62), the mean number of upward crossings of a given level a per unit interval du can be expressed as

$$\begin{aligned}\frac{E\{U(a)\}}{du} &= \frac{a}{2\sqrt{\pi}\pi\sigma}e^{-a^2}\int_0^\infty \mathsf{R}' e^{-\frac{\mathsf{R}'^2}{16\pi^2\sigma^2}}d\mathsf{R}' \\ &= 4\sqrt{\pi}\sigma a e^{-a^2}. \end{aligned} \tag{3.69}$$

The outage probability for the maximum sidelobe peak is the probability that at least one peak exceeds the level a, i.e.,

$$\begin{aligned}\mathrm{Pr}_{\mathrm{out}} &= \mathrm{Pr}\{U(a) \geq 1\} \\ &= \sum_{k=1}^{\infty}\mathrm{Pr}\{U(a) \geq k\} \\ &\leq \sum_{k=1}^{\infty} k\,\mathrm{Pr}\{U(a) \geq k\} \\ &= E\{U(a)\}. \end{aligned} \tag{3.70}$$

Thus, we can conclude that the outage probability is upper bounded by $E\{U(a)\}$.

Integrating (3.69) over the whole sidelobe region, we obtain that

$$\begin{aligned}\mathrm{Pr}_{\mathrm{out}} &\leq E\{U(a)\} \\ &= 2\int_{\phi_{\mathrm{Sidelobe}}}^{\pi} 4\sqrt{\pi}\sigma a e^{-a^2}du \\ &= 8\sqrt{\pi}\left(1-\sin\left(\frac{\phi_{\mathrm{Sidelobe}}}{2}\right)\right)\sigma a e^{-a^2}. \end{aligned} \tag{3.71}$$

Moreover, for low values of ϕ_{Sidelobe}, the upper bound (3.71) can be simplified as

$$\mathrm{Pr}_{\mathrm{out}} \leq 8\sqrt{\pi}\sigma\sqrt{NP_0}e^{-NP_0}, \quad NP_0 > \frac{1}{2} \tag{3.72}$$

where $a = \sqrt{NP_0}$ and $E\{\mathsf{R}(u)\} = 1/\sqrt{2}$ in the sidelobe region. The expression (3.72) shows the relationship between the probability of maximum sidelobe level P_0, the cluster size N, and the cluster area. It can be seen that increasing the cluster area results in higher outage probability, while increasing the cluster size N reduces this probability. Therefore, we can conclude that if the interference is our main concern, it is better to use small size clusters with large number of sensor nodes at each cluster.

Fig. 3.11 shows the upper bounds on the sidelobe maximum with a given outage probability for both uniform and Gaussian spatial distributions. It can be seen that for the same number of sensor nodes N and outage probability $\mathrm{Pr}_{\mathrm{out}}$, the

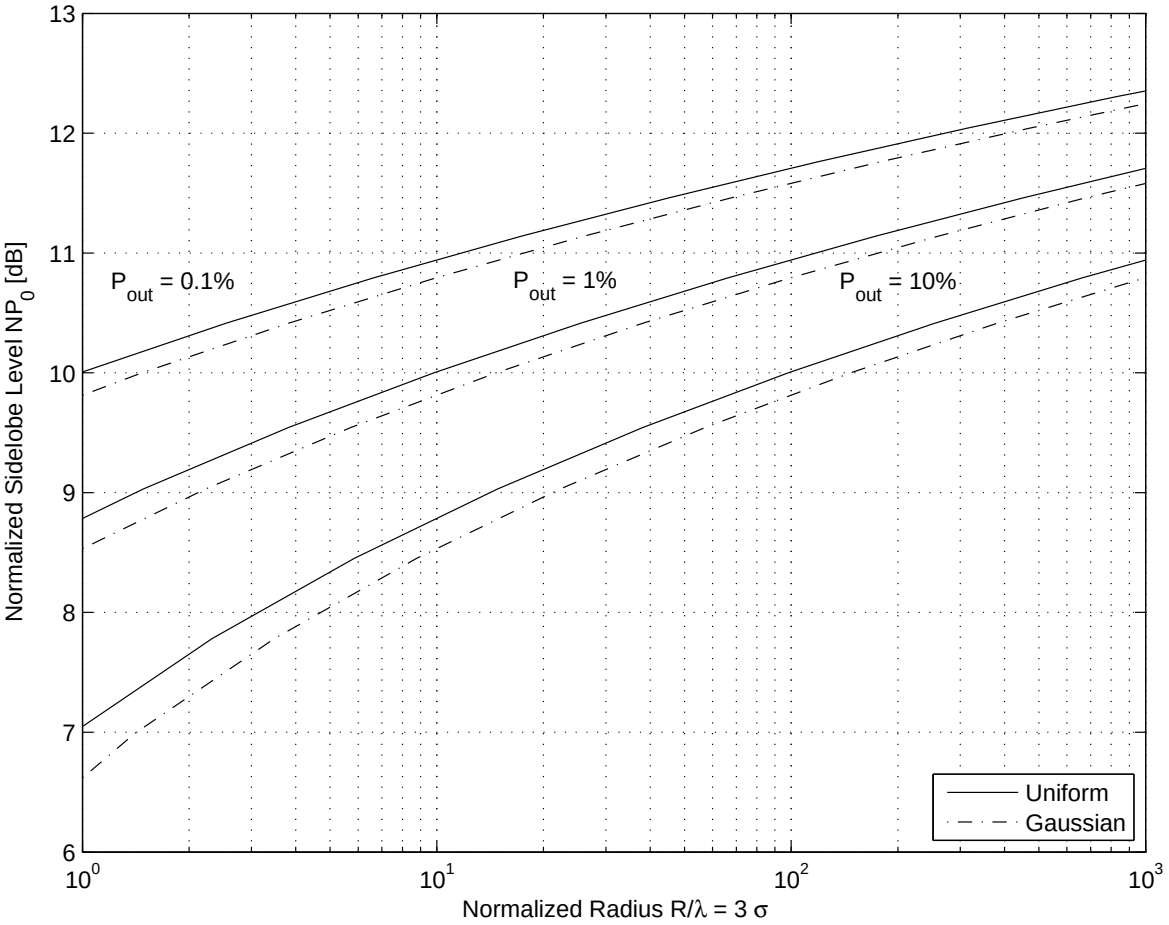

Figure 3.11. The upper bound on the sidelobe maximum with a given outage probability $\mathrm{Pr}_{\mathrm{out}}$ for both uniform and Gaussian spatial distributions: $N = 16, \tilde{R} = 3\sigma$.

level of interference to neighboring clusters is lower in the case of Gaussian spatial distribution and the value of the maximum peak in the sidelobe region increases with increasing the normalized radius $\tilde{R} = 3\sigma$.

3.5 Conclusions

Gaussian pdf has been proposed as a realistic model for sensor node spatial distribution within a cluster of WSN. The characteristics of the average beampattern have been studied and compared with corresponding characteristics in the case of uniform sensor node spatial distribution. It has been shown that for Gaussian spatial distribution, the beampattern has wider mainlobe and lower chance of large sidelobes as compared to the case of uniform spatial distribution. The outage probability achieves lower value in the case of Gaussian distribution than similar characteristics in the case of uniform distribution. Consequently, it results in smaller interference to the neighboring clusters. Although higher directivity can be achieved if sensor nodes are uniformly distributed. The directivity can be increased simply by spreading the sensor nodes over larger area, and therefore, it can be controlled only at the network deployment stage. The overall conclusion is that the CB provides better performance in terms of the characteristics, which can not be controlled at the network deployment stage, if sensor nodes are deployed according to Gaussian pdf as compared to the case of uniform pdf.

Chapter 4

Sidelobe Control in Collaborative Beamforming via Node Selection and Multi-Link Collaborative Beamforming

4.1 Introduction

Another significant concern in CB design is the uncontrolled sidelobes of the sample beampattern due to the random sensor node locations. Although it has been shown in the previous chapter that, for both uniform and Gaussian spatial distribution, the CB sample beampattern has almost-deterministic mainlobe which is similar to the average mainlobe. The sidelobes of the CB sample beampattern depend on the sensor node locations and, thus, are random [14], [89], [191]. In addition, the aforementioned cross-layer information sharing scheme of [159] results in higher sidelobes even for the average CB beampattern. High sidelobe levels can lead to unacceptable interference levels at the directions of unintended BSs/APs. Therefore, the sidelobe control problem arises for CB in the context of WSNs. Indeed, lower interference at unintended BSs/APs achieved by the sidelobe control has the potential to increase the WSN transmission rate by enabling multi-link CB.

The problem of high sidelobe levels of the average CB beampattern has been discussed in [174]. It has been suggested in [174] to use only sensor nodes placed in multiple concentric rings instead of using all nodes in the coverage area to achieve higher directivity. However, a narrower ring with larger radius results in the average beampattern with narrower mainlobe and leads to larger sidelobe peak levels in some directions. Moreover, only the average beampattern behavior is considered in [174],

while it is the sample beampattern behavior that is of practical concern for the sidelobe control in WSNs.

Due to the inherent distributed nature of WSNs, the sidelobe control has to be achieved with minimum data overhead and knowledge of the channel information. Unfortunately, traditional sidelobe control techniques developed in classical array processing [192], [193] cannot be applied in the context of WSNs due to their unacceptably high complexity and the requirement of centralized processing. Indeed, to apply the centralized beamforming weight design in the WSNs, a node or BS/AP has to collect the location and channel information from all sensor nodes and, thus, significantly increase the corresponding overhead in the network. Note that for the same reasons, the recently developed network beamforming techniques [194], [195] are restricted to the applications in the relay networks only.

In this chapter, we formulate and study the sidelobe control problem in the CB sample beampattern using node selection. It enables us to introduce the interference reduction capabilities for WSNs, which in turns, enables multi-link CB versus the single-link CB of [14] and [89]. The enabling concept for achieving sidelobe control by node selection is the randomness of the node locations in WSNs. Indeed, different combinations of sensor nodes result in beampatterns with different sidelobes. Note also that a similar technique based on random selection is used in other signal processing problems such as, for example, multiple choice sequences for OFDM [196]. Typical WSNs consist of hundreds or thousands of sensor nodes. It guarantees that a large range of sidelobe levels can be achieved by simply selecting different combinations of sensor nodes. Selecting different combinations of nodes is equivalent to assigning different beamforming weights, which are determined by node locations and corresponding channel gains. Therefore, the beamforming design boils down to selection of an acceptable combination of such weights. Thus, we develop a random node selection algorithm with low-rate feedback. As compared to the optimal beamforming weights design, our algorithm does not depend on channel gain measurements/estimates and does not suffer from the finite precision problem related to the need of communicating the channel gain to a central point. Thus, it suits well the WSN applications since it avoids complex computations and additional communications accompanied by central beamforming weight design. Note that a central point is still required for performing the scheduling functions to arrange the order of node selection for communication with the BSs/APs. Such scheduling functions

are, however, much simpler than the central beamforming weights design.

The performance of the proposed algorithm is analyzed in terms of i) the average number of trials required to select collaborative nodes, ii) the distribution of the resulting interference, and iii) the corresponding average SINR and transmission rate.

4.2 System and Signal Model

4.2.1 System Model

We consider a WSN with sensor nodes randomly placed over a plane as shown in Fig. 4.1. Multiple BSs/APs, denoted as $\mathcal{D} = \{d_0, d_1, \ldots, d_D\}$, are located outside and far apart from the coverage area of each individual node at directions $\varphi_0, \varphi_1, \ldots, \varphi_D$, respectively. Due to limited power of individual sensor nodes, direct transmission to the BSs/APs is impossible and sensor nodes have to employ CB for uplink transmission.

Uplink transmission is a burst traffic for which the nodes are idle most of the time and have sudden transmissions. Thus, a time-slotted transmission scheme, where nodes are allowed to transmit at the beginning of each time slot, can be, for example, adopted.

The downlink transmissions from different BSs/APs are only control data broadcasted over separate error-free control channels. In practice, the BSs/APs typically can be connected to each other with almost no delay communication links and can simply use one control channel. The BSs/APs can use high power transmission and, therefore, the downlink is less challenging and can be organized as direct transmission.

The distance between nodes in one cluster of WSN is small so that the power consumed for communication among sensor nodes can be neglected. Each sensor node is equipped with a single antenna used for both transmission and reception. To identify different nodes in a cluster, each node has a unique identification (ID) sequence that is included in each transmission.

At each time slot, a set $\mathcal{S} = \{s_0, s_1, \ldots, s_S\}$ of source nodes is active. However, only $K + 1$ source–destination pairs are allowed to communicate. This can be organized at the higher media access layer through scheduling or random access protocol. For example, BSs/APs can simply perform the scheduling function. Here

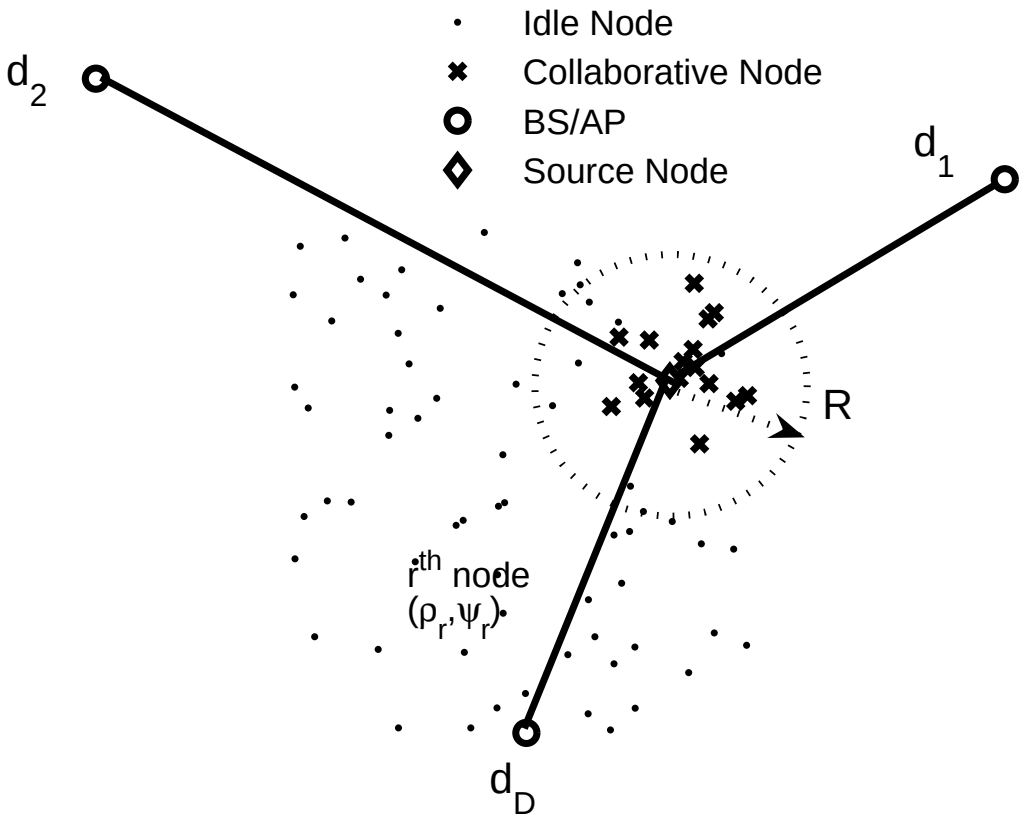

Figure 4.1. WSN model with multiple BSs/APs.

$K+1 = \min\{\text{card}(\mathcal{S}), \text{card}(\mathcal{D})\}$ where $\text{card}(\cdot)$ denotes the cardinality of a set, and the kth source–destination pair is denoted as s_k–d_k. For source node s_k, the coverage area is, ideally, a circle with a radius which depends on the power allocated for the node-to-node communication.

Let $\mathcal{M}^k$ be a set of nodes in the coverage area of the node s_k. Then the rth collaborative node, denoted as c_r, $r \in \mathcal{M}^k$, has polar coordinates (ρ_r, ϕ_r) relative, for example, to the source node s_k. The Euclidean distance between the collaborative node c_r and a point (ϱ, ϕ) in the same plane is given as

$$\begin{aligned} \delta_r(\phi) &\triangleq \sqrt{\varrho^2 + \rho_r^2 - 2\rho_r \varrho \cos(\phi - \phi_r)} \\ &\approx \varrho - \rho_r \cos(\phi - \phi_r) \end{aligned} \tag{4.1}$$

where $\varrho \gg \rho_r$ in the far-field region.

The array factor for the set of sensor nodes $\mathcal{M}^k$ in a plane can be defined as

$$\mathbb{F}^k(\phi) \triangleq \sum_{r \in \mathcal{M}^k} \sqrt{P_r} e^{j\psi_r^k} e^{-j\psi_r(\phi)} \tag{4.2}$$

where P_r is the transmit power of the rth sensor node, ψ_r^k is the initial phase of the rth sensor node's carrier when CB transmits to d_k, and $\psi_r(\phi)$ is the phase delay due to propagation at the point (ϱ, ϕ) given as

$$\psi_r(\phi) = (2\pi/\lambda)\delta_r(\phi) \tag{4.3}$$

with λ being the wavelength of the carrier.

Then the far-field beampattern corresponding to the set of sensor nodes $\mathcal{M}^k$ can be found from (4.2) as

$$\mathbb{P}^k(\phi) \triangleq \left|\mathbb{F}^k(\phi)\right|^2 = \left| \sum_{r \in \mathcal{M}^k} \sqrt{P_r} e^{j\psi_r^k} e^{-j\psi_r(\phi)} \right|^2 \tag{4.4}$$

where $|\cdot|^2$ denotes the magnitude of a complex number. The mainlobe of the beampattern is formed toward the direction of d_k while collaborative node $c_r, r \in \mathcal{M}^k$ is synchronized with the initial phase $\psi_r^k = -(2\pi/\lambda)\rho_r \cos(\varphi_k - \phi_r)$ using the knowledge of the node location. Alternatively synchronization can be performed without any knowledge of the node locations [144]– [150]. Note that the synchronization step has to be done at the network deployment stage to enable CB irrespective to whether it is the single-link CB of [14] and [89] or the multi-link CB of this chapter. Synchronization with multiple BSs/APs is a straightforward process with overhead increasing only linearly with the number of the BSs/APs.

4.2.2 Channel Model

In this chapter, we use a channel model which is more realistic than the one used in Chapter 3. Two types of fading effects attenuate the signal during propagation through wireless channels, namely, small-scale and large-scale fading. Small-scale fading, alternatively called Rayleigh fading, occurs when signal propagates in large number of multiple reflective paths and there is no LOS signal component. The envelope of the received signal at the distention is distributed according to a Rayleigh pdf. The channel gains are modeled as circularly symmetric complex Gaussian random variables with zero mean and arbitrary variance. Rayleigh fading is a widely accepted model that captures the effect of the signal reflections during propagation in the urban environments [187].

On the other hand, large-scale fading is the attenuation in the signal power due to propagation over long distances and is affected by hills, forests, buildings, etc. in the signal path. Large-scale fading has two components, the first is the path loss due to propagation distance which decays according to the nth-power law. The second is the attenuation variation about mean and it follows the log-normal distribution which represents the flactuation/shadowing effect in the channel coefficients.

In the following analysis, we consider the channel characteristics near ground in outdoor WSN applications of interest, i.e., the scenarios in which CB is needed. Sensor nodes are deployed randomly on the ground and the antenna heights are very low, so that the transmitted signals are obstructed mainly by the ground [197]. In such case, the small-scale fading can be neglected and the large-scale fading is considered to be the dominant factor for the channel attenuation. Then, the channel coefficient between collaborative nodes in $\mathcal{M}^k$ and BSs/APs can be modeled as a log-normal distributed random variable. Moreover, sensor nodes and any surrounding objects are static which suggests that the channel attenuation varies very slowly with time [197], [198]. Therefore, the channel variations over time can be neglected and the channel can be considered to be time-invariant.

The channel coefficient for rth collaborative node which serves kth source–destination pair can be modeled as

$$h_{rk} = a_{rk} b_{rk}, \tag{4.5}$$

where a_{rk} is assumed to be a lognormal distributed random variable which represents the flactuation/shadowing effect in the channel coefficient, i.e., $a_{rk} \sim \exp\{\mathcal{N}(0, \sigma^2)\}$

with σ^2 being the variance of the corresponding zero-mean Gaussian distribution, where the lognormal pdf is given as

$$f_a(a) = \frac{1}{a\sigma\sqrt{2\pi}} \exp^{-\frac{(\ln(a))^2}{2\sigma^2}} \qquad 0 \leq a < \infty. \tag{4.6}$$

The other factor b_{rk} is the attenuation/path loss effect in the channel due to propagation distance. Thus, it depends on the distance between c_r and d_k and the path loss exponent. Assuming that all nodes in $\mathcal{M}^k$ are close to each other, the pass losses from the nodes in $\mathcal{M}^k$ to the BS/AP d_k are equal to each other, i.e., $b_{rk} = b_k$, $r \in \mathcal{M}^k$ [157]. Moreover, since all BSs/APs are located far apart from the cluster of collaborative nodes, the network can be viewed as homogeneous and the attenuation effects of different paths can be assumed approximately equal to each other, i.e., $b_k = b$ [160]. Note that even if the attenuation effects for different BSs/APs are different, they can be compensated by adjusting the gains of the corresponding receivers or the power/number of the corresponding collaborative nodes participating in CB. Therefore, the channel model simplifies to

$$h_{rk} = a_{rk}. \tag{4.7}$$

4.2.3 CB and Corresponding Signal Model

Consider a two–step transmission which consists of the information sharing and the actual CB steps. Information sharing aims at broadcasting the data from one source node to all other nodes in its coverage area. Specifically, in this step, the source node s_k broadcasts the data symbol z_k to all nodes in its coverage area $\mathcal{M}^k$, where the data symbol z_k belongs to a codebook of zero mean, unit power, and independent symbols, i.e., $E\{z_k\} = 0$, $\left|z_k^2\right| = 1$, and $E\{z_k z_n\} = 0$ for $n \neq k$.

In the case of multiple source nodes, data sharing can be achieved over orthogonal channels in frequency, time, or code to avoid collisions. Note that the use of time orthogonal channels requires scheduling which can be achieved by an appropriate MAC protocol or using the BSs/APs as a central scheduler. Alternatively, the existing collision resolution schemes can be used [157], [199].

We assume that the power used for broadcasting the data by the source node is high enough so that each collaborative node c_r can successfully decode the received symbol from the source node s_k.

During the CB step, each collaborative node $c_r, r \in \mathcal{M}^k$ targeting d_k transmits the signal

$$t_r = z_k \sqrt{P_r}\, e^{j\psi_r^k}, \quad r \in \mathcal{M}^k. \tag{4.8}$$

Then the received signal at angle ϕ from all collaborative sets $\mathcal{M}^k,\ \forall k \in \{0, 1, \ldots, K\}$ can be written as

$$g(\phi) = \sum_k z_k \sum_{r \in \mathcal{M}^k} \sqrt{P_r}\, a_{rk}\, e^{j\psi_r^k}\, e^{-j\psi_r(\phi)} + w \tag{4.9}$$

where $w \sim \mathcal{CN}(0, \sigma_w^2)$ is the additive white Gaussian noise (AWGN) at the direction ϕ. The received noise power σ_w^2 at BSs/APs can be measured in the absence of data transmission and, therefore, is assumed to be known at each BS/AP.

The received signal at the BS/AP d_{k^*} can be written as

$$\begin{aligned} g_{k^*} &\triangleq g(\varphi_{k^*}) \\ &= z_{k^*} \sum_{r \in \mathcal{M}^{k^*}} \sqrt{P_r} a_{rk^*} + \sum_{k \neq k^*} z_k \sum_{r \in \mathcal{M}^k} \sqrt{P_r} a_{rk^*} e^{-j(\psi_r^{k^*} - \psi_r^k)} + w \\ &= z_{k^*} \sum_{r \in \mathcal{M}^{k^*}} \sqrt{P_r} a_{rk^*} + \sum_{k \neq k^*} z_k \sum_{r \in \mathcal{M}^k} \sqrt{P_r} a_{rk^*} \left(\mathsf{x}_r^{(k^*,k)} - j\mathsf{y}_r^{(k^*,k)} \right) + w \end{aligned} \tag{4.10}$$

where

$$\mathsf{x}_r^{(k^*,k)} = \mathcal{R}\left\{ e^{-j(\psi_r^{k^*} - \psi_r^k)} \right\} \tag{4.11}$$

and

$$\mathsf{y}_r^{(k^*,k)} = \mathcal{I}\left\{ e^{-j(\psi_r^{k^*} - \psi_r^k)} \right\}. \tag{4.12}$$

As shown in [89], the array factor has a random behavior on the sidelobe region[1] and therefore, $\mathsf{x}_r^{(k^*,k)}$ and $\mathsf{y}_r^{(k^*,k)}$ are independent random variables.

It can be further shown that $\mathsf{u} \in \left\{ \mathsf{x}_r^{(k^*,k)}, \mathsf{y}_r^{(k^*,k)} \right\}$ has the mean $m_{\mathsf{u}} = m_{\mathsf{x}_r^{(k^*,k)}} = m_{\mathsf{y}_r^{(k^*,k)}} = E\{\mathsf{u}\} = 0$ and variance $\sigma_{\mathsf{u}}^2 = \sigma_{\mathsf{x}_r^{(k^*,k)}}^2 = \sigma_{\mathsf{y}_r^{(k^*,k)}}^2 = E\left\{\mathsf{u}^2\right\} = 0.5$. Let the angles ψ_r^k and $\psi_r^{k^*}$ be uniform distributed in the interval $[-\pi, \pi]$, i.e., $\psi \sim \mathcal{U}[-\pi, \pi]$. Since the mod-$2\pi$ sum of two uniform random variables on [0,2π] is again uniform on [0,2π], it can be found that the difference $\Delta = \psi_r^k - \psi_r^{k^*}$ has uniform distribution on [0,2π]. Using the equality $u = \mathcal{R}\left\{e^{j\Delta}\right\} = \cos(\Delta)$, the distribution of $u \in \left\{ x_r^{(k^*,k)}, y_r^{(k^*,k)} \right\}$ can be found as

$$f(u) = \frac{1}{\pi\sqrt{1 - u^2}}. \tag{4.13}$$

[1]It is worth noting that in typical WSNs, there is no need to put BSs/APs close to each other and BSs/APs are well separated. Therefore, when forming a beampattern with a mainlobe towards certain BS/AP, other unintended BSs/APs will be in the sidelobe region of that beampattern.

The mean can be then easily found as $m_u = 0$ and the variance as $\sigma_u^2 = 0.5$. Similar result can be also derived for $u \triangleq \mathcal{I}\left\{e^{j\Delta}\right\} = \sin(\Delta)$ in the same way.

Moreover, the first term in (4.10) is the signal received at the BS/AP d_{k^*} from the desired set of collaborative nodes $\mathcal{M}^{k^*}$ and the second term represents the interference caused by other sets of nodes $\mathcal{M}^k, \forall k \neq k^*$ with $\mathcal{M}^k \cap \mathcal{M}^n = \varnothing$, $k \neq n$.

4.3 Sidelobe Control via Node Selection

As mentioned before, the randomness of the node locations provides additional degrees of freedom for controlling the beampattern sidelobes. Thus, to achieve desired sidelobes, it is required to select a subset of collaborative nodes from the candidate nodes in the coverage area of each source node. Node selection is performed at the network deployment stage and is repeated only when the network configuration changes. Note that the selection process can not be done during data transmission and, if needed, any BS/AP can stop the transmission for all collaborative nodes at any time to perform node selection and then continue the transmission after.

Let $\mathcal{N}^k$ be a set of collaborative nodes to be selected from $\mathcal{M}^k$, i.e., $\mathcal{N}^k \subset \mathcal{M}^k$, to beamform data symbols to d_k. We aim at assigning a set of collaborative nodes $\mathcal{N}^k \subset \mathcal{M}^k$ to each source–destination pair s_k–d_k. Note that according to [14] and [89], the mainlobe of the beampattern is stable for different subsets of $\mathcal{M}^k$ as long as the coverage area does not change and each cluster of the WSN consists of a sufficiently large number of sensor nodes.

In order to achieve a beampattern with low level sidelobes toward the unintended BSs/APs, we develop a low-complexity node selection algorithm which guarantees that the sidelobe levels at the unintended BSs/APs are below a certain prescribed value(s). Such algorithm should utilize only the knowledge of the receive interference-to-noise ratio (INR), denoted as η, at the unintended destinations and requires only low-rate (essentiality, one-bit) feedback from the unintended BSs/APs at each trial.

To select such a collaborative set, the nodes can be tested one by one or a group of nodes by a group of nodes. The latter is preferable since it can significantly reduce the data overhead in the system. Indeed, while testing one node or a group of nodes, we need to check if the corresponding CB sample beampattern sidelobe level reduces in the unintended direction(s) and then send one 'approve/reject' bit per one node in the first case, or per a group of nodes in the second case. Therefore, if every

group of nodes consists of a larger number of sensor nodes, less 'approve/reject' bits have to be sent in total. Note that the node selection is performed for one source–destination pair at a time and a schedule that arranges the source nodes order in the node selection process is maintained by the BSs/APs or a MAC protocol. Moreover, only nodes that are not assigned to any other source–destination pairs are available as candidate nodes for selection.

Consider the source node s_{k^*}, let the number of nodes in its coverage area is M, the number of collaborative nodes needed to be selected is $N \leq M$, and the size of one group of nodes to be tested in each trial is $L \leq N$. Using the selection principle highlighted above, the selection process can be organized in the following two steps.

Step 1: **Selection.** Source node s_{k^*} initiates the node selection by broadcasting the *select message* to the nodes in its coverage area, namely the set $\mathcal{M}^{k^*}$, and randomly selects a subset $\mathcal{L}^{k^*}$ of L candidate nodes from $\mathcal{M}^{k^*}$.

Nodes can be assigned to the set $\mathcal{L}^{k^*}$ by using any of the following two methods. The first one is a centralized method in which the source node s_{k^*} maintains a table of IDs of all candidate nodes in its coverage area and broadcasts the IDs of the nodes randomly assigned to the set $\mathcal{L}^{k^*}$. The disadvantage of this method is that each source node has to keep records of all other nodes in its coverage area. Moreover, this method requires extensive data exchange between the source and candidate nodes and, therefore, it is suitable only for small WSNs.

Alternatively, in the second method, node assignment task is distributed among the source and collaborative nodes. In particular, if collaborative nodes receive the *select message*, each node starts a random delay using an internal timer. After the random delay, the candidate node responds by the *offer message* which contains the ID of this node. Then the source node responds by the *approval message* which requires only 1 bit of feedback.

If a collision occurs and two collaborative nodes transmit the *offer message* at the same time, the source node responds by the *approval message* with a different bit value and the timers in both nodes start over new random delays.

The process repeats and the source node s_{k^*} keeps sending the *select message* until L candidate nodes are assigned and the set $\mathcal{L}^{k^*}$ is constructed. Assignment of $\mathcal{L}^{k^*}$ can be performed in one time-slot by setting the limits of random

timer appropriately, so that the candidate set $\mathcal{L}^{k^*}$ is ready for transmission at the beginning of the next time slot.

Step 2: **Test.** Once the candidate subset $\mathcal{L}^{k^*}$ is assigned, it transmits a *test message* containing the intended BS/AP ID at the beginning of the next time-slot to the intended destination d_{k^*} using CB. While the intended destination d_{k^*} receives a predetermined signal power level, the interference power levels at the unintended destination(s) $d_k, \forall k \neq k^*$ are random because of the random sidelobes of the CB beampattern.

At this step, all unintended BSs/APs with different IDs measure the receive INR η. If η is higher than a predetermined threshold value η_{thr}, the *reject message* is sent back to the candidate set $\mathcal{L}^{k^*}$. If multiple BSs/APs send *reject messages*, only the first *reject message* is sufficient to reject the candidate set.

Another possibility is that BSs/APs coordinate transmissions and only one *reject message* is transmitted for multiple BSs/APs. In this case, the nodes in the candidate set $\mathcal{L}^{k^*}$ are all returned to the set of nodes $\mathcal{M}^{k^*}$ and can be used in future trials.

If no *reject message* is received from any of the unintended BSs/APs after a predetermined *waiting time*, then the candidate set $\mathcal{L}^{k^*}$ is approved and each node from $\mathcal{L}^{k^*}$ stores the IDs of the source node s_{k^*} and the destination d_{k^*}.

Then the collaborative nodes assigned to serve the source–destination pair s_{k^*}–d_{k^*} do not participate in future trials. In this way, we can avoid an overlap between sets of nodes serving different BSs/APs. Note that the *waiting time* has to be set long enough so that the BSs/APs can measure the INR over longer time to assure that the INR variations are in an acceptable range.

In order to select N collaborative nodes, the Selection and Test steps are repeated until N/L candidate sets $\mathcal{L}_l^{k^*}$, $l = 1, 2, \ldots, N/L$, are approved. It is assumed for simplicity that N/L is an integer number. If N/L is not integer, it is still easy to adjust the size of the candidate set $\mathcal{L}^{k^*}$ in the last trial of the algorithm only. Then the so obtained set of approved collaborative nodes is $\mathcal{N}^{k^*} = \bigcup_l \mathcal{L}_l^{k^*}$. Once $\mathcal{N}^{k^*}$ is constructed, the source node s_{k^*} broadcasts the *end message*. The timing diagram of the node selection process is shown in Fig. 4.2 and the pseudocode of the node selection algorithm is also given in Table 1.

Node selection algorithm

Initial values:

N and L are predetermined at the Source Node s_{k^*}.

η_{thr} is predetermined at the unintended Destinations d_k, $k = \{0, 1, \ldots, D\}$.

1: At s_{k^*}: (Counter $l \leftarrow 1$).
2: **If** (Counter $l < \frac{N}{L}$),
3: **Then:** { s_{k^*} broadcasts the *select message*.
4: A candidate set $\mathcal{L}_l^{k^*}$ is constructed.
5: Using CB, the nodes in $\mathcal{L}_l^{k^*}$ transmit the *test message*.}
6: **Otherwise:** {Go to 12.}
7: At any $d_k, \forall k \neq k^*$: **If** (The receive INR $\eta > \eta_{\text{thr}}$),
8: **Then** { d_k sends the *reject message* to $\mathcal{L}_l^{k^*}$.}
9: **Else** { No *reject message* is received.
10: $\mathcal{L}_l^{k^*}$ is approved and the corresponding nodes store the IDs of s_{k^*} and d_{k^*}.
11: At s_{k^*}: (Counter $l \leftarrow$ Counter $l + 1$). **Go to** 2.}
12: s_{k^*} broadcasts the *end message*.

Table 4.1. Table 1: Node selection algorithm for CB sidelobe control.

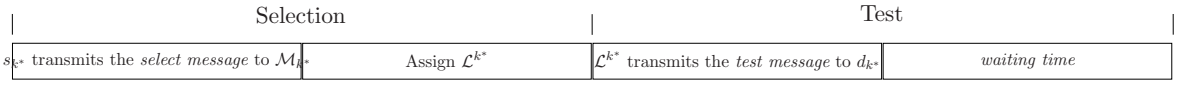

Figure 4.2. Timing diagram for node selection process.

Although the proposed node selection strategy does not guarantee the optimal result of centralized beamforming strategies (which require global knowledge of the channel information and, therefore, a very significant data overhead in the network), it has practically important advantages for WSNs since it can be run in sensor nodes with simple hardware, it is scalable and uses minimum control feedback from the unintended BSs/APs. Finally, note that once the collaborative nodes are assigned for each source node, the links between different source-destination pairs have minimum interference to each other and are independent. Then the actual data communication is a directional (unicast) transmission to a specific BSs/APs which can be straightforwardly implemented based on scheduling or any appropriate random access protocol.

4.4 Performance Analysis

In this section, we analyze the proposed node selection algorithm in terms of i) the average number of trials required for selecting a set of collaborative nodes, ii) the CCDF of the received INR η, and iii) the achievable average SINR and corresponding transmission rate. The first characteristic allows to estimate the average run time of the algorithm, while the second characteristic is needed to estimate the achievable interference levels versus the corresponding interference threshold values. The achievable average SINR and transmission rate aim at emphasizing the improvements that the multi-link CB with node selection provides as compared to the multi-link CB without node selection and single-link CB of [14] and [89].

For simplicity, but without lose of generality, we assume in our further analysis that each node in the network utilizes the same amount of power for each CB transmission, i.e., $P_r = P$, $\forall r$ in (4.10).[2]

4.4.1 Average Number of Trials

It is worth reminding that the node selection for the set $\mathcal{N}^{k^*}$ which serves the link s_{k^*}–d_{k^*} is performed for one source–destination pair at a time. We assume that the total transmit power budget for each tested candidate set of nodes is kept the same in each trial of CB transmission for any number of collaborative nodes. In particular, the power per one sensor node in $\mathcal{L}_l^{k^*}$ during the selection process has to

[2]The general case follows straightforwardly from our analysis by substituting corresponding P_r's $\forall r$.

be set as

$$P = \frac{\sigma_w^2 \gamma}{L} \tag{4.14}$$

where γ is the power budget for single CB transmission normalized to σ_w^2. Then the SNR at the intended BS/AP is

$$SNR = 10 \log_{10}(L\gamma) \quad [\mathrm{d}B] \tag{4.15}$$

where the factor L is the corresponding array gain. The power consumed for running the node selection algorithm is proportional to the average number of trials in the algorithm. Therefore, it is preferable to construct a set of collaborative nodes with less number of trials.

In order to derive the average number of trials for the node selection algorithm, we, first, need to find the probability that a candidate set of nodes $\mathcal{L}_l^{k^*}$ is approved as part of the set of collaborative nodes $\mathcal{N}^{k^*}$. This probability is the same as the probability that the set $\mathcal{L}_l^{k^*}$ generates an acceptable interference at the unintended BSs/APs. Since we assumed that only one set of collaborative nodes $\mathcal{N}^{k^*}$ is constructed at a time, there is no interference present from other candidate sets. Using (4.10), the interference power received at the unintended BS/AP d_k from the tested candidate set of nodes $\mathcal{L}_l^{k^*}$ which targets the intended BS/AP d_{k^*} can be written as

$$\begin{aligned} I\left(\varphi_k \left| \mathcal{L}_l^{k^*} \right.\right) &= \sqrt{\frac{\sigma_w^2 \gamma}{L}} z_{k^*} \sum_{r \in \mathcal{L}_l^{k^*}} a_{rk} \left(\mathsf{x}_r^{(k^*,k)} - j \mathsf{y}_r^{(k^*,k)} \right) \\ &= z_{k^*} \left(\mathsf{X}_l^{(k^*,k)} - j \mathsf{Y}_l^{(k^*,k)} \right) \end{aligned} \tag{4.16}$$

where

$$\begin{aligned} \mathsf{X}_l^{(k^*,k)} &\triangleq \sqrt{\frac{\sigma_w^2 \gamma}{L}} \sum_{r \in \mathcal{L}_l^{k^*}} a_{rk} \mathsf{x}_r^{(k^*,k)} \\ \mathsf{Y}_l^{(k^*,k)} &\triangleq \sqrt{\frac{\sigma_w^2 \gamma}{L}} \sum_{r \in \mathcal{L}_l^{k^*}} a_{rk} \mathsf{y}_r^{(k^*,k)} \end{aligned} \tag{4.17}$$

can be approximated by zero-mean Gaussian random variables with variances

$$\begin{aligned} \sigma_{\mathsf{X}}^2 &= E\left\{ \left(\mathsf{X}_l^{(k^*,k)} \right)^2 \right\} \\ &= E\left\{ \left(\sqrt{\frac{\sigma_w^2 \gamma}{L}} \sum_{r \in \mathcal{L}_l^{k^*}} a_{rk} \mathsf{x}_r^{(k^*,k)} \right)^2 \right\} \end{aligned}$$

$$
\begin{aligned}
&= \frac{\sigma_w^2\gamma}{L} E\left\{\left(\sum_{r\in\mathcal{L}_l^{k^*}} a_{rk}\mathsf{x}_r^{(k^*,k)}\right)^2\right\} \\
&= \sigma_w^2\gamma E\left\{a_{rk}^2\right\} E\left\{\left(\mathsf{x}_r^{(k^*,k)}\right)^2\right\} \qquad (4.18)
\end{aligned}
$$

The expected values in (4.18) are given by

$$
\begin{aligned}
E\left\{a_{rk}^2\right\} &= \sigma_a^2 + m_a^2 \\
E\left\{\left(\mathsf{x}_r^{(k^*,k)}\right)^2\right\} &= \sigma_u^2 \qquad (4.19)
\end{aligned}
$$

Thus, the following is valid

$$
\sigma_{\mathsf{X}}^2 = \sigma_{\mathsf{Y}}^2 = \gamma\sigma_w^2\sigma_u^2\left(\sigma_a^2 + m_a^2\right) \qquad (4.20)
$$

where m_a and σ_a^2 are the mean and variance of the lognormal distributed a_{rk} given by [200]

$$
\begin{aligned}
m_a &= e^{m+\frac{\sigma^2}{2}} \\
\sigma_a^2 &= \left(e^{\sigma^2-1}\right)e^{2m+\sigma^2} \qquad (4.21)
\end{aligned}
$$

Using (4.16) and the fact that $|z_{k^*}|^2 = 1$, the received interference power at the unintended BS/AP d_k from the candidate set of nodes $\mathcal{L}_l^{k^*}$ can be expressed as

$$
\left|I\left(\varphi_k \left| \mathcal{L}_l^{k^*}\right.\right)\right|^2 = \left(\mathsf{X}_l^{(k^*,k)}\right)^2 + \left(\mathsf{Y}_l^{(k^*,k)}\right)^2. \qquad (4.22)
$$

Then the probability that the candidate set of nodes $\mathcal{L}_l^{k^*}$ is approved to join the set of collaborative nodes $\mathcal{N}^{k^*}$, i.e., the probability that the INR η from $\mathcal{L}_l^{k^*}$ at the unintended BS/AP d_k is lower than the threshold value η_{thr}, can be found as

$$
\begin{aligned}
p' \triangleq \Pr\left\{\eta < \eta_{\text{thr}}\right\} &= \Pr\left\{\frac{\left|I(\varphi_k \left| \mathcal{L}_l^{k^*}\right.)\right|^2}{\sigma_w^2} < \eta_{\text{thr}}\right\} \\
&= \Pr\left\{\frac{\left(\mathsf{X}_l^{(k^*,k)}\right)^2 + \left(\mathsf{Y}_l^{(k^*,k)}\right)^2}{\sigma_w^2} < \eta_{\text{thr}}\right\} \\
&= 1 - \exp\left(-\frac{\eta_{\text{thr}}\sigma_w^2}{2\sigma_{\mathsf{X}}^2}\right) \qquad (4.23)
\end{aligned}
$$

where the INR

$$
\eta = \frac{\left(\mathsf{X}_l^{(k^*,k)}\right)^2 + \left(\mathsf{Y}_l^{(k^*,k)}\right)^2}{\sigma_w^2} \qquad (4.24)
$$

is the summation of the squared zero-mean Gaussian random variables each with variance σ_{X}^2 multiplied by $\frac{1}{\sigma_w^2}$. The INR η is exponentially distributed random variable with the pdf

$$f\left(\eta \;\middle|\; \frac{\sigma_w^2}{2\sigma_{\mathsf{X}}^2}\right) = \begin{cases} \frac{\sigma_w^2}{2\sigma_{\mathsf{X}}^2} \exp\left\{-\frac{\sigma_w^2 \eta}{2\sigma_{\mathsf{X}}^2}\right\}, & \eta \geq 0 \\ 0, & \eta < 0. \end{cases} \tag{4.25}$$

It is worth noting that any value of η_{thr} in the distribution range of the INR η will result in non-zero value of p'. Indeed, the interference power $\left|I\left(\varphi_k \left| \mathcal{L}_l^{k^*}\right.\right)\right|^2$ depends on the set $\mathcal{L}_l^{k^*}$. Although the number of possible combinations for constructing $\mathcal{L}_l^{k^*}$ is finite. It equals to

$$\binom{M}{L} = \frac{M!}{L!(M-L)!}, \tag{4.26}$$

which is very large number for typical WSNs consisting of hundreds or thousands of sensor nodes. For example, if 256 candidate nodes have to be selected from 512 nodes, the number of combinations is 4.7255×10^{152} each corresponding to different value of the beampattern levels. Different values of the interference power $\left|I\left(\varphi_k \left| \mathcal{L}_l^{k^*}\right.\right)\right|^2$, which correspond to different combinations of $\mathcal{L}_l^{k^*}$, cover the same range of the beampattern levels that can be achieved using L collaborative nodes. Once we set η_{thr} to a value from that achievable range of beampattern levels, the number of trials for selecting $\mathcal{N}^{k^*}$ should be finite.

It is also important to note that $\mathsf{X}_l^{(k^*,k)}$ and $\mathsf{Y}_l^{(k^*,k)}$ are defined through the independent random variables $\mathsf{x}_r^{(k^*,k)}$ and $\mathsf{y}_r^{(k^*,k)}$, respectively, and the channel gains a_{rk} which are also independent random variables for different directions $\varphi_k, \forall k \neq k^*$. Therefore, $\mathsf{X}_l^{(k^*,k)}$ and $\mathsf{Y}_l^{(k^*,k)}$ are independent random variables $\forall k \neq k^*$ and the interference levels caused by $\mathcal{L}_l^{k^*}$ at different directions $\varphi_k, \forall k \neq k^*$, $\left|I\left(\varphi_k \left| \mathcal{L}_l^{k^*}\right.\right)\right|^2$, are also independent random variables. If D unintended BSs/APs are present in the neighborhood of the set of candidate collaborative nodes $\mathcal{L}_l^{k^*}$, the probability that the INR from $\mathcal{L}_l^{k^*}$ at any one of these unintended BSs/APs is lower than the threshold value η_{thr} is given by (4.23). Therefore, the probability that $\mathcal{L}_l^{k^*}$ is approved by all BSs/APs is the product of the probabilities that $\mathcal{L}_l^{k^*}$ is approved by each of the unintended BSs/APs, that is,

$$p = \left(1 - \exp\left(-\frac{\eta_{\text{thr}}\sigma_w^2}{2\sigma_{\mathsf{X}}^2}\right)\right)^D. \tag{4.27}$$

It can be seen from (4.27) that p decreases if the threshold η_{thr} decreases or the number D of unintended BSs/APs increases.

Using (4.27), a closed-form expression for the average number of trials can be derived. Since the candidate nodes are selected randomly at each trial, the algorithm itself can be viewed as a Bernoulli process. Since $T_0 = N/L$ of these Bernoulli trials must be successful among the first T trials in order to construct $\mathcal{N}^{k^*}$, the probability distribution of the number of trials T is, in fact, negative binomial distribution [201, p. 82], that is,

$$\Pr\{T = t\} = \binom{t-1}{T_0-1} p^{T_0} (1-p)^{t-T_0}. \tag{4.28}$$

The expression for the mean of the negative binomial distribution is derived as follows. Consider an infinite sequence of independent Bernoulli trials with probability of success p. Let Z_1 denote the number of trials before the first successful trial. Then Z_1 is geometric distributed random variable $Z_1 \sim \text{Geom}(p)$, that is,

$$\Pr(Z_1 = k) = (1-p)^{k-1}p, \quad k = 1, 2, \cdots, \infty. \tag{4.29}$$

The corresponding moment generating function (MGF) for (4.29) is

$$\begin{aligned} M_{Z_1}(t) &\triangleq E\{e^{tZ_1}\} = \sum_{k=1}^{\infty} e^{tk}(1-p)^{k-1}p \\ &= pe^t \sum_{l=0}^{\infty} \left((1-p)e^t\right)^l = \frac{pe^t}{1-(1-p)e^t}. \end{aligned} \tag{4.30}$$

Therefore, the average value of Z_1 can be found as

$$\begin{aligned} E\{Z_1\} &= \frac{d}{dt} M_{Z_1}(t)\Big|_{t=0} = \frac{(1-(1-p)e^t)(pe^t) - ((p-1)e^t)(pe^t)}{(1-(1-p)e^t)^2}\Big|_{t=0} \\ &= \frac{pe^t}{(1-(1-p)e^t)^2}\Big|_{t=0} = \frac{p}{p^2} = \frac{1}{p}. \end{aligned} \tag{4.31}$$

Similarly, we can find the average number of trials between the first and second successful trials $E\{Z_2\}$, second and third successful trials $E\{Z_3\}$, and so on until the $T_0 = N/L$-th successful trial. Since $Z_1, Z_2, \cdots, Z_{T_0}$ are independent identically geometric distributed random variables, i.e., $Z_i \sim \text{Geom}(p)$, the summation $T = \sum_{i=1}^{T_0} Z_i$ is negative binomial distributed, i.e., $T = \sum_{i=1}^{T_0} Z_i \sim \text{NegBin}(T_0, p)$, with average

$$E\left\{\sum_{i=1}^{T_0} Z_i\right\} = T_0 E\{Z_i\} = \frac{T_0}{p} = \frac{N}{L \cdot p} \tag{4.32}$$

where the fact that $Z_1, Z_2, \cdots, Z_{T_0}$ are independent identically distributed is used again.

Using (4.28) and the expression for the mean of the negative binomial distribution, the average number of trials for the proposed node selection algorithm can be obtained as

$$E\{T\} = \frac{T_0}{p} = \frac{N}{L \cdot p}. \tag{4.33}$$

It can be seen from (4.33) that the average number of trials is proportional to the size of the set of collaborative nodes $\mathcal{N}^{k^*}$, but it is inverse proportional to the size of the candidate set of nodes $\mathcal{L}_l^{k^*}$ and to the probability that the set $\mathcal{L}_l^{k^*}$ is approved to join the set $\mathcal{N}^{k^*}$. Therefore, less number of trials is required in average for the proposed node selection algorithm if L is chosen to be large for a certain value of N. Moreover, if the probability p is large, then less number of trials is required.

4.4.2 CCDF of Interference

Once the collaborative nodes are assigned for each source-destination pair, the links between different source-destination pairs have minimum interference to each other and can be used independently for the multi-link CB. In this subsection, we study the CCDF of the interference occurring during simultaneous multi-link CB communications of $K+1$ different source-destination pairs.

At the intended destination d_{k^*}, other K collaborative sets that target different $d_k, \forall k \neq k^*$ destinations are interfering. These sets are $\mathcal{N}^k, \forall k \neq k^*$ and their union is denoted hereafter as $\bigcup \mathcal{N}^{k \neq k^*}$. Using (4.16), the total interference collected at the destination d_{k^*} from all K interfering collaborative sets can be expressed as

$$I\left(\varphi_{k^*} \,\middle|\, \bigcup \mathcal{N}^{k \neq k^*}\right) = \sqrt{\frac{\sigma_w^2 \gamma}{N}} \sum_{k \neq k^*} z_k \sum_{r \in \mathcal{N}^k} a_{k^* r} \left(\mathsf{x}_r^{(k^*,k)} - j\mathsf{y}_r^{(k^*,k)}\right) \tag{4.34}$$

where the power per one collaborative sensor node is $P = \sigma_w^2 \gamma / N$ in this case, and the SNR at the intended BS/AP is $10 \log_{10}(N\gamma)$ dB.

Using the fact that $\mathcal{N}^k = \bigcup \mathcal{L}_l^k$ and multiplying and dividing the right hand side of (4.34) by $\sqrt{L}$, the total interference at d_{k^*} can be expressed as

$$\begin{aligned} I\left(\varphi_{k^*} \,\middle|\, \bigcup \mathcal{N}^{k \neq k^*}\right) &= \sqrt{\frac{L}{N}} \sum_{k \neq k^*} z_k \sum_{l=1}^{N/L} \sum_{r \in \mathcal{L}_l^k} \sqrt{\frac{\sigma_w^2 \gamma}{L}} \left(a_{rk} \mathsf{x}_r^{(k^*,k)} - j a_{rk} \mathsf{y}_r^{(k^*,k)}\right) \\ &= \sqrt{\frac{L}{N}} \sum_{k \neq k^*} z_k \sum_{l=1}^{N/L} \left(\tilde{\mathsf{X}}_l^{(k^*,k)} - j\, \tilde{\mathsf{Y}}_l^{(k^*,k)}\right) \end{aligned} \tag{4.35}$$

where $\tilde{\mathsf{X}}_l^{(k^*,k)}$ and $\tilde{\mathsf{Y}}_l^{(k^*,k)}$ are zero mean truncated Gaussian distributed random variables corresponding to $\mathsf{X}_l^{(k^*,k)}$ and $\mathsf{Y}_l^{(k^*,k)}$ of (4.16) for only approved candidate subsets. It can be shown that the marginal conditional pdf of $\tilde{\mathsf{U}}_l^{(k^*,k)} \in \left\{\tilde{\mathsf{X}}_l^{(k^*,k)}, \tilde{\mathsf{Y}}_l^{(k^*,k)}\right\}$ is [202, p. 191]

$$\begin{aligned} f\left(\tilde{\mathsf{U}}_l^{(k^*,k)} \,\middle|\, \eta \leq \ \eta_{\text{thr}}\right) &= f\left(\tilde{\mathsf{U}}_l^{(k^*,k)} \,\middle|\, \left(\tilde{\mathsf{X}}_l^{(k^*,k)}\right)^2 + \left(\tilde{\mathsf{Y}}_l^{(k^*,k)}\right)^2 \leq \sigma_w^2 \eta_{\text{thr}}\right) \\ &= \frac{1}{\sqrt{2\pi\sigma_{\mathsf{X}}^2}}\left[1 - \exp\left(-\frac{\sigma_w^2\eta_{\text{thr}}}{2\sigma_{\mathsf{X}}^2}\right)\right]^{-1} \\ &\times \left[1 - 2\ \mathrm{Q}\left(\frac{\sqrt{\sigma_w^2\eta_{\text{thr}} - \left(\tilde{\mathsf{U}}_l^{(k^*,k)}\right)^2}}{\sigma_{\mathsf{X}}}\right)\right] \\ &\times \exp\left(-\frac{\left(\tilde{\mathsf{U}}_l^{(k^*,k)}\right)^2}{2\sigma_{\mathsf{X}}^2}\right), \quad |\tilde{\mathsf{U}}_l^{(k^*,k)}| \leq \sqrt{\sigma_w^2\ \eta_{\text{thr}}} \end{aligned} \tag{4.36}$$

where $\mathrm{Q}(x) = 1/\sqrt{2\pi}\int_x^\infty \exp(-u^2/2)\,du$ is the Q-function of the Gaussian distribution.

Using (4.35), the total INR at d_{k^*} can be expressed as

$$\begin{aligned} \eta &= \frac{1}{\sigma_w^2}\left|I\left(\varphi_{k^*}\left|\bigcup \mathcal{N}^{k\neq k^*}\right.\right)\right|^2 \\ &= \frac{L}{N\sigma_w^2}\sum_{k\neq k^*}\left(\left(\sum_{l=1}^{N/L}\tilde{\mathsf{X}}_l^{(k^*,k)}\right)^2 + \left(\sum_{l=1}^{N/L}\tilde{\mathsf{Y}}_l^{(k^*,k)}\right)^2\right) \\ &= \sum_{k\neq k^*}\left(\left(\sqrt{\frac{L}{N\sigma_w^2}}\sum_{l=1}^{N/L}\tilde{\mathsf{X}}_l^{(k^*,k)}\right)^2 + \left(\sqrt{\frac{L}{N\sigma_w^2}}\sum_{l=1}^{N/L}\tilde{\mathsf{Y}}_l^{(k^*,k)}\right)^2\right). \end{aligned} \tag{4.37}$$

Based on the central limit theorem, both summation terms in (4.37) corresponding to the real and imaginary parts of the INR from each set of collaborative nodes, i.e., $\sqrt{L/N\sigma_w^2}\sum_{l=1}^{N/L}\tilde{\mathsf{X}}_l^{(k^*,k)}$ and $\sqrt{L/N\sigma_w^2}\sum_{l=1}^{N/L}\tilde{\mathsf{Y}}_l^{(k^*,k)}$, are zero mean Gaussian distributed random variables with variance for both given as

$$\begin{aligned} \sigma_\Sigma^2 &= E\left\{\left(\sqrt{\frac{L}{N\sigma_w^2}}\sum_{l=1}^{N/L}\tilde{\mathsf{X}}_l^{(k^*,k)}\right)^2\right\} \\ &= E\left\{\left(\sqrt{\frac{L}{N\sigma_w^2}}\sum_{l=1}^{N/L}\tilde{\mathsf{Y}}_l^{(k^*,k)}\right)^2\right\} \\ &= \frac{\sigma_{\mathsf{X}}^2(1-(1+\beta)e^{-\beta})}{\sigma_w^2(1-e^{-\beta})} \end{aligned} \tag{4.38}$$

where $\beta = \sigma_w^2 \eta_{\text{thr}} / 2\sigma_{\mathsf{X}}^2$.

Therefore, the total INR η collected at d_{k^*} from all collaborative sets is a sum of exponentially distributed random variables (see (4.37)) and can be shown to be Erlang distributed, that is,

$$f\left(\eta \mid K, \alpha\right) = \frac{\alpha^K (\eta)^{K-1} \exp\left(-\alpha\eta\right)}{(K-1)!}, \quad \text{for } K > 0, \eta \geq 0,\ \alpha = \frac{1}{2\sigma_{\sum}^2}. \tag{4.39}$$

Finally, using (4.39), the CCDF of the INR can be expressed in closed-form as

$$\Pr\left\{\eta \geq \eta_0\right\} = \sum_{k=0}^{K-1} \frac{(\alpha\eta_0)^k e^{-\alpha\eta_0}}{k!}. \tag{4.40}$$

4.4.3 SINR and Transmission Rate

The average SINR at the intended BS/AP d_{k^*} for the proposed multi-link CB with node selection can be found as

$$\gamma_{\text{ML}}^{k^*} = \frac{E\left\{\left|\sqrt{P}\sum_{r\in\mathcal{N}^{k^*}} a_{rk^*}\right|^2\right\}}{E\left\{|I\left(\varphi_{k^*} \mid \bigcup \mathcal{N}^{k\neq k^*}\right)|^2\right\} + \sigma_w^2}. \tag{4.41}$$

Using the facts that

$$E\left\{\left|\sqrt{P}\sum_{r\in\mathcal{N}^{k^*}} a_{rk^*}\right|^2\right\} = P(N\sigma_a^2 + N^2 m_a^2) \tag{4.42}$$

and

$$E\left\{|I(\varphi_{k^*} \mid \bigcup \mathcal{N}^{k\neq k^*})|^2\right\} = 2K\sigma_I^2 \tag{4.43}$$

where the latter one follows from (4.38) with $\sigma_I^2 = \sigma_{\sum}^2 \sigma_w^2$, the average SINR (4.41) can be rewritten as

$$\begin{aligned} \gamma_{\text{ML}}^{k^*} &= \frac{P(N\sigma_a^2 + N^2 m_a^2)}{2K\sigma_I^2 + \sigma_w^2} \\ &= \frac{\gamma\sigma_w^2(\sigma_a^2 + Nm_a^2)}{2K\sigma_I^2 + \sigma_w^2}. \end{aligned} \tag{4.44}$$

Since $K+1$ source–destination links are used simultaneously, the transmission rate in bits/sec/Hz of the multi-link CB with node selection can be expressed as

$$\begin{aligned} C_{\text{ML}} &= (K+1)\log_2(1+\gamma_{ML}^{k^*}) \\ &= (K+1)\log_2\left(1 + \frac{\gamma\sigma_w^2(\sigma_a^2 + Nm_a^2)}{2K\sigma_I^2 + \sigma_w^2}\right). \end{aligned} \tag{4.45}$$

Similarly, using (4.41), the average SINR at the intended BS/AP d_{k^*} for the multi-link CB without node selection can be found as

$$\begin{aligned}\bar{\gamma}_{\mathrm{ML}}^{k^*} &= \frac{P(N\sigma_a^2 + N^2 m_a^2)}{2K\sigma_{\mathsf{X}}^2 + \sigma_w^2} \\ &= \frac{\gamma\sigma_w^2(\sigma_a^2 + Nm_a^2)}{2K\sigma_{\mathsf{X}}^2 + \sigma_w^2}\end{aligned} \tag{4.46}$$

where $E\left\{|I(\varphi_{k^*} \mid \bigcup \mathcal{N}^{k\neq k^*})|^2\right\} = 2K\sigma_{\mathsf{X}}^2$ in this case, i.e., σ_I^2 in (4.44) is substituted by σ_{X}^2 in (4.46). Then the corresponding transmission rate can be expressed as

$$C'_{\mathrm{ML}} = (K+1)\log_2\left(1 + \frac{\gamma\sigma_w^2(\sigma_a^2 + Nm_a^2)}{2K\sigma_{\mathsf{X}}^2 + \sigma_w^2}\right). \tag{4.47}$$

Finally, in the single-link CB case, the interference is not present and the SNR at the intended BS/AP d_{k^*} can be found as

$$\begin{aligned}\gamma_{\mathrm{SL}}^{k^*} &= \frac{E\left\{\left|\sqrt{P}\sum_{r\in\mathcal{M}^{k^*}} a_{rk^*}\right|^2\right\}}{\sigma_w^2} \\ &= \frac{P(M\sigma_a^2 + M^2 m_a^2)}{\sigma_w^2} \\ &= \gamma((K+1)\sigma_a^2 + (K+1)^2 N m_a^2)\end{aligned} \tag{4.48}$$

where the number of sensor nodes used in the single-link CB case is the same as the total number of sensor nodes used in all links in the multi-link CB case, i.e., for fare comparison with the multi-link CB case $M = (K+1)N$. Thus, the power per one collaborative sensor node is $P = \sigma_w^2\gamma/N$. Then the corresponding transmission rate is given as

$$C_{\mathrm{SL}} = \log_2(1 + \gamma((K+1)\sigma_a^2 + (K+1)^2 N m_a^2)). \tag{4.49}$$

It can be seen that although there is no interference for the single-link CB and better SNR that SINR in the multi-link CB can be achieved, the single-link CB transmission rate improvement over the multi-link CB is only logarithmic, while the multi-link CB transmission rate improvement over the single-link CB due to multiple links is linear. Moreover, sidelobe control via node selection achieves isolation between different links in the multi-link CB and, thus, the interference is minimized that leads to increased link transmission rate as well.

Finally, note that since the node selection has to be done at the deployment stage of WSN and repeated only when the network configuration changes, the transmission rate lose because of the overhead spent on node selection is insignificant since it is

run in a much slower time scale than the actual data transmission. Moreover, this overhead can be controlled if necessary and depends on the size of the candidate set of nodes L and the threshold η_{thr}.

4.5 Simulation Results

In this section, we aim at demonstrating the advantages of the proposed node selection algorithm for the multi-link CB beampattern sidelobe control and verifying the accuracy of the derived analytical expressions. Throughout this section the following set up is considered, unless otherwise is specified. The sensor nodes are assumed to be uniformly distributed over a disk with radius $R = 2\lambda$. The total number of sensor nodes in the coverage area of the transmitting source node is $M = 512$ and the desired number of collaborative nodes to be selected is $N = 256$. The power budget for all N collaborative nodes γ equals to 20 dB, where all power values are normalized to σ_w^2. The size of a group of candidate sensor nodes L is taken to be equal to 32 and the INR threshold value at the unintended BSs/APs is set to $\eta_{\text{thr}} = 10$ dB. The intended BS/AP is located at the direction $\varphi_0 = 0^o$ in all scenarios, while the direction to the unintended BS/AP is $\varphi_1 = 65^o$ in the scenarios with only one unintended BS/AP. In the scenarios with multiple unintended BSs/APs, the directions are defined in corresponding scenarios. Moreover, we always assume for simplicity, but without any loss of generality, that η_{thr} is the same for all BSs/APs. Indeed, the node selection is performed based on the 'accept/reject' bit from the corresponding BS/AP, that is, the threshold η_{thr} is used only at the BS/AP. Therefore, it is straightforward to use different threshold values at different BSs/APs without any change to the node selection algorithm.

4.5.1 Sample CB Beampattern

Scenario 1: In this scenario, $D = 4$ unintended BSs/APs are present and the corresponding directions are $\varphi_1 = -140^o$, $\varphi_2 = -70^o$, $\varphi_3 = 70^o$, and $\varphi_4 = 140^o$. Fig. 4.3 shows the sample beampattern corresponding to the multi-link CB with node selection and compares it to the sample beampattern corresponding to the multi-link CB without node selection and the average beampattern. It can be seen from the figure that the CB with node selection achieves the lowest sidelobes in the directions of unintended BSs/APs, while the sidelobes of the CB without node selection are uncontrolled and high in the directions of unintended BSs/APs. Moreover, Fig. 4.4

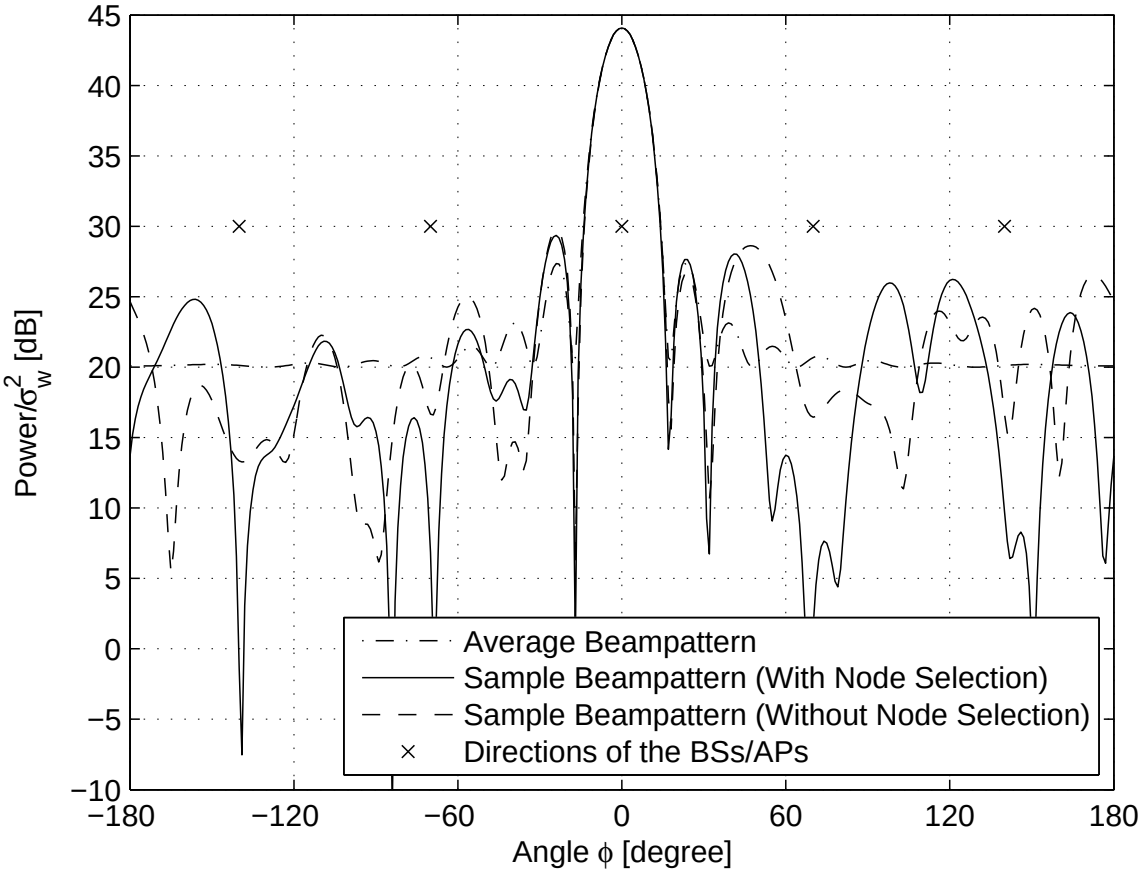

Figure 4.3. Beampattern: The intended BS/AP is located at $\varphi_0 = 0^o$ and 4 unintended BSs/APs at directions $\varphi_1 = -140^o$, $\varphi_2 = -70^o$, $\varphi_3 = 70^o$, and $\varphi_4 = 140^o$: $M = 512$, $N = 256$, $L = 32$, $\varphi_0 = 0^o$, and $\eta_{\text{thr}} = 10$ dB.

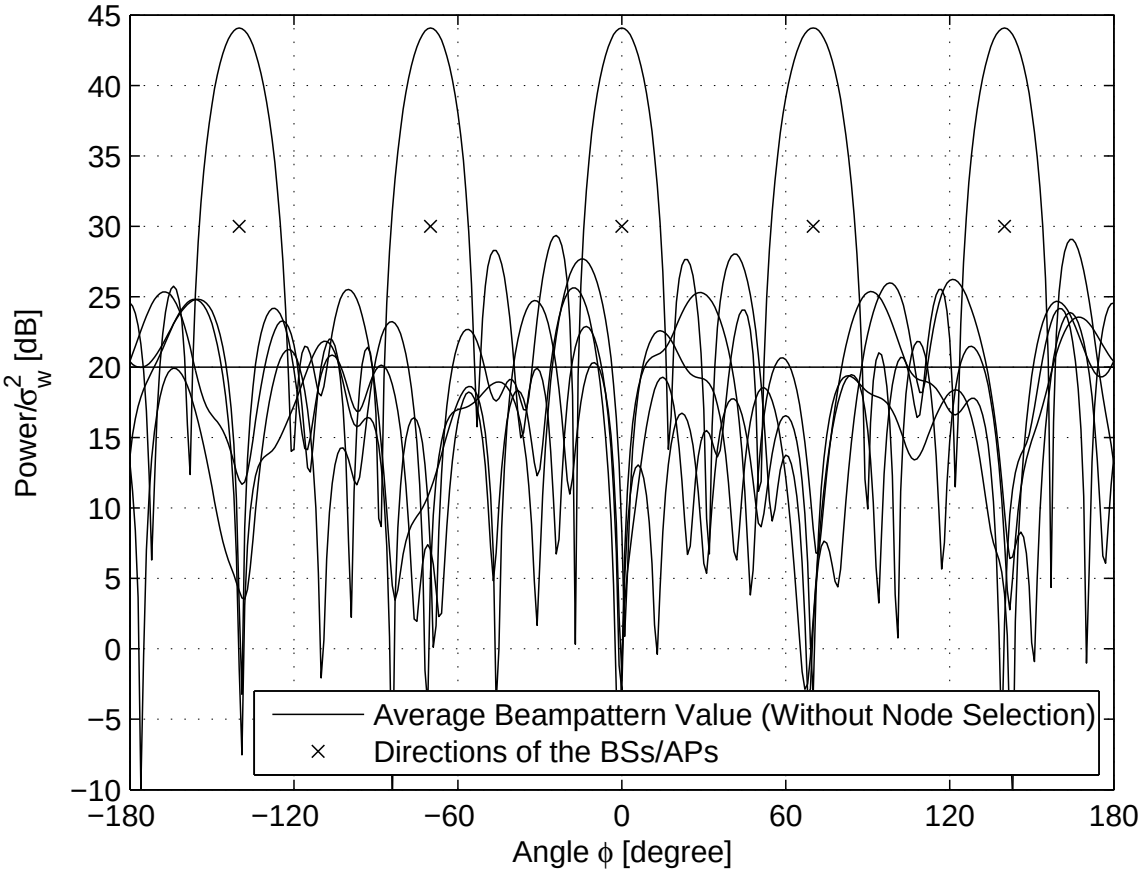

Figure 4.4. Beampattern: Multi-link beampatterns with BSs/APs at directions $\varphi_0 = 0^o$, $\varphi_1 = -140^o$, $\varphi_2 = -70^o$, $\varphi_3 = 70^o$, and $\varphi_4 = 140^o$: $M = 512$, $N = 256$, $L = 32$, and $\eta_{\text{thr}} = 10$ dB.

shows the beampatterns of the multi-link CBs with node selection for all sets of collaborative nodes. It can be seen from the figure that each beampattern has minimum interference at the directions of the mainlobes of the other beampatterns.

Scenario 2: In this scenario, it is required to limit the interference in the range $\phi \in [25^o\, 45^o]$. The beampattern of the CB with node selection and the average beampattern are shown in Fig. 4.5. It can be seen from the figure that the CB with node selection is able to achieve a beampattern with sufficiently low sidelobes over the whole range $\phi \in [25^o\, 45^o]$. Note that this case corresponds, for example, to the situation when the unintended BS/AP is actually another cluster of sensor nodes distributed over space, which, therefore, cannot be viewed as a point in space.

Scenario 3: In the last scenario, we assume that $D = 4$ unintended Bs/APs are located at the directions corresponding to the largest peaks of the average beampattern. Therefore, the locations of the unintended BSs/APs are actually the worst possible locations in terms of the corresponding average interference levels. Fig. 4.6 shows the average beampattern and the beampattern of the CB with node selection. As it can be seen from the figure, using the node selection, we can achieve minimum interference levels at the directions of unintended BSs/APs even in this case.

4.5.2 Average Number of Trials

The two parameters in the node selection algorithm are the INR threshold η_{thr} and the size L of the candidate set of nodes $\mathcal{L}^{k^*}$ for fixed N.

In this example, the INR threshold value changes in the range $\eta_{\text{thr}} = [0\, 30]$ dB. The parameters of the Gaussian distribution corresponding to the lognormal distribution of the channel coefficients are $m = 0$ and $\sigma^2 = 0.2$. Monte Carlo simulations are carried over using 1000 runs to obtain average results.

Fig. 4.7 demonstrates the effect of the threshold η_{thr} on the average number of trials required to select the set of collaborative nodes $\mathcal{N}^k$ using the sets of candidate nodes of different sizes $L \in \{16, 32, 64, 128\}$. It can be seen from the figure that the curves obtained using the closed-form expression (4.33) for the average number of trials are in good agreement with the simulation results. It can also be seen that by decreasing the threshold η_{thr}, the number of trials increases. Moreover, the number of trials for fixed N can be controlled using L. Indeed, as L increases, the number of trials decreases.

In our next example, we study the effect of the number of unintended BSs/APs

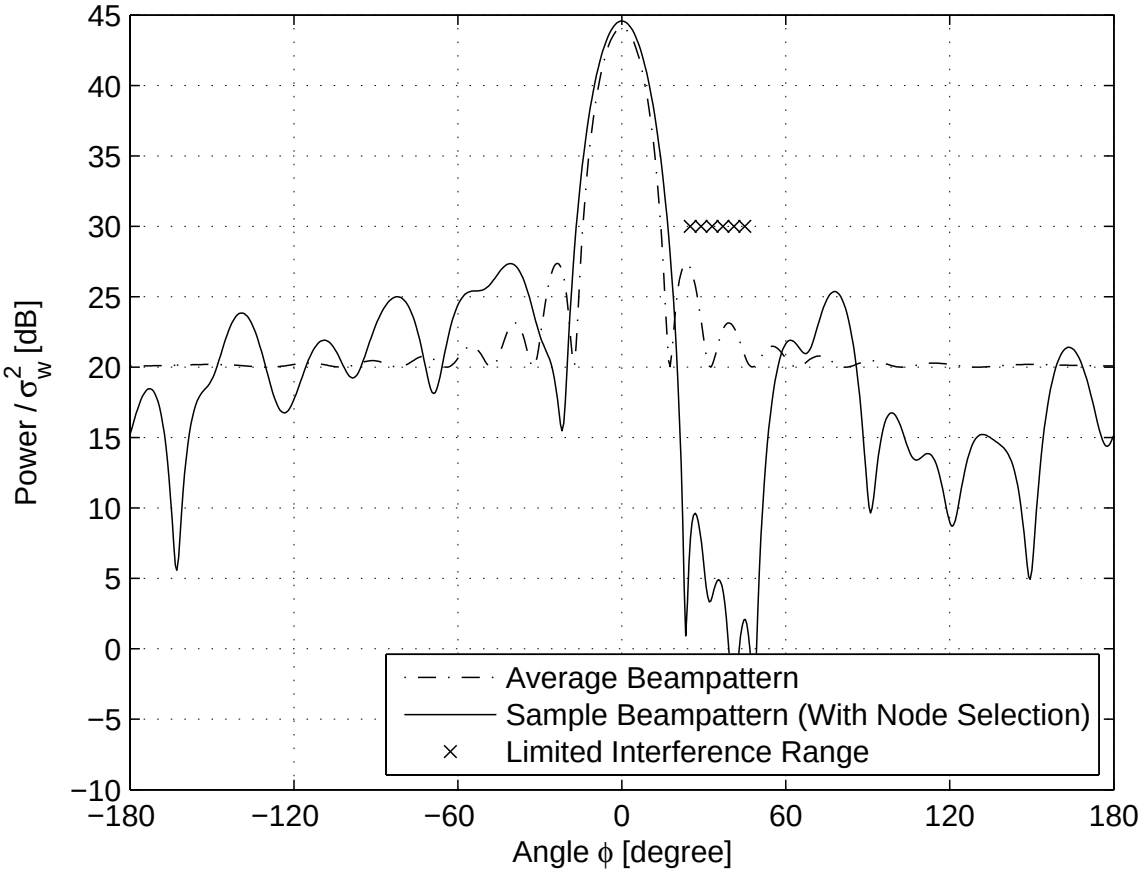

Figure 4.5. Beampattern: The interference is limited in the range $\phi \in [25^o\, 45^o]$: $M = 512$, $N = 256$, $L = 32$, $\varphi_0 = 0^o$, and $\eta_{\text{thr}} = 10$ dB.

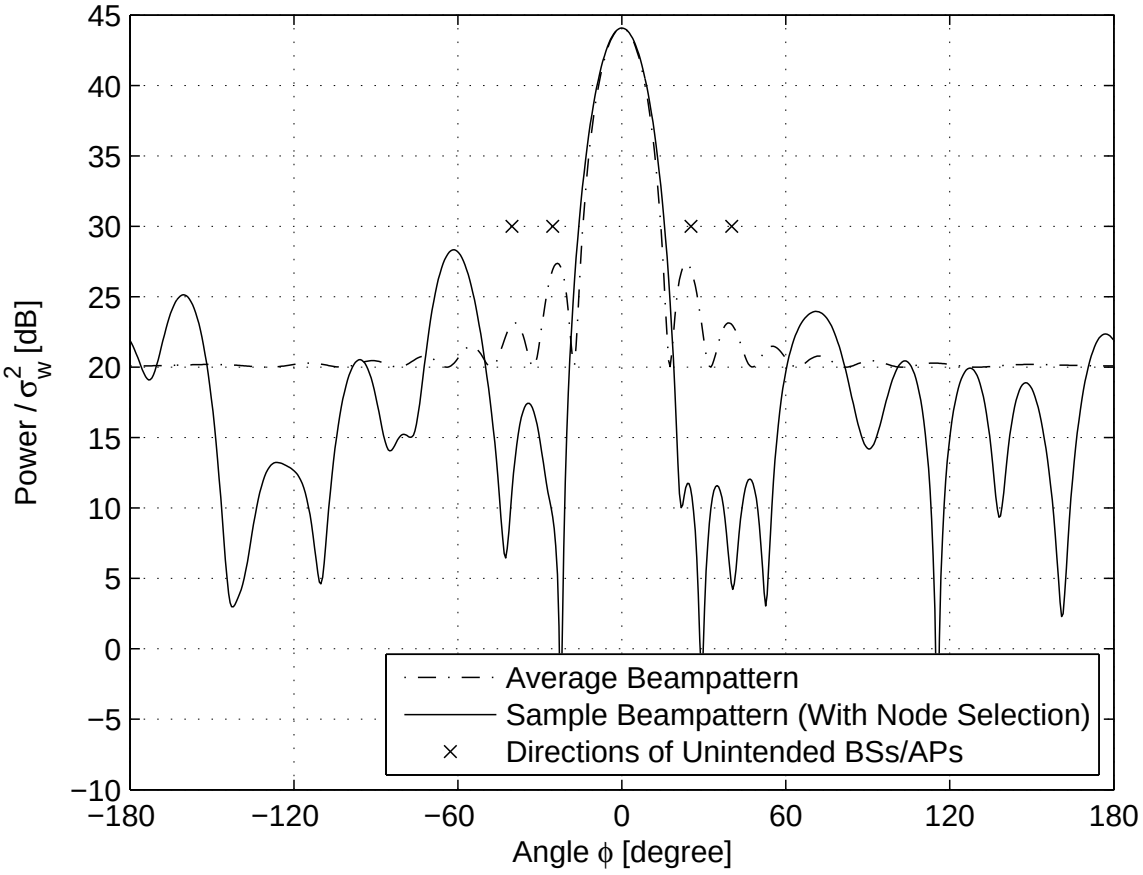

Figure 4.6. Beampattern: The unintended BSs/APs are at directions corresponding to the peaks of the average beampattern: $M = 512$, $N = 256$, $L = 32$, $\varphi_0 = 0^o$, and $\eta_{\text{thr}} = 10$ dB.

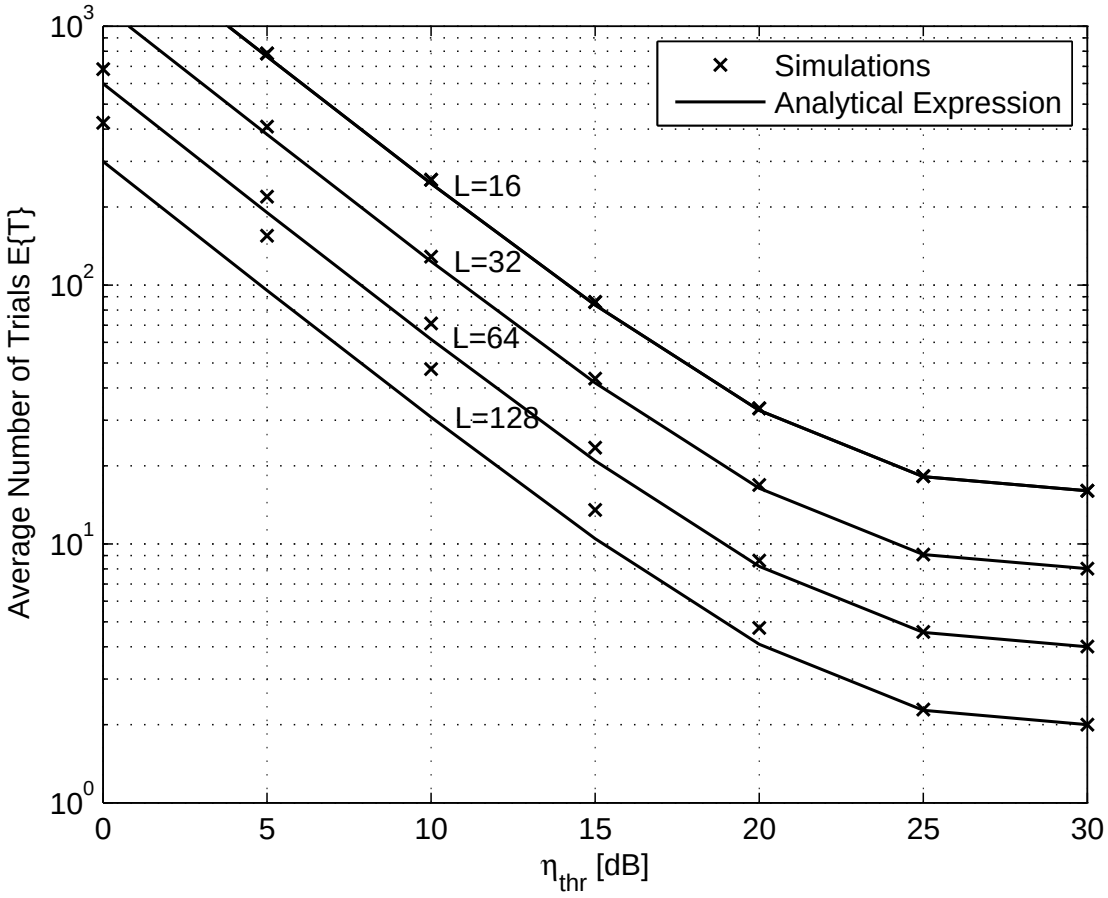

Figure 4.7. Average number of trials $E\{T\}$ versus threshold η_{thr}: $M = 512$, $N = 256$, $\varphi_0 = 0^o$, and $\varphi_1 = 65^o$.

D to the performance of the node selection algorithm.

In Fig. 4.8, the average number of trials is plotted versus the threshold η_{thr} for different values of $D \in \{1, 2, 3\}$. It can be seen from this figure that as D increases, the average number of trials of the node selection algorithm increases exponentially if the threshold η_{thr} is low. Finally, it can be observed that the analytical and simulation results are in a good agreement with each other.

4.5.3 CCDF of the Beampattern Level

Fig. 4.9 depicts the probability that the interference exceeds certain level, i.e., it shows the CCDF of interference for different values of $\eta_{\text{thr}} \in \{-5, 0, 5, 10\}$. In addition, Fig. 4.10 illustrates the CCDF of the interference for different numbers of active collaborative sets $K \in \{1, 2, 3\}$. It can be seen from Fig. 4.9 that the CCDF of the interference increases as η_{thr} decreases. Moreover, as can be observed from Fig. 4.10, the CCDF of the interference increases if K increases. The latter fact agrees with the intuition that for larger number of collaborative sets transmitting simultaneously, the overall received interference by all BSs/APs must be higher. The simulation results in both figures closely agree with our analytical results as well.

4.5.4 SINR and Transmission Rate

In Fig. 4.11, the SNR of the single-link CB (4.44) and the SINR for one link of the multi-link CB with node selection (4.46) and without node selection (4.48) are plotted versus the threshold value η_{thr} for different numbers of collaborative sets $K \in \{1, 2, 3\}$ and compared with the simulation results. Since the single-link CB does not have interference, it can be seen that it achieves higher SNR than the SINR achieved by one link of the multi-link CB. Moreover, it can be seen from this figure that the SINR of the multi-link CB with node selection increases as the threshold η_{thr} decreases. The SINR is lower for the multi-link CB if larger number of collaborative sets, $K + 1$, is transmitting simultaneously because of the increased interference. In the case of the single-link CB, larger K results in increase of M since $M = (K + 1)N$. Therefore, more collaborative nodes are available for the single-link CB with larger K and the SNR increase can be observed.

In Fig. 4.12, the corresponding total transmission rates computed according to the expressions (4.45), (4.47), and (4.49) are plotted and compared with the

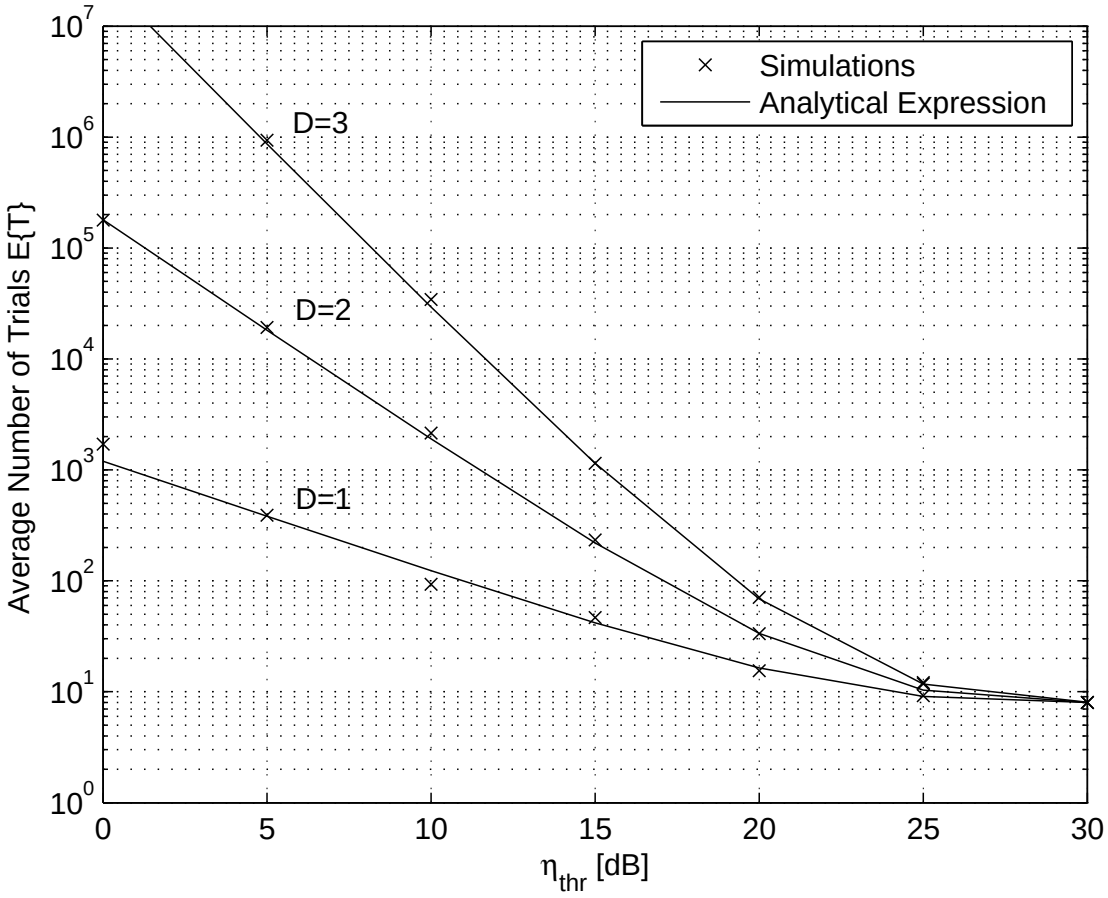

Figure 4.8. Average number of trials $E\{T\}$ versus threshold η_{thr} for different values of D: $M = 512$, $N = 256$, $L = 32$, and $\varphi_0 = 0^o$.

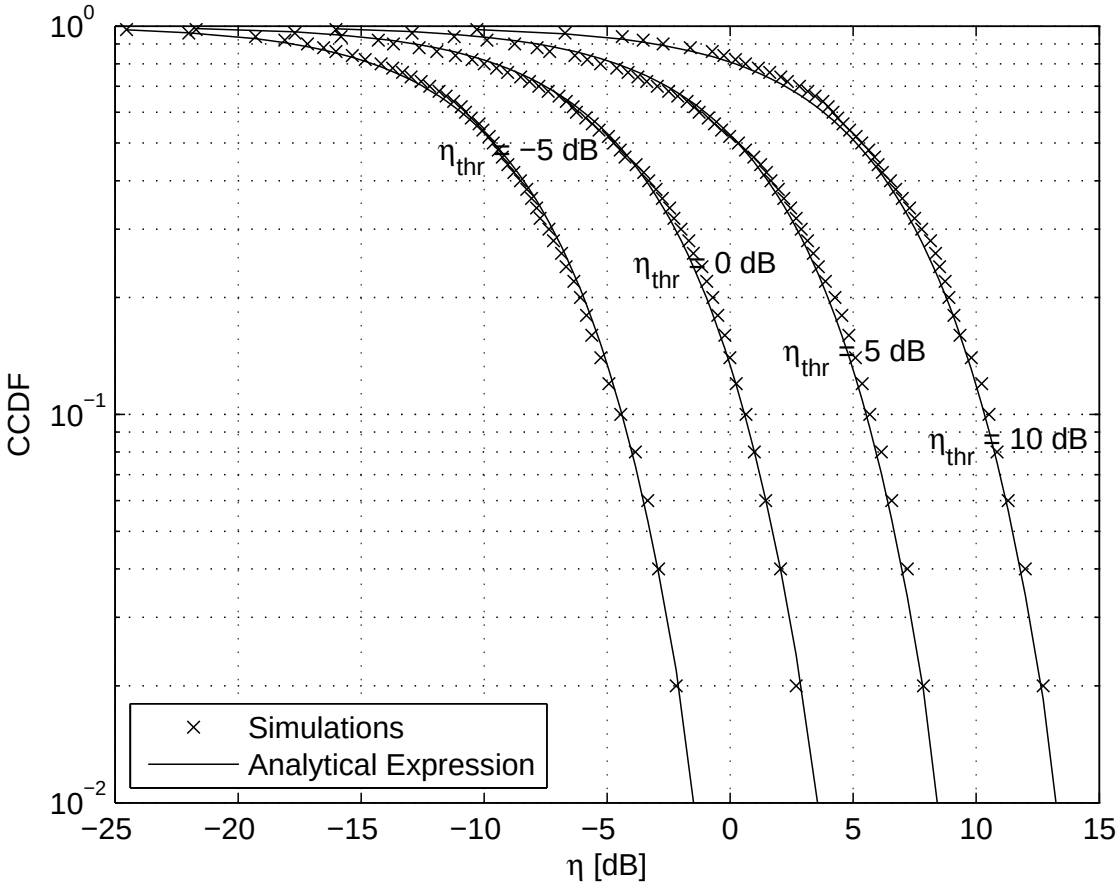

Figure 4.9. The CCDF of the INR for different values of the threshold η_{thr}: $M = 512$, $N = 256$, $L = 32$, $\varphi_0 = 0^o$, and $\varphi_1 = 65^o$.

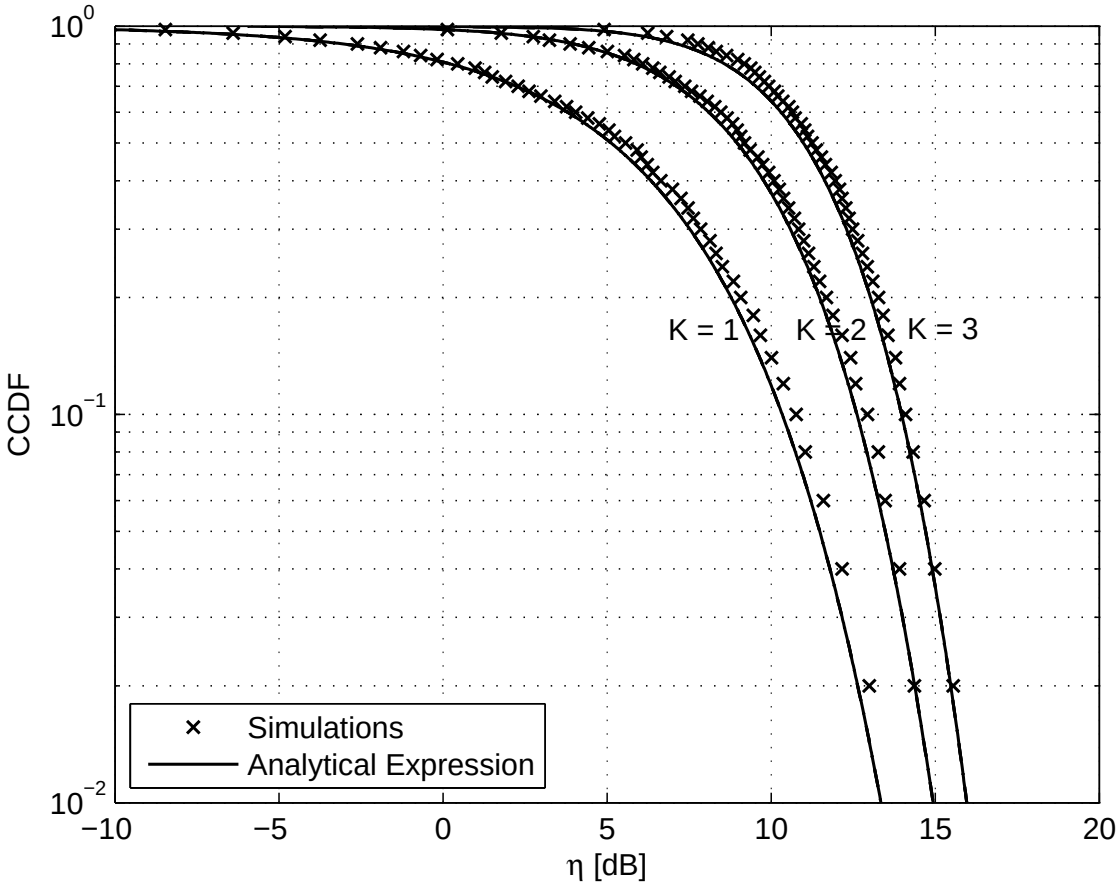

Figure 4.10. The CCDF of the INR for different values of K: $M = 512$, $N = 256$, $L = 32$, $\varphi_0 = 0^o$, and $\eta_{\text{thr}} = 10$ dB.

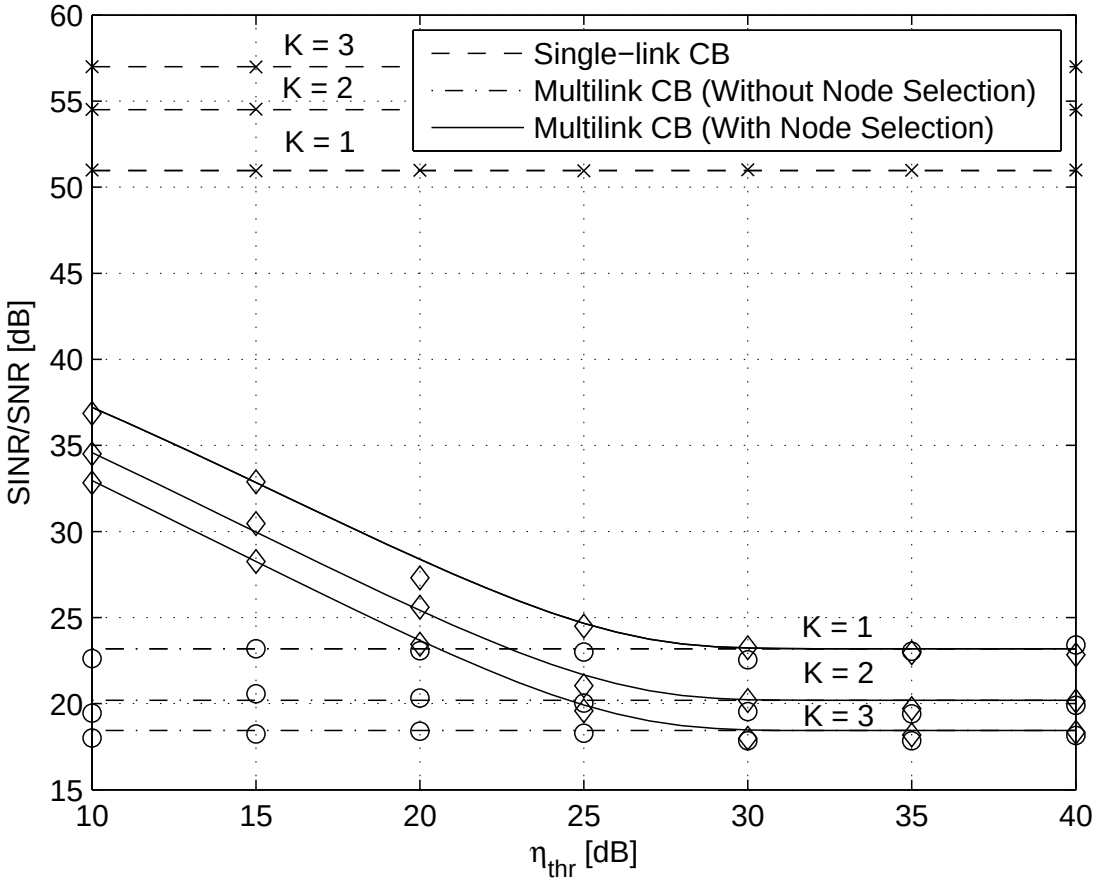

Figure 4.11. The SNR of the single-link CB and the SINR of the multi-link CBs with and without node selection for different values of K: $M = 512$, $N = 256$, $L = 32$, and $\varphi_0 = 0^o$.

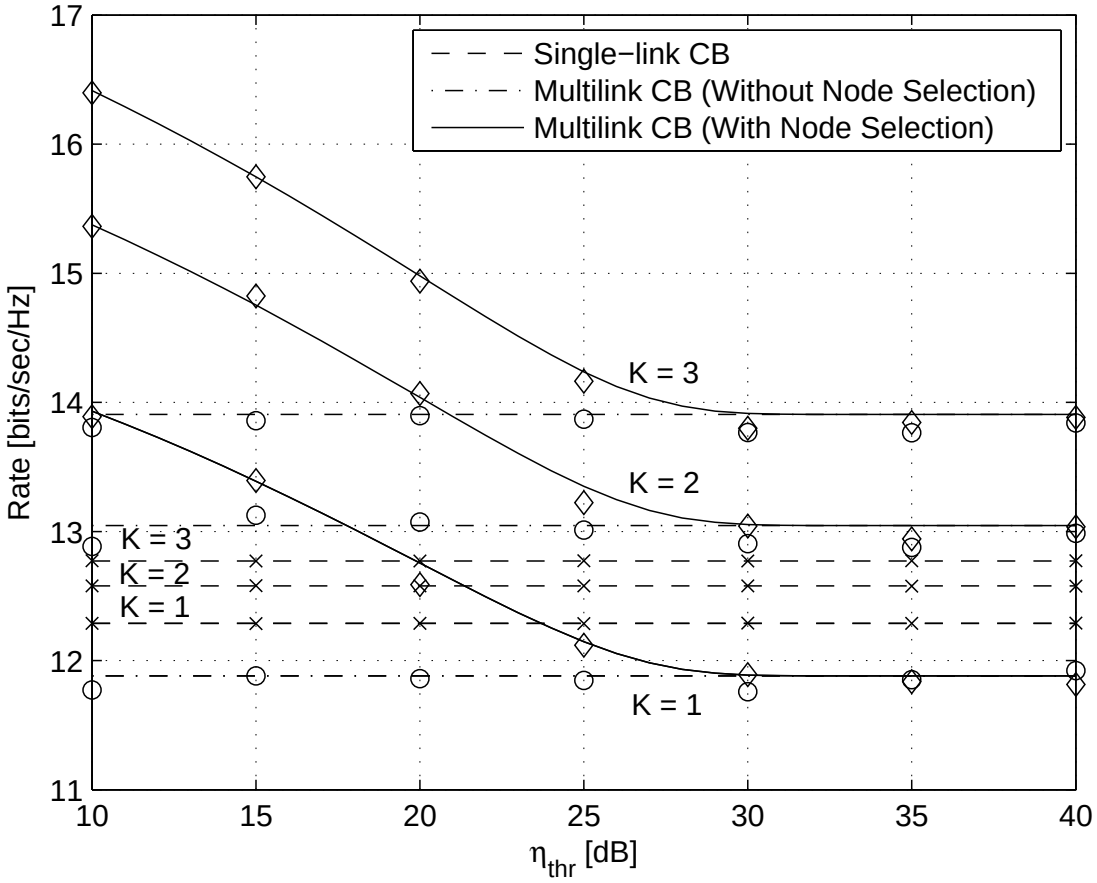

Figure 4.12. The transmission rate of the single- and multi-link CBs with and without node selection for different values of K: $M = 512$, $N = 256$, $L = 32$, and $\varphi_0 = 0^o$.

simulation results. It can be seen from this figure that for $K > 1$, the transmission rate of the multi-link CB with and without node selection is larger than that achieved by the single-link CB. Moreover, higher transmission rate can be achieved by the multi-link CB with node selection as the threshold η_{thr} decreases.

Comparing Figs. 4.7 and 4.12 to each other, we can observe a tradeoff between the average number of trials required for node selection and the achieved transmission rate. Particularly, higher transmission rate is achieved by using smaller values of η_{thr} in the multi-link CB with node selection or larger number of collaborative sets transmitting simultaneously (see Fig. 4.12). This transmission rate increase is achieved at the expense of larger number of trials in the selection algorithm (see Fig. 4.7).

4.6 Conclusions

Node selection has been introduced for the multi-link CB sidelobe control in the context WSNs and an efficient algorithm with low overhead has been developed and analyzed. The expressions for the average number of trials required for the proposed node selection algorithm and the CCDF of the interference of the multi-link CB with node selection have been derived. Moreover, the transmission rate for the multi-link CB with and without node selection has been analyzed and compared to that of the single-link CB. From both the analytical and simulation results, we have seen that the multi-link CB with node selection has perfect interference suppression capabilities as compared to the multi-link CB without node selection. It has been also shown that the transmission rate achievable by the multi-link CB with node selection is significantly higher than that of the multi-link CB without node selection and single-link CB. Although our theoretical analysis is approximate, the numerical results show close agreement with our analytical results.

Chapter 5

Power Control for Collaborative Beamforming

5.1 Introduction

Energy conservation is a critical issue in WSNs where sensor nodes are mounted with batteries of limited capacity as energy sources. Moreover, sensor nodes are usually deployed in difficult-to-access areas and their batteries can not be replaced once the WSN is deployed. Accordingly, sensor node lifetime is mainly limited by the battery lifetime.

Energy harvesting can be used as an alternative source to power sensor nodes. In this method, a harvesting device is mounted at the sensor node to extract energy from the surrounding renewable sources such as light, temperature, or vibration. Unfortunately, these sources often do not provide sufficient energy, and thus, the extracted energy from these sources is limited for the existing current technology. As a result, sensor nodes are still energy constrained and energy efficiency becomes the most critical design requirement in WSNs. It is required to reduce the consumed energy at individual sensor nodes to extend the WSN lifetime.

Another point about energy capabilities of sensor nodes is the energy consumption rate. Typical WSNs have identical nodes with sensing, data processing, and communication capabilities. However, the surrounding environment determines the priority and the load of these tasks for each sensor node. Although sensor nodes typically start with the same energy capacity once the WSN deployed, the energy consumption rate for individual sensor nodes can be very different due to the corresponding assigned tasks. As a result, different sensor nodes will have different residual energies at their batteries with progress of time. To maintain network con-

nectivity and avoid uncovered regions in WSNs, sensor nodes are required to deplete their energies over the same period.

Since increasing the energy capabilities of sensor nodes is not feasible with the current technology, prolonging the WSV lifetime is addressed in this chapter by implementing energy efficient schemes. Among different energy costs in sensor nodes, energy consumed because of communication has received considerable attention over the past few years. Wireless transmission dominates the energy consumption in sensor nodes where the RF transceiver runs radio analog circuits. Energy-efficient communication in WSNs is addressed in the network layer using multi-hop transmission. Specifically, routing techniques have been designed to minimize the overall energy consumption in WSNs [139]–[141], [203]. Some factors such as the hop length and the number of hops in multi-hop transmission are optimized to minimize the energy consumption in WSNs. Optimizing the frame sizes and coding techniques in single-hop transmission [204] and multi-hop routing [205] is also considered to increase the energy-efficiency of communication in WSNs. Additionally, scheduling techniques are proposed to balance energy consumption among sensor nodes and increase the network lifetime [206].

However, multi-hop transmission is not always the best choice for energy-efficient communication in WSNs. Generally, single-hop transmission is almost always more power efficient than multi-hop routing [84]. Moreover, the overhead of MAC and routing protocols increases for multi-hop routing as compared to single-hop transmission and this increases the associated energy consumption. Another problem with multi-hop routing is the fact that sensor nodes located close to the destination are part of the paths of many routes. Thus, these sensor nodes deplete their energy faster than other sensor nodes in the WSN.

Energy-efficient communication can be addressed in the PHY layer by implementing CB. In this technique, single-hop transmission is established using a cluster of sensor nodes. It helps to avoid the overhead of multi-hop transmission and the corresponding energy cost. Moreover, CB inherently spread the energy cost over a group of collaborative sensor nodes and achieves directional gain at the destination [207].

In conventional CB, weights are designed to cancel out the phase difference due to propagation delay and channel phase shift that helps to achieve coherent transmission. Different methods are introduced in literature to consider other factors

in designing the CB weights or improve the energy consumption pattern for CB. For example, CB weight design is proposed in [91] to maximize the received SNR at the BS/AP. In [208], sensor node scheduling is proposed for CB where the participating sensor nodes are selected in each round of transmission to balance the remaining energies at all sensor nodes. A game-theoretic model is used in [175] for power control among different WSN clusters utilizing CB for transmission. The power-saving effect of CB is studied in [207] with the assumption of free-space channels between the sensor nodes and the BS/AP.

The energy consumption behavior in CB with power control should be investigated in more details. Implementing equal power CB with sensor nodes having different energy budgets can lead to the situation when some sensor nodes drain out of energy faster than the others. In this chapter, CB with power control is exploited to prolong the overall network lifetime. A novel strategy is proposed to achieve this goal by balancing the lifetime of individual sensor nodes instead of balancing their energy consumption. Residual Energy Information (REI) available at each sensor node is utilized to adjust the transmission power of each sensor node while achieving the required average SNR at the BS/AP. The proposed algorithm requires significantly low overhead and computational complexity as compared to the centralized algorithms. However, the proposed algorithm does not guarantee globally optimum CB power control. Note that in WSNs, distributed algorithms are generally preferred over centralized protocols even when it offers only sub-optimal solutions [209]. In addition, energy consumption model is proposed for CB in WSNs to study the effect of CB power control on the network life time. Simulation results show that CB with power control outperforms equal power CB in terms of the network lifetime and the achieved SNR at the destination.

5.2 Signal and Channel Models

We consider a cluster of N sensor nodes randomly placed over a plane and one BS/AP, denoted as $\mathcal{D}$, at a point (ϱ_D, φ_D) in the same plane according to the geometrical model of Chapter 3. The distances between sensor nodes are typically much smaller than the distance between the cluster center and the BS/AP. Thus, the path losses in the channels from sensor nodes to the BS/AP due to distances are approximately the same and the pass loss effect on the channel model is not considered in the analysis. The wireless channel attenuation/fluctuation for rth col-

laborative node is modeled as a_r which is a lognormal distributed random variable, i.e., $a_r \sim \exp\{\mathcal{N}(0, \sigma^2)\}$. We also assume that sensor nodes are frequency and phase synchronized.

During the information sharing step, each sensor transmits its measurement to the other sensor nodes in the cluster using any of the information sharing techniques presented in Chapter 2. Collaborative sensor nodes use the same codebook with zero mean, unit power, and independent symbols, denoted as z, i.e., $E\{z_n\} = 0$, $|z_n 2| = 1$, and $E\{z_n z_m\} = 0$ for $n \neq m$.

During the CB step, each collaborative node $c_r, r = 1, 2, \ldots, N$, transmits the signal

$$t_r = z\ w_r\ e^{j\psi_r}, \qquad r = 1, 2, \ldots, N, \tag{5.1}$$

where $w_r e^{j\psi_r}$ is the CB weight for senor node c_r and ψ_r is the initial phase of its carrier. The real value weight amplitude w_r controls the transmission power since $P_r = w_r^2$. The Euclidean distance between the collaborative node c_r and a point (ϱ_D, ϕ) in the same plane is given as

$$\delta_r(\phi) \triangleq \sqrt{\varrho^2 + \rho_r^2 - 2\rho_r \varrho \cos(\phi - \phi_r)} \approx \varrho - \rho_r \cos(\phi - \phi_r) \tag{5.2}$$

where $\varrho \gg \rho_r$ in the far-field region. Thus, the initial phase of each sensor node carrier is set as $\psi_r = (2\pi/\lambda)\delta_r(\varphi_{\mathcal{D}})$ to achieve coherent addition at the destination $\mathcal{D}$. Then, the received signal at angle ϕ from all collaborative nodes can be written as

$$g(\phi) = z \sum_{r=1}^{N} w_r e^{j\psi_r}\ a_r\ \ e^{-j\theta_r(\phi)} + w \tag{5.3}$$

where $w \sim \mathcal{CN}(0, \sigma_w^2)$ is the AWGN at the direction ϕ.

The received signal at the BS/AP can be written as

$$y \triangleq z \sum_{r=1}^{N} w_r a_r + w \tag{5.4}$$

In the following, we refer to w_r as the CB weights for simplicity, however, the actual CB weight is $w_r e^{j\psi_r}$.

5.3 Power Control Strategy for CB

In this section, we present an energy consumption model for WSNs with focus on the energy dissipation corresponding to CB transmission. We introduce new definition

for the network lifetime for WSNs implementing CB for long distance transmission. Finally, we propose a low-complexity power control strategy that is implemented in a distributed manner and, thus, matches the constrains and requirements of WSNs. The power control strategy aims at extending the network lifetime by balancing lifetimes of individual sensor nodes. Power control for CB transmission is considered a PHY layer solution for extending the network lifetime.

5.3.1 Energy Consumption Model

A popular energy consumption model has been introduced in the literature for the communication task in sensor nodes [208], [210], [211]. This model is commonly used for the analysis of the MAC and network layer protocols designed in order to maximize the network lifetime. Other tasks such as sensing and processing are assumed to have smaller energy consumption as the energy consumed for communication [143]. The model considers the energy consumed by the RF transceiver hardware in both transmission and reception. The consumed energy in the transmitter is dissipated on the circuit electronics and the power amplifier, where most of the consumed energy goes to the power amplifier. On the other hand, the receiver does not have power amplifier and the energy is dissipated on the the circuit electronics only. Therefore, less energy is consumed during reception than during transmission.

The minimum energy consumed by the transmitter to achieve certain SNR γ, at the destination can be expressed as

$$E_{tx} = E_{tx}^{\mathrm{e}} + E^{\mathrm{a}} \tag{5.5}$$

where E_{tx}^{e} represents the energy consumption of the transmitter electronics and E^{a} is the energy consumed by the transmit power amplifier. The energy E_{tx}^{e} is consumed in the transmitter hardware, including the oscillator, frequency synthesizer, mixers, filters, baseband processing, etc. This energy is considered constant for specific hardware. However, E^{a} is the transmitted energy and it have to compensate the attenuation due to propagation distance. If free-space propagation is considered, E^{a} can be modeled as

$$E^{\mathrm{a}} = e\ d^{\alpha} \tag{5.6}$$

where e is the received energy at the destination corresponding to γ, d represents the distance over which data is being communicated, and α represents the path loss

exponent. The energy consumed at the receiver can be expressed as

$$E_{\mathrm{r}x} = E_{\mathrm{r}x}^{\mathrm{e}} \tag{5.7}$$

where $E_{\mathrm{r}x}^{\mathrm{e}}$ represents the energy consumption of the receiver electronics. Similar to $E_{\mathrm{t}x}^{\mathrm{e}}$, $E_{\mathrm{r}x}^{\mathrm{e}}$ is considered constant for specific hardware.

In the following analysis, we modify the energy consumption model to consider the energy consumed for CB transmission in WSNs. In our scenario, the destination is the BS/AP which has unconstrained power source. Thus, the energy consumed at reception $E_{\mathrm{r}x}$ is not considered here. We are interested in the effect of CB weights on the energy consumption behavior and, thus, neglect $E_{\mathrm{t}x}^{\mathrm{e}}$ in the following. Energy consumed in intra-cluster transmissions for data sharing is neglected in our analysis. The energy consumption in the power amplifier depends on the CB weight. To achieve the required SNR γ at the BS/AP, CB with power control is used for transmission and CB weight w_r is assigned for each sensor node $c_r, r = 1, 2, \ldots, N$. Hence, the transmitted power P_r^{a} from each individual sensor node is given as

$$P_r^{\mathrm{a}} = w_r^2, \qquad r = 1, 2, \ldots, N. \tag{5.8}$$

A time-slotted transmission model is considered and sensor nodes transmit data to the BS/AP over time slot t of length T seconds. The energy consumed at the power amplifier of sensor node c_r during the tth time-slot for CB transmission, denoted as e_r^t, is given by

$$e_r^t = w_r^2 \;\; T = P^{\mathrm{a}} \;\; T = E^{\mathrm{a}}, \qquad r = 1, 2, \ldots, N. \tag{5.9}$$

5.3.2 Network Lifetime

The network lifetime, denoted hereafter as T_0, has many definitions in the literature. However, the common understanding of the network lifetime is the time period until the WSN stops performing its assigned tasks [212]. The definition is, however, different from one application to another depending on the criteria according to which the network is recognized as not functional. In the context of WSNs utilizing CB for transmission, two main tasks should be performed in order for the network to be functional. First, sensor nodes are required to collect information from the surrounding environment. Second, sensor nodes are required to communicate the collected information to the far away BS/AP using CB. Thus, we define the network lifetime as the time period during which the WSN is covering the sensing field with

more than a certain percentage of sensor nodes and also is able to achieve acceptable SNR at the BS/AP.

5.3.3 Power Control Strategy

In this section, we propose a simple power control scheme for CB aiming at balancing the lifetimes of individual sensor nodes to maximize the overall network lifetime. Power control for CB should achieve the following requirements:

- The CB weights should balance the lifetime of individual sensor nodes instead of balancing the energy consumption for individual transmissions.
- It should be guaranteed that the received SNR γ at the BS/AP achieves a predetermined average value $\bar{\gamma} \triangleq E\{\gamma\}$.

Let us introduce the vector $\boldsymbol{u} = [u_1, u_2, \ldots, u_N] \in [0,1]^N$ as the normalized CB weight vector and w_{max} as the maximum CB weight. Then, the CB weight vector is $\boldsymbol{w} = [w_1, w_2, \ldots, w_N] \in [0, w_{\max}]^N$ where $w_r = w_{max}\ u_r, \quad r, 1, 2, \ldots, N$. Also, let us introduce the vector $\boldsymbol{E} = [E_1, E_2, \ldots, E_N] \in [0, E_{\max}]^N$ as the REI vector and E_{max} as the maximum energy available at each node. Note that E_{max} is bounded by the battery capacity.

To achieve the aforementioned requirements, power control is divided into two steps. Namely, the first step is to calculate a normalized CB weights based on the REI at each sensor node to balance the lifetime of individual sensor nodes. The second step is to find a scaling factor, i.e., maximum CB weight, to achieve the required average SNR $\bar{\gamma}$ at the targeted BS/AP.

To find the normalized CB weights $\boldsymbol{u}$, assume that each sensor node is able to measure its own REI $E_r, r = 1, 2, \ldots, N$. The normalized CB weight vector is designed to balance the lifetime of different sensor nodes so that we set larger CB weights to sensor nodes with larger REI. A simple choice to the normalized CB weights can be expressed as

$$u_r = \frac{E_r}{E_{\max}}, \qquad r = 1, 2, \ldots, N. \tag{5.10}$$

While the normalized weight vector $\boldsymbol{u}$ is arbitrary, the scaling factor w_{max} corresponding to arbitrary $\boldsymbol{u}$ is used to adjust the average received SNR at the BS/AP.

The average SNR $\bar{\gamma}$ at the intended BS/AP $\mathcal{D}$ can be then found as

$$\begin{aligned}\bar{\gamma} = E\{\gamma\} &= \frac{E\left\{\left|z\sum_{r=1}^{N} w_r a_r\right|^2\right\}}{\sigma_w^2} \\ &= \frac{\sum_{r=1}^{N} E\left\{w_r^2\right\} E\left\{a_r^2\right\} + \sum_{r=1}^{N}\sum_{j=1,j\neq r}^{N} E\left\{w_r\right\} E\left\{a_r\right\} E\left\{w_j\right\} E\left\{a_j\right\}}{\sigma_w^2} \\ &= \frac{w_{max}^2 N\sigma_u^2\sigma_a^2 + N(N-1)w_{max}^2 m_u^2 m_a^2}{\sigma_w^2}. \end{aligned} \tag{5.11}$$

Then, the maximum transmission CB weight corresponding to the average SNR (5.11) at the intended BS/AP can be expressed as

$$w_{max} = \sqrt{\frac{\bar{\gamma}\sigma_w^2}{N\sigma_u^2\sigma_a^2 + N(N-1)m_u^2 m_a^2}} \tag{5.12}$$

where σ_u^2 and m_u are the mean and the variance of the normalized CB weights, respectively. These mean and variance can be found from the mean m_E and variance σ_E^2 of REI as

$$\begin{aligned} m_u &= \frac{m_E}{E_{max}} \\ \sigma_u^2 &= \frac{\sigma_E^2}{E_{max}^2} \end{aligned} \tag{5.13}$$

where m_E and σ_E^2 can be obtained through consensus or distributed estimation algorithms. Note that the number of sensor nodes N in the cluster should be large enough to achieve the required SNR with $w_{max} \leq W_{max}$ where W_{max} corresponds to the maximum transmitted power specified by the sensor node transmitter rating.

Let E_r^0 to be the initial energy available at the collaborative node c_r. Then the residual energy at the sensor node c_r at the end of the t_0th transmission round is

$$E_r^{t_0} = E_r^0 - \sum_{t=1}^{t_0} e_r^t. \tag{5.14}$$

The residual energy at each sensor when the network dies, denoted as e_r^w, is given by

$$e_r^w = E_r^{T_0} = E_r^0 - \sum_{t=1}^{T_0} e_r^t. \tag{5.15}$$

Finally, the wasted energy is defined as the total unused energy in the network when it dies and it is given by

$$E_w = \sum_{r=1}^{N} e_r^w. \tag{5.16}$$

5.4 Simulation Results

In this section, numerical simulations are used to illustrate the effect of CB with power control on the network lifetime. We consider a cluster of uniformly distributed sensor nodes over a disk with radius $R = 2\lambda$. The BS/AP is located at the direction $\varphi_D = 0^o$. The total number of collaborative nodes in the cluster is $N = 256$. The required average SNR at the BS/AP $\bar{\gamma}$ is set to 20 dB and the noise power σ_w^2 is set to 0.05 W. The energies at different sensor nodes are assumed to be uniformly distributed between 0 and E_{max}, i.e., $E_r \sim \mathcal{U}[0, E_{\max}], r = 1, 2, \ldots, N$, however, other distributions can be also used. The maximum energy available at each sensor nodes E_{max} is set to 2 J and thus $m_E = 1$ J.

Equal power CB weights are used as the benchmark for comparison. In this case, the CB weights can be found as

$$w_{\max} = \sqrt{\frac{\bar{\gamma}\sigma_w^2}{N\sigma_a^2 + N(N-1)m_a^2}} \tag{5.17}$$

Each sensor node transmits in discrete values, thus quantized CB weights are used in simulation. We quantize the CB weights into 8 levels from 0 to w_{max}. The cluster of sensor nodes is considered dead when more than 90% of the sensor nodes deplete energy or the achieved SNR at the BS/AP with CB reduces by 3 dB below the nominal average value.

Fig. 5.1 shows the percentage of sensor nodes in life. It can be seen that it changes with time for both cases of equal power CB and CB with power control. As expected, the percentage of sensor nodes in life decay linearly with time in the case of equal power CB because the initial energies at sensor nodes are not equal. In the case of CB with power control, the percentage of sensor node in life is almost constant at the beginning and then drops abruptly.

Fig. 5.2 shows the received SNR at the BS/AP versus time. The SNR demonstrates similar behavior as the percentage of sensor nodes in life. For equal power CB, SNR decays linearly because the sensor nodes are lost over time linearly as well. While for CB with power control, SNR is stable over the network lifetime and drops sharply due to the the drop in the percentage of sensor nodes in life.

Fig. 5.3 shows the total available energy at all sensor nodes versus time. The network starts with total initial energy of 256 J. Then the energy decreases linearly for both cases of equal power CB and CB with power control. However, the decay

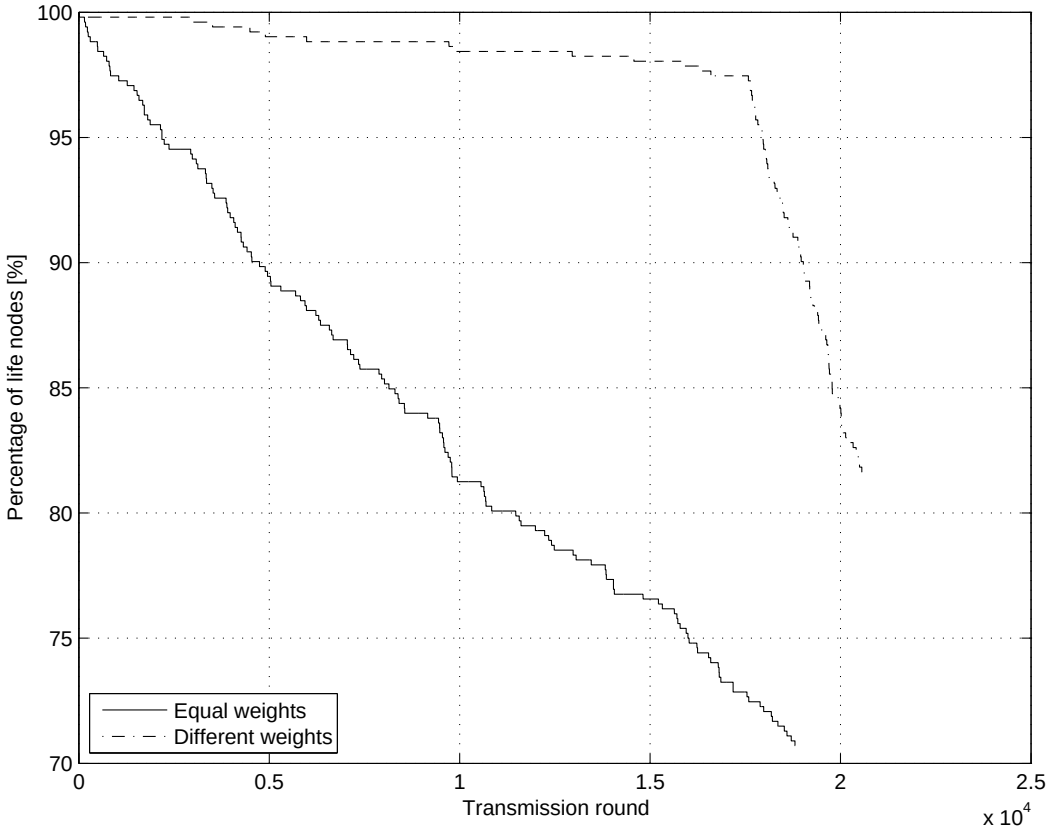

Figure 5.1. Percentage of sensor nodes in life versus time.

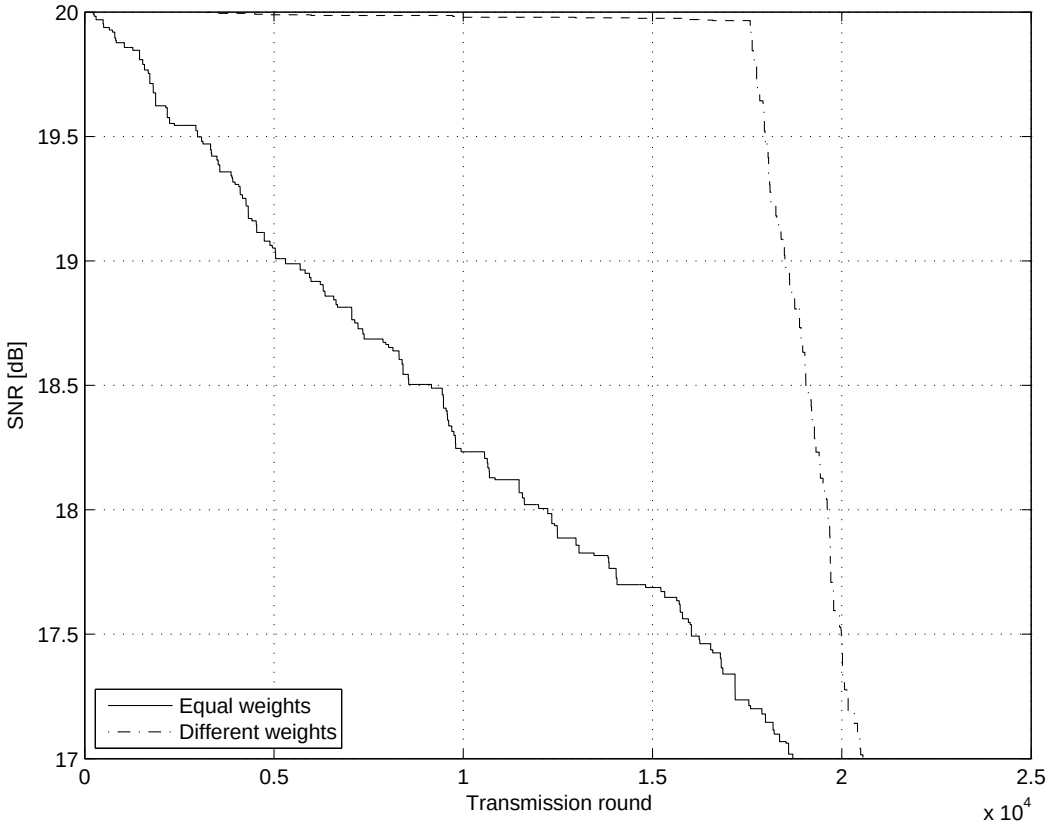

Figure 5.2. Received SNR γ at the BS/AP versus time.

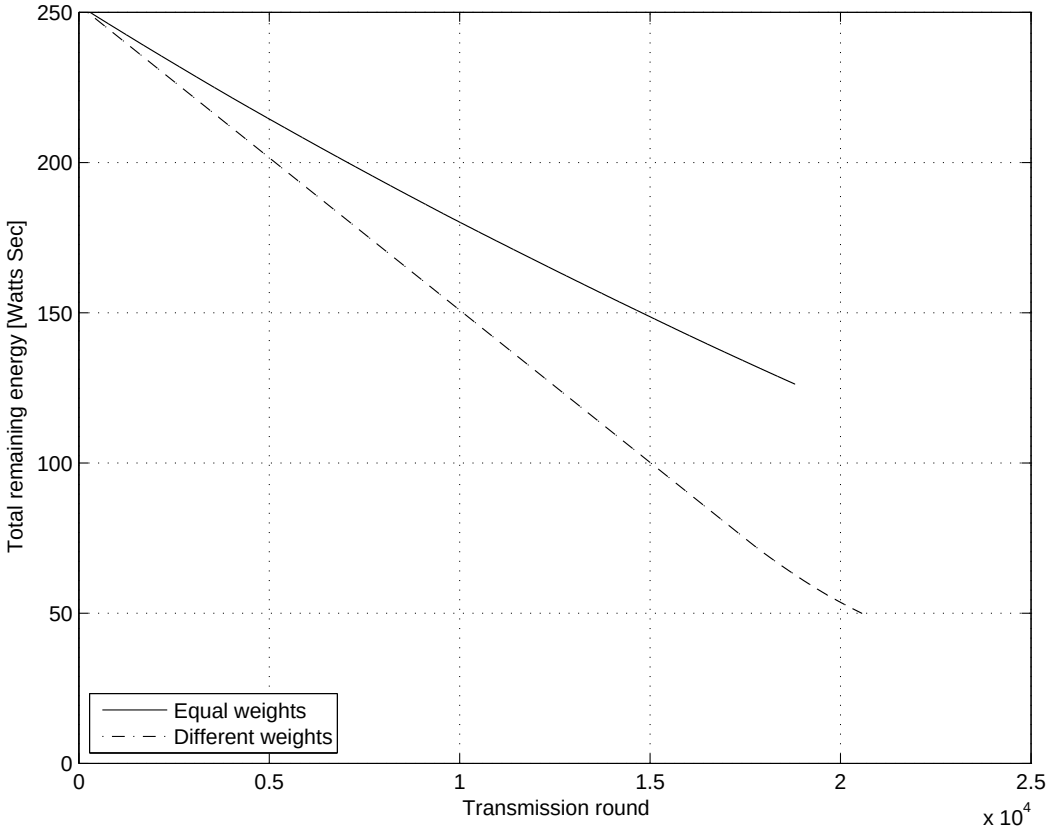

Figure 5.3. Total available energy at all sensor nodes versus time.

rate is higher for the case of CB with power control and this results in less wasted energy E_w when the network dies. It clearly demonstrates the advantage of using CB power control strategy where sensor node manage to use most of the WSN's energy. In the case of equal CB powers, most of sensor nodes die or unable to achieve acceptable SNR when still about half of WSN's initial energy is wasted.

5.5 Conclusions

We analyzed the energy consumption behavior in a cluster of sensor nodes due to CB transmission. In particular, we modeled the circuit energy consumption to target CB transmission and focus on energy dissipated at the power amplifier. Power control algorithm for CB weights is introduced as a PHY layer solution to the problem of extending the WSN lifetime. A strategy for power control that considers the remaining energy at each sensor node is proposed. Only the local energy level and the average energy available at the cluster are required for our power control strategy. While the proposed strategy is very simple, simulation results illustrate the improvements of the network lifetime due to the CB power control. More complicated and sophisticated power control strategies are expected to improve the lifetime even further. However, the implementation complexity should be taken into account in designing new schemes.

Chapter 6

Concluding Remarks and Future Work

6.1 Conclusions

This thesis addressed different aspect od CB for WSNs. Two directions related to the CB beampatten have been investigated, namely the effect of the sensor nodes spatial distribution on the CB beampattern and node selection for CB sidelobe control. Also, Power control is introduced for CB to balance the lifetime of individual sensor nodes having different energy budgets.

We have started with studying the effect of spatial distribution of sensor nodes on the CB beampattern. Gaussian spatial distribution is proposed as a realistic distribution of sensor nodes and its CB beampattern is compared with the CB beampattern of uniformly spatial distribution for sensor nodes. The average characteristics and the random behavior of the beampatter were considered. Our results show that the CB beampattern has similar characteristics for both uniform and Gaussian spatial distributions. However, Gaussian distribution have better performance than uniform distribution in terms of lower sidelobe levels. Also, it has been shown that the control of the cluster area is an effective way to control the width of the mainlobe of the CB beampattern for any spatial distribution of sensor nodes.

The results from our analysis of the CB beampattern characteristics have showed that the mainlobe is almost deterministic for arbitrary realizations of WSNs. On the other hand, the sidelobes of CB beampattern are random and depend mainly on the sensor node locations. To achieve more controlled CB beampattern, sidelobe control using node selection has been introduced in CB. Node selection algorithm with low feedback overhead was introduced to reduce the interference at directions of

unintended BSs/APs. The proposed node selection algorithm has showed promising results for sidelobe control. Moreover, multi-link CB with sidelobe control is utilized to increase the transmission rate compared to the conventional single-link CB.

Finally, power control is introduced for CB to prolong the WSN lifetime. The proposed power control strategy utilized the REI available at each sensor node to balance the lifetime of individual sensor nodes while achieving the required SNR at the destination. It has been shown that even simple power control strategy is able to balance the remaining energy available at individual sensor nodes and prolong the network lifetime.

6.2 Proposed Future Work

Many research directions and open problems need to be investigated to reach practical implementation for CB in WSNs.

Multi-link CB provides new strategy for data transmission in WSNs. It has been shown that higher SINR and increased data rates are achieved with multi-link CB utilizing sidelobe control. However, our analysis considered the PHY layer only, specifically reducing the cross interference among different links using sidelobe control. To implement Multi-link CB, it is required to investigate the associated algorithms in the MAC and network layers. Clustering techniques should be specifically designed to assign sensor nodes to different collaborative groups utilizing CB.

Energy-efficient transmission is the main motivation to implement CB in WSNs, however, some research still need to be done to even improve the energy consumption behavior of sensor nodes. A more realistic energy consumption model for sensor nodes that considers energy consumption in the sensing and processing tasks should be proposed.

Also, the proposed power control strategy in this thesis is considered a starting point to investigate the potential advantages of power control for CB. It is expected to find a tradeoff between the network lifetime and the complexity of the power control algorithm. Moreover, sensor node scheduling and the estimated CSI at the sensor node can also be considered in designing power control algorithms for CB.

Bibliography

[1] J. Yick, B. Mukherjee, and D. Ghosal, "Wireless sensor network survey," *Computer Networks*, vol. 52, pp. 2292–2330, August 2008.

[2] I. F. Akyildiz, W. Su, Y. Sankarasubramaniam, and E. Cayirci, "Wireless sensor networks: a survey," *Computer Networks*, vol. 38, no. 4, pp. 393 – 422, 2002.

[3] ——, "A survey on sensor networks," *IEEE Communications Magazine*, vol. 40, no. 8, pp. 102–114, Aug. 2002.

[4] C.-Y. Chong and S. Kumar, "Sensor networks: Evolution, opportunities, and challenges," *Proceedings of the IEEE*, vol. 91, no. 8, pp. 1247 – 1256, 2003.

[5] D. Puccinelli and M. Haenggi, "Wireless sensor networks: Applications and challenges of ubiquitous sensing," *IEEE Circuits and Systems Magazine*, vol. 5, no. 3, pp. 19–31, 2005.

[6] A. Flammini, P. Ferrari, D. Marioli, E. Sisinni, and A. Taroni, "Wired and wireless sensor networks for industrial applications," *Microelectronics Journal*, vol. 40, no. 9, pp. 1322 – 1336, 2009.

[7] H. Wang, D. Estrin, and L. Girod, "Preprocessing in a tiered sensor network for habitat monitoring," *EURASIP Journal on Applied Signal Processing*, vol. 2003, pp. 392–401, January 2003.

[8] A. Giridhar and P. Kumar, "Toward a theory of in-network computation in wireless sensor networks," *IEEE Communications Magazine*, vol. 44, no. 4, pp. 98 – 107, 2006.

[9] M. Wang, J. Cao, B. Chen, Y. Xu, and J. Li, "Distributed processing in wireless sensor networks for structural health monitoring," in *Ubiquitous Intelligence and Computing*, ser. Lecture Notes in Computer Science, 2007, vol. 4611, pp. 103–112.

[10] S. Pileggi, C. Palau, and M. Esteve, "Multimode wsn: Improving robustness, fault tolerance and performance of randomly deployed wireless sensor network," in *Second International Conference on Computational Intelligence, Communication Systems and Networks, 2010, CICSyN'10*, 2010, pp. 112 –117.

[11] H. Alwan and A. Agarwal, "A survey on fault tolerant routing techniques in wireless sensor networks," in *Third International Conference on Sensor Technologies and Applications, 2009, SENSORCOMM '09*, 2009, pp. 366 – 371.

[12] T. Nieberg, S. Dulman, P. Havinga, L. Hoesel, and J. Wu, "Collaborative algorithms for communication in wireless sensor networks," in *Ambient Intelligence: Impact on Embedded Sytem Design*, 2004, pp. 271–294.

[13] S. K. Singh, M. Singh, and D. Singh, "Routing protocols in wireless sensor networks a survey," *International Journal of Computer Science and Engineering Survey (IJCSES)*, vol. 1, no. 2, pp. 63–83, 2010.

[14] H. Ochiai, P. Mitran, H. V. Poor, and V. Tarokh, "Collaborative beamforming for distributed wireless ad hoc sensor networks," *IEEE Trans. on Signal Processing*, vol. 53, no. 11, pp. 4110–4124, Nov. 2005.

[15] R. Mudumbai, G. Barriac, and U. Madhow, "On the feasibility of distributed beamforming in wireless networks," *IEEE Trans. Wireless Communications*, vol. 6, no. 5, pp. 1754–1763, May 2007.

[16] D. Culler, D. Estrin, and M. Srivastava, "Overview of sensor networks," *Computer*, vol. 37, no. 8, pp. 41–49, Aug. 2004.

[17] Y. Yu, V. K. Prasanna, and B. Krishnamachari, *Information Processing and Routing in Wireless Sensor Networks*. River Edge, NJ: World Scientific Publishing Co., Inc., 2007.

[18] D. Estrin, L. Girod, G. Pottie, and M. Srivastava, "Instrumenting the world with wireless sensor networks," in *IEEE International Conference on Acoustics, Speech, and Signal Processing, 2001, ICASSP '01*, 2001.

[19] M. Tubaishat and S. Madria, "Sensor networks: An overview," *IEEE Potentials*, vol. 22, no. 2, pp. 20–23, 2003.

[20] D. Cook and S. Das, *Smart Environments: Technology, protocols and applications*. Wiley-Interscience, 2004.

[21] C.-C. Shen, W. Plishker, S. Bhattacharyya, and N. Goldsman, "An energy-driven design methodology for distributing dsp applications across wireless sensor networks," in *28th IEEE International Real-Time Systems Symposium, 2007, RTSS 2007*, 2007, pp. 214 –226.

[22] R. Kumar, V. Tsiatsis, and M. B. Srivastava, "Computation hierarchy for in-network processing," in *2nd ACM international conference on Wireless sensor networks and applications 2003, WSNA '03*, 2003, pp. 68–77.

[23] M. Singh and V. K. Prasanna, "A hierarchical model for distributed collaborative computation in wireless sensor networks," *International Parallel and Distributed Processing Symposium*, vol. 0, p. 166b, 2003.

[24] M. Rabbat and R. Nowak, "Distributed optimization in sensor networks," in *3rd international symposium on Information processing in sensor networks, 2004, IPSN '04*, 2004, pp. 20–27.

[25] J. Elson, L. Girod, and D. Estrin, "Fine-grained network time synchronization using reference broadcasts," *SIGOPS Oper. Syst. Rev.*, vol. 36, pp. 147–163, December 2002.

[26] W. Su and I. F. Akyildiz, "Time-diffusion synchronization protocol for wireless sensor networks," *IEEE/ACM Trans. Netw.*, vol. 13, pp. 384–397, April 2005.

[27] S. Ganeriwal and M. R. Kumar, "Network-wide time synchronization in sensor networks," *NESL Technical Report*, May 2003.

[28] D. Niculescu and B. Nath, "Ad hoc positioning system (APS)," vol. 5, 2001, pp. 2926–2931.

[29] A. Savvides, C.-C. Han, and M. B. Strivastava, "Dynamic fine-grained localization in ad-hoc networks of sensors," in *7th annual international conference on Mobile Computing and Networking, 2001, MobiCom '01*, 2001, pp. 166–179.

[30] A. D'Costa and A. Sayeed, "Collaborative signal processing for distributed classification in sensor networks," in *Information Processing in Sensor Networks*, ser. Lecture Notes in Computer Science, 2003, vol. 2634, pp. 558–558.

[31] F. Zhao, J. Shin, and J. Reich, "Information-driven dynamic sensor collaboration," *IEEE Signal Processing Magazine*, vol. 19, no. 2, pp. 61–72, Mar. 2002.

[32] S. K. R. Prakash Ishwar; Rohit Puri; Sandeep Pradhan, "On compression for robust estimation in sensor networks," in *Information Theory, 2003. Proceedings. IEEE International Symposium on*, July 2003, p. 193.

[33] M. Sartipi and F. Fekri, "Source and channel coding in wireless sensor networks using ldpc codes," in *First Annual IEEE Communications Society Conference on Sensor and Ad Hoc Communications and Networks, 2004, IEEE SECON 2004*, Oct 2004, pp. 309 – 316.

[34] P. Baronti, P. Pillai, V. W. Chook, S. Chessa, A. Gotta, and Y. F. Hu, "Wireless sensor networks: A survey on the state of the art and the 802.15.4 and zigbee standards," *Computer Communications*, vol. 30, no. 7, pp. 1655 – 1695, 2007.

[35] N. Srivastava, "Challenges of next-generation wireless sensor networks and its impact on society," *Journal of Telecommunications*, vol. 1, pp. 128–133, Feb. 2010.

[36] T. Arampatzis, J. Lygeros, and S. Manesis, "A survey of applications of wireless sensors and wireless sensor networks," in *Intelligent Control, 2005. Proceedings of the 2005 IEEE International Symposium on, Mediterrean Conference on Control and Automation*, 2005, pp. 719 –724.

[37] M. Kuorilehto, M. Hännikäinen, and T. D. Hämäläinen, "A survey of application distribution in wireless sensor networks," *EURASIP Journal on Wireless Communications and Networking*, vol. 2005, pp. 774–788, October 2005.

[38] C. F. Garcia-Hernandez, P. H. Ibarguengoytia-Gonzalez, J. Garcia-Hernandez, and J. A. Perez-Diaz, "Wireless sensor networks and applications: a survey," *International Journal of Computer Science and Network Security*, vol. 17, no. 3, pp. 264 –273, 2007.

[39] G. J. Pottie and W. J. Kaiser, "Wireless integrated network sensors," *Commun. ACM*, vol. 43, pp. 51–58, May 2000.

[40] A. Kunnath and M. Ramesh, "Integrating geophone network to real-time wireless sensor network system for landslide detection," in *First International Conference on Sensor Device Technologies and Applications, 2010, SENSORDEVICES'10*, 2010, pp. 167 –171.

[41] L. Yu, N. Wang, and X. Meng, "Real-time forest fire detection with wireless sensor networks," in *International Conference on Wireless Communications, Networking and Mobile Computing, 2005*, vol. 2, 2005, pp. 1214 – 1217.

[42] J. Zhang, W. Li, Z. Yin, S. Liu, and X. Guo, "Forest fire detection system based on wireless sensor network," in *4th IEEE Conference on Industrial Electronics and Applications, 2009, ICIEA 2009*, May 2009, pp. 520 –523.

[43] N.-B. Chang and D.-H. Guo, "Urban flash flood monitoring, mapping and forecasting via a tailored sensor network system," in *IEEE International Conference on Networking, Sensing and Control, 2006, ICNSC'06*, 0 2006.

[44] F. Kreit, G. Barberio, C. Subramanian, I. Kostanic, and J. Pinelli, "Performance testing of the wireless sensor network system for hurricane monitoring," in *First International Conference on Sensor Device Technologies and Applications, 2010, SENSORDEVICES'10*, 2010, pp. 63 –72.

[45] R. Pon, M. A. Batalin, V. Chen, A. Kansal, D. Liu, M. Rahimi, L. Shirachi, A. Somasundra, Y. Yu, M. Hansen, W. J. Kaiser, M. Srivastava, G. Sukhatme, and D. Estrin, "Coordinated static and mobile sensing for environmental monitoring," in *Distributed Computing in Sensor Systems*, ser. Lecture Notes in Computer Science, 2005, vol. 3560, pp. 403–405.

[46] G. Barrenetxea, F. Ingelrest, G. Schaefer, and M. Vetterli, "Wireless sensor networks for environmental monitoring: The sensorscope experience," in *Communications, 2008 IEEE International Zurich Seminar on*, 2008, pp. 98 –101.

[47] H. Liu, Z. Meng, and S. Cui, "A wireless sensor network prototype for environmental monitoring in greenhouses," in *International Conference on Wireless Communications, Networking and Mobile Computing, 2007, WiCom'07*, 2007, pp. 2344 –2347.

[48] R. Cardell-Oliver, K. Smettem, M. Kranz, and K. Mayer, "Field testing a wireless sensor network for reactive environmental monitoring [soil moisture measurement]," in *Intelligent Sensors, Sensor Networks and Information Processing Conference, 2004. Proceedings of the 2004*, 2004, pp. 7 – 12.

[49] J. Davis and R. Sloan, "Wireless sensor networks for industrial processes," in *Location Technologies, 2007. The Institution of Engineering and Technology Seminar on*, 2007, pp. 1 –8.

[50] S. Thiele, S. Schone, F. Voigt, M. Da Silva, and U. Hampel, "Design of a neutrally buoyant self-powered multi-parameter sensor for data logging in flow applications," in *IEEE Sensors, 2009*, 2009, pp. 1927 –1930.

[51] P. Jiang, H. Ren, L. Zhang, Z. Wang, and A. Xue, "Reliable application of wireless sensor networks in industrial process control," in *Intelligent Control and Automation, 2006. WCICA 2006. The Sixth World Congress on*, 0 2006.

[52] M. Bertocco, G. Gamba, A. Sona, and S. Vitturi, "Experimental characterization of wireless sensor networks for industrial applications," *IEEE Trans. on Instrumentation and Measurement*, vol. 57, no. 8, pp. 1537 –1546, 2008.

[53] J. H. Taylor and J. Slipp, "An integrated testbed for advanced wireless networked control systems technology," in *36th Annual Conference on IEEE Industrial Electronics Society, 2010, IECON 2010*, 2010, pp. 2101 –2106.

[54] M. Antoniou, M. Boon, P. Green, P. Green, and T. York, "Wireless sensor networks for industrial processes," in *IEEE Sensors Applications Symposium, 2009, SAS 2009*, 2009, pp. 13 –18.

[55] S. Shin, T. Kwon, G.-Y. Jo, Y. Park, and H. Rhy, "An experimental study of hierarchical intrusion detection for wireless industrial sensor networks," *IEEE Trans. on Industrial Informatics*, vol. 6, no. 4, pp. 744 –757, 2010.

[56] D. Christin, P. S. Mogre, and M. Hollick, "Survey on wireless sensor network technologies for industrial automation: The security and quality of service perspectives," *Future Internet*, vol. 2, no. 2, pp. 96–125, 2010.

[57] Y. Wan, L. Li, J. He, X. Zhang, and Q. Wang, "Anshan: Wireless sensor networks for equipment fault diagnosis in the process industry," in *5th Annual IEEE Communications Society Conference on Sensor, Mesh and Ad Hoc Communications and Networks, 2008, SECON '08*, 2008, pp. 314 –322.

[58] P. Pramod, S. Srikanth, N. Vivek, M. Patil, and C. Sarat, "Intelligent intrusion detection system (in2ds) using wireless sensor networks," in *International Conference on Networking, Sensing and Control, 2009, ICNSC '09*, 2009, pp. 587 –591.

[59] A. Chehri, P. Fortier, and P.-M. Tardif, "Security monitoring using wireless sensor networks," in *Fifth Annual Conference on Communication Networks and Services Research, 2007, CNSR'07*, May 2007, pp. 13 –17.

[60] C. Pham and A. Makhoul, "Performance study of multiple cover-set strategies for mission-critical video surveillance with wireless video sensors," in *IEEE 6th International Conference on Wireless and Mobile Computing, Networking and Communications, 2010, WiMob'10*, 2010, pp. 208 –216.

[61] D. Dudek, C. Haas, A. Kuntz, M. Zitterbart, D. Kruger, P. Rothenpieler, D. Pfisterer, and S. Fischer, "A wireless sensor network for border surveillanc," in *7th ACM Conference on Embedded Networked Sensor Systems, 2009, SenSys 2009*, November 2009, p. 303 304.

[62] K. Sha, W. Shi, and O. Watkins, "Using wireless sensor networks for fire rescue applications: Requirements and challenges," in *IEEE International Conference on Electro/information Technology, 2006*, May 2006, pp. 239 –244.

[63] F. Hu, M. Jiang, L. Celentano, and Y. Xiao, "Robust medical ad hoc sensor networks (masn) with wavelet-based ecg data mining," *Ad Hoc Netw.*, vol. 6, pp. 986–1012, September 2008.

[64] M. W. D. Malan, T. R. F. Fulford-Jones and S. Moulton, "Code-blue: An ad hoc sensor network infrastructure for emergency medical care," in *in Proc. MobiSys 2004 Workshop Applications Mobile Embedded Systems (WAMES 2004)*, Boston, MA, 2004, p. 1214.

[65] K. Martinez, J. Hart, and R. Ong, "Environmental sensor networks," *Computer*, vol. 37, no. 8, pp. 50 – 56, 2004.

[66] J. Rabaey, M. Ammer, J. da Silva, J.L., D. Patel, and S. Roundy, "Picoradio supports ad hoc ultra-low power wireless networking," *Computer*, vol. 33, no. 7, pp. 42 –48, Jul. 2000.

[67] I. Marin, E. Arceredillo, A. Zuloaga, and J. Arias, "Wireless sensor networks: a survey on ultra-low power-aware design," 2005.

[68] B. H. Calhoun, D. C. Daly, N. Verma, D. F. Finchelstein, D. D. Wentzloff, A. Wang, S.-H. Cho, and A. P. Chandrakasan, "Design considerations for ultra-low energy wireless microsensor nodes," *IEEE Trans. on Computers*, vol. 54, no. 6, pp. 727–740, 2005.

[69] C. Cordeiro and D. P. Agrawal, *Ad hoc & sensor networks: Theory and applications*. World scientific publishing, 2006.

[70] C. Buratti, A. Conti, D. Dardari, and R. Verdone, "An overview on wireless sensor networks technology and evolution," *Sensors*, vol. 9, no. 9, pp. 6869–6896, 2009.

[71] Y. Chae and Y. Kwon, "Traffic adaptive ieee 802.15.4 medium access control," *International Journal of Pervasive Computing and Communications*, vol. 4, no. 2, pp. 198 – 212, 2008.

[72] J. Polastre, R. Szewczyk, and D. Culler, "Telos: enabling ultra-low power wireless research," in *IPSN '05: Proceedings of the 4th international symposium on Information processing in sensor networks*, Piscataway, NJ, USA, 2005.

[73] A. Mainwaring, D. Culler, J. Polastre, R. Szewczyk, and J. Anderson, "Wireless sensor networks for habitat monitoring," in *Proceedings of the 1st ACM international workshop on Wireless sensor networks and applications*, ser. WSNA '02, 2002, pp. 88–97.

[74] R. Szewczyk, E. Osterweil, J. Polastre, M. Hamilton, A. Mainwaring, and D. Estrin, "Habitat monitoring with sensor networks," *Commun. ACM*, vol. 47, pp. 34–40, June 2004.

[75] D. Mascarenas, E. Flynn, C. Farrar, G. Park, and M. Todd, "A mobile host approach for wireless powering and interrogation of structural health monitoring sensor networks," *IEEE Sensors Journal*, vol. 9, no. 12, pp. 1719 –1726, 2009.

[76] P. De Mil, B. Jooris, L. Tytgat, R. Catteeuw, I. Moerman, P. Demeester, and A. Kamerman, "Design and implementation of a generic energy-harvesting framework applied to the evaluation of a large-scale electronic shelf-labeling wireless sensor network," *EURASIP J. Wirel. Commun. Netw.*, vol. 2010, pp. 7:1–7:14, February 2010.

[77] Y. K. Tan and S. Panda, "Optimized wind energy harvesting system using resistance emulator and active rectifier for wireless sensor nodes," *IEEE Trans. on Power Electronics*, vol. 26, no. 1, pp. 38 –50, 2011.

[78] I. Demirkol, C. Ersoy, and F. Alagoz, "Mac protocols for wireless sensor networks: a survey," *IEEE Communications Magazine*, vol. 44, no. 4, pp. 115 – 121, 2006.

[79] K. Akkaya and M. Younis, "A survey on routing protocols for wireless sensor networks," *Ad Hoc Networks*, vol. 3, no. 3, pp. 325 – 349, 2005.

[80] J. Al-Karaki and A. Kamal, "Routing techniques in wireless sensor networks: a survey," *IEEE Wireless Communications*, vol. 11, no. 6, pp. 6 – 28, 2004.

[81] L. Tong, Q. Zhao, and S. Adireddy, "Sensor networks with mobile agents," in *in Proc. 2003 Military Communications Intl Symp*, 2003, pp. 688–693.

[82] P. Gupta and P. Kumar, "The capacity of wireless networks," *Information Theory, IEEE Trans. on*, vol. 46, no. 2, pp. 388 –404, Mar. 2000.

[83] H. Gharavi and K. Ban, "Multihop sensor network design for wide-band communications," *Proceedings of the IEEE*, vol. 91, no. 8, pp. 1221 – 1234, 2003.

[84] Q. Wang, M. Hempstead, and W. Yang, "A realistic power consumption model for wireless sensor network devices," in *3rd Annual IEEE Communications Society on Sensor and Ad Hoc Communications and Networks, 2006, SECON '06*, vol. 1, 2006, pp. 286 –295.

[85] A. Kalis and A. Kanatas, "Cooperative beam forming in smart dust: Getting rid of multihop communications," *IEEE Pervasive Computing*, vol. 9, pp. 47–53, July 2010.

[86] C. Wang, Q. Yin, J. Zhang, B. Hao, and W. Li, "Distributed transmit beamforming without phase feedback," *EURASIP J. Wirel. Commun. Netw.*, vol. 2010, pp. 1–8, January 2010.

[87] O. Younis and S. Fahmy, "Heed: A hybrid, energy-efficient, distributed clustering approach for ad hoc sensor networks," *IEEE Trans. on Mobile Computing*, vol. 3, pp. 366–379, 2004.

[88] R. Ramanathan, "On the performance of ad hoc networks with beamforming antennas," in *ACM MobiHoc*, 2001, pp. 95–105.

[89] M. F. A. Ahmed and S. A. Vorobyov, "Collaborative beamforming for wireless sensor networks with gaussian distributed sensor nodes," *IEEE Trans. on Wireless Communications*, vol. 8, no. 2, pp. 638–643, Feb. 2009.

[90] Z. Han and H. V. Poor, "Lifetime improvement in wireless sensor networks via collaborative beamforming and cooperative transmission," *IET Microwaves, Antennas, and Propagation*, vol. 1, no. 6, pp. 1103–1110, Dec. 2007.

[91] S. Betz, H. Poor, and A. Petropulu, "Cooperative beamforming and power control," in *Conference Record of the Forty-First Asilomar Conference on Signals, Systems and Computers, 2007, ACSSC'07*, 2007, pp. 2117 –2123.

[92] M. Kiese, C. Hartmann, J. Lamberty, and R. Vilzmann, "On connectivity limits in ad hoc networks with beamforming antennas," *EURASIP J. Wirel. Commun. Netw.*, vol. 2009, February 2009.

[93] R. Ramanathan, in *Proc. 2nd ACM international symposium on Mobile ad hoc networking and computing*.

[94] Y. Lo, "A mathematical theory of antenna arrays with randomly spaced elements," *IEEE Trans. Antennas and Propagation*, vol. 12, no. 3, pp. 257–268, May 1964.

[95] B. Steinberg, *Principles of Aperture and Array System Design*. New York, USA: Wiley, 1976.

[96] V. Agrawal and Y. Lo, "Distribution of sidelobe level in random arrays," *Proceedings of the IEEE*, vol. 57, no. 10, pp. 1764 – 1765, 1969.

[97] A. S. Shifrin, *Statistical antenna theory*. Golem Press, 1971.

[98] B. Steinberg, "The peak sidelobe of the phased array having randomly located elements," *IEEE Trans. on Antennas and Propagation*, vol. 20, no. 2, pp. 129 – 136, Mar. 1972.

[99] A. Akdagli and K. Guney, "Shaped-beam pattern synthesis of equally and unequally spaced linear antenna arrays using a modified tabu search algorithm," *Microwave and Optical Technology Letters*, vol. 36, no. 1, p. 1620, January 2003.

[100] J. A. R. Azevedo, "Synthesis of planar arrays with elements in concentric rings," *IEEE Trans. on Antennas and Propagation*, 2010.

[101] A. Panicali and Y. Lo, "A probabilistic approach to large circular and spherical arrays," *IEEE Trans. on Antennas and Propagation*, vol. 17, no. 4, pp. 514 – 522, Jul. 1969.

[102] B. Kumar and G. Branner, "Generalized analytical technique for the synthesis of unequally spaced arrays with linear, planar, cylindrical or spherical geometry," *IEEE Trans. on Antennas and Propagation*, vol. 53, no. 2, pp. 621 –634, 2005.

[103] O. Bucci, M. D'Urso, T. Isernia, P. Angeletti, and G. Toso, "Deterministic synthesis of uniform amplitude sparse arrays via new density taper techniques," *IEEE Trans. on Antennas and Propagation*, vol. 58, no. 6, pp. 1949 –1958, 2010.

[104] D. Jenn, Y. Loke, M. Tong, E. C. Yeo, and R. Broadston, "Distributed phased arrays with wireless beamforming," in *Conference Record of the Forty-First Asilomar Conference on Signals, Systems and Computers, 2007, ACSSC'07*, 2007, pp. 948 –952.

[105] A. R. Hunt, "Image formation through walls using a distributed radar sensor array," *Applied Image Pattern Recognition Workshop,*, vol. 0, p. 232, 2003.

[106] R. Heimiller, J. Belyea, and P. Tomlinson, "Distributed array radar," *IEEE Trans. on Aerospace and Electronic Systems*, vol. AES-19, no. 6, pp. 831 –839, 1983.

[107] E. Attia and K. Abend, "An experimental demonstration of a distributed array radar," in *Antennas and Propagation Society International Symposium, 1991. AP-S. Digest*, Jun. 1991, pp. 1720 –1723 vol.3.

[108] M. Haleem and A. Haimovich, "On the distribution of ambiguity levels in mimo radar," in *42nd Asilomar Conference on Signals, Systems and Computers, 2008*, 2008, pp. 198 –202.

[109] H. Steyskal, J. Schindler, P. Franchi, and R. Mailloux, "Pattern synthesis for techsat21-a distributed spacebased radar system," in *Aerospace Conference, 2001, IEEE Proceedings.*, 2001.

[110] ——, "Pattern synthesis for techsat21 - a distributed space-based radar system," *IEEE Antennas and Propagation Magazine*, vol. 45, no. 4, pp. 19 – 25, 2003.

[111] J. Schindler and H. Steyskal, "Sparse, random array processing for space-based radar," in *System Theory, 2004. Proceedings of the Thirty-Sixth Southeastern Symposium on*, 2004.

[112] G. Toso, C. Mangenot, and A. Roederer, "Sparse and thinned arrays for multiple beam satellite applications," in *The Second European Conference on Antennas and Propagation, 2007, EuCAP'07*, 2007, pp. 1 –4.

[113] M. Gregory and D. Werner, "Ultrawideband aperiodic antenna arrays based on optimized raised power series representations," *IEEE Trans. on Antennas and Propagation*, vol. 58, no. 3, pp. 756 –764, 2010.

[114] T. Spence and D. Werner, "Design of broadband planar arrays based on the optimization of aperiodic tilings," *IEEE Trans. on Antennas and Propagation*, vol. 56, no. 1, pp. 76 –86, 2008.

[115] S. Goss, L. Frizzell, J. Kouzmanoff, J. Barich, and J. Yang, "Sparse random ultrasound phased array for focal surgery," *IEEE Trans. on Ultrasonics, Ferroelectrics and Frequency Control*, vol. 43, no. 6, pp. 1111 –1121, Nov. 1996.

[116] S. Holm and B. Elgetun, "Properties of the beampattern of weight- and layout-optimized sparse arrays," *IEEE Trans. on Ultrasonics, Ferroelectrics and Frequency Control*, vol. 44, no. 5, pp. 983 –991, Sep. 1997.

[117] S. Goudos, V. Moysiadou, T. Samaras, K. Siakavara, and J. Sahalos, "Application of a comprehensive learning particle swarm optimizer to unequally spaced linear array synthesis with sidelobe level suppression and null control," *IEEE Antennas and Wireless Propagation Letters*, 2010.

[118] Y. Bar-Ness and A. Haimovich, "Synthesis of random antenna array patterns with prescribed nulls," *IEEE Trans. on Antennas and Propagation*, vol. 32, no. 12, pp. 1298 – 1307, Dec. 1984.

[119] N. Jin and Y. Rahmat-Samii, "Advances in particle swarm optimization for antenna designs: Real-number, binary, single-objective and multiobjective implementations," *IEEE Trans. on Antennas and Propagation*, vol. 55, no. 3, pp. 556 –567, 2007.

[120] Y. Liu, Z. Nie, and Q. H. Liu, "Reducing the number of elements in a linear antenna array by the matrix pencil method," *IEEE Trans. on Antennas and Propagation*, vol. 56, no. 9, pp. 2955 –2962, 2008.

[121] L. Cen, W. Ser, Z. L. Yu, S. Rahardja, and W. Cen, "Linear sparse array synthesis with minimum number of sensors," *IEEE Trans. on Antennas and Propagation*, vol. 58, no. 3, pp. 720 –726, 2010.

[122] X. Ren, J. Azevedo, and A. Casimiro, "Synthesis of non-uniformly spaced arrays using the fourier transform and window techniques," *IET Microwaves, Antennas, and Propagation*, vol. 3, no. 8, pp. 1245 –1253, 2009.

[123] Y.-B. Tian and J. Qian, "Improve the performance of a linear array by changing the spaces among array elements in terms of genetic algorithm," *IEEE Trans. on Antennas and Propagation*, vol. 53, no. 7, pp. 2226 – 2230, 2005.

[124] F. Ares-Pena, J. Rodriguez-Gonzalez, E. Villanueva-Lopez, and S. Rengarajan, "Genetic algorithms in the design and optimization of antenna array patterns," *IEEE Trans. on Antennas and Propagation*, vol. 47, no. 3, pp. 506 –510, Mar. 1999.

[125] A. Tennant, M. Dawoud, and A. Anderson, "Array pattern nulling by element position perturbations using a genetic algorithm," *Electronics Letters*, vol. 30, no. 3, pp. 174 –176, Feb. 1994.

[126] D. Kurup, M. Himdi, and A. Rydberg, "Synthesis of uniform amplitude unequally spaced antenna arrays using the differential evolution algorithm," *IEEE Trans. on Antennas and Propagation*, vol. 51, no. 9, pp. 2210 – 2217, Sep. 2003.

[127] V. Murino, A. Trucco, and C. Regazzoni, "Synthesis of unequally spaced arrays by simulated annealing," *IEEE Trans. on Signal Processing*, vol. 44, no. 1, pp. 119 –122, Jan. 1996.

[128] A. Rodriguez, R. Munoz, H. Estevez, E. Ares, and E. Moreno, "Synthesis of planar arrays with arbitrary geometry generating arbitrary footprint patterns," *IEEE Trans. on Antennas and Propagation*, vol. 52, no. 9, pp. 2484 – 2488, 2004.

[129] M. Khodier and C. Christodoulou, "Linear array geometry synthesis with minimum sidelobe level and null control using particle swarm optimization," *IEEE Trans. on Antennas and Propagation*, vol. 53, no. 8, pp. 2674 – 2679, 2005.

[130] R. Harrington, "Sidelobe reduction by nonuniform element spacing," *IRE Trans. on Antennas and Propagation*, vol. 9, no. 2, pp. 187 –192, 1961.

[131] B. Kumar and G. Branner, "Design of unequally spaced arrays for performance improvement," *IEEE Trans. on Antennas and Propagation*, vol. 47, no. 3, pp. 511 –523, Mar. 1999.

[132] R. Willey, "Space tapaering of linear and planar arrays," *Antennas and Propagation, IRE Trans. on*, vol. 10, no. 4, pp. 369 –377, 1962.

[133] B. Fuchs, "Shaped beam synthesis of arbitrary arrays via linear programming," *IEEE Antennas and Wireless Propagation Letters*, 2010.

[134] H. Schjaer-Jacobsen and K. Madsen, "Synthesis of nonuniformly spaced arrays using a general nonlinear minimax optimisation method," *IEEE Trans. on Antennas and Propagation*, vol. 24, no. 4, pp. 501 – 506, Jul. 1976.

[135] R. Mailloux and E. Cohen, "Statistically thinned arrays with quantized element weights," *IEEE Trans. on Antennas and Propagation*, vol. 39, no. 4, pp. 436 –447, Apr. 1991.

[136] T. Maher and D. Cheng, "Random removal of radiators from large linear arrays," *IEEE Trans. on Antennas and Propagation*, vol. 11, no. 2, pp. 106 – 112, Mar. 1963.

[137] M. Donvito and S. Kassam, "Characterization of the random array peak sidelobe," *IEEE Trans. on Antennas and Propagation*, vol. 27, no. 3, pp. 379 – 385, May 1979.

[138]

[139] J.-H. Chang and L. Tassiulas, "Maximum lifetime routing in wireless sensor networks," *Networking, IEEE/ACM Trans. on*, vol. 12, no. 4, pp. 609 – 619, 2004.

[140] M. Gatzianas and L. Georgiadis, "A distributed algorithm for maximum lifetime routing in sensor networks with mobile sink," *IEEE Trans. on Wireless Communications*, vol. 7, no. 3, pp. 984 –994, 2008.

[141] R. Madan and S. Lall, "Distributed algorithms for maximum lifetime routing in wireless sensor networks," *IEEE Trans. on Wireless Communications*, vol. 5, no. 8, pp. 2185 –2193, 2006.

[142] G. Barriac, R. Mudumbai, and U. Madhow, "Distributed beamforming for information transfer in sensor networks," in *Proceedings of the Third International Symposium on Information processing in Sensor Networks (IPSN), IPSN 2004*, Apr. 2004, pp. 81–88.

[143] D. Wang, B. Xie, and D. Agrawal, "Coverage and lifetime optimization of wireless sensor networks with gaussian distribution," *Mobile Computing, IEEE Transactions on*, vol. 7, no. 12, pp. 1444 –1458, 2008.

[144] R. Mudumbai, B. Wild, U. Madhow, and K. Ramchandran, "Distributed beamforming using 1 bit feedback: from concept to realization," in *Proc. of 44'th Allerton Conference on Communication, Control and Signal Processing*, Sept 2006, pp. 1020–1027.

[145] R. Mudumbai, J. Hespanha, U. Madhow, and G. Barriac, "Distributed transmit beamforming using feedback control," *IEEE Trans. on Information Theory*, vol. 56, no. 1, pp. 411 –426, 2010.

[146] S. Sigg and M. Beigl, "Algorithms for closed-loop feedback based distributed adaptive beamforming in wireless sensor networks," in *5th International Conference on Intelligent Sensors, Sensor Networks and Information Processing, 2009, ISSNIP'09*, 2009, pp. 25 –30.

[147] S. Song, J. Thompson, P.-J. Chung, and P. Grant, "Improving the one-bit feedback algorithm for distributed beamforming," in *IEEE Wireless Communications and Networking Conference (WCNC), 2010*, 2010, pp. 1 –6.

[148] J. A. Bucklew and W. A. Sethares, "Convergence of a class of decentralized beamforming algorithms," in *IEEE/SP 14th Workshop on Statistical Signal Processing 2007, SSP '07*, Aug. 2007, pp. 123–125.

[149] Y.-S. Tu and G. J. Pottie, "Coherent cooperative transmission from multiple adjacent antennas to a distant stationary antenna through awgn channels," in *Vehicular Technology Conference, 2002. VTC Spring 2002. IEEE 55th*, vol. 1, 2002, pp. 130 – 134.

[150] D. R. Brown and H. V. Poor, "Time-slotted round-trip carrier synchronization for distributed beamforming," *IEEE Trans. on Signal Processing*, vol. 56, no. 11, pp. 5630–5643, Nov. 2008.

[151] I. Brown, D.R., G. Prince, and J. McNeill, "A method for carrier frequency and phase synchronization of two autonomous cooperative transmitters," in *Signal Processing Advances in Wireless Communications, 2005 IEEE 6th Workshop on*, 2005, pp. 260 – 264.

[152] I. Ozil and D. Brown, "Time-slotted round-trip carrier synchronization," in *Conference Record of the Forty-First Asilomar Conference on Signals, Systems and Computers, 2007, ACSSC 2007*, 2007, pp. 1781 –1785.

[153] M. Ferguson, "On the control, stability, and waiting time in a slotted aloha random-access system," *IEEE Trans. on Commun.*, vol. 23, no. 11, pp. 1306 – 1311, Nov. 1975.

[154] M. H. Ngo, V. Krishnamurthy, and L. Tong, "Optimal channel-aware aloha protocol for random access in wlans with multipacket reception and decentralized channel state information," *IEEE Trans. on Signal Processing*, vol. 56, no. 6, pp. 2575 –2588, 2008.

[155] Y.-W. P. Hong, C.-K. Lin, and S.-H. Wang, "Exploiting cooperative advantages in slotted aloha random access networks," *IEEE Trans. on Information Theory*, vol. 56, no. 8, pp. 3828 –3846, 2010.

[156] M. Tsatsanis, R. Zhang, and S. Banerjee, "Network-assisted diversity for random access wireless networks," *IEEE Trans. on Signal Processing*, vol. 48, no. 3, pp. 702 –711, Mar. 2000.

[157] R. Lin and A. P. Petropulu, "A new wireless network medium access protocol based on cooperation," *IEEE Trans. on Signal Processing*, vol. 53, no. 12, pp. 4675–4684, Dec. 2005.

[158] L. Dong and A. P. Petropulu, "Multichannel alliances: A cooperative cross-layer scheme for wireless networks," *IEEE Trans. on Signal Processing*, vol. 56, no. 2, pp. 771 –784, 2008.

[159] L. Dong, A. P. Petropulu, and H. V. Poor, "A cross-layer approach to collaborative beamforming for wireless ad hoc networks," *IEEE Trans. on Signal Processing*, vol. 56, pp. 2981–2993, Jul. 2008.

[160] A. P. Petropulu, L. Dong, and H. V. Poor, "Weighted cross-layer cooperative beamforming for wireless networks," *IEEE Trans. on Signal Processing*, vol. 57, no. 8, pp. 3240–3252, Aug. 2009.

[161] R. Mudumbai, J. Hespanha, U. Madhow, and G. Barriac, "Scalable feedback control for distributed beamforming in sensor networks," in *International Symposium on Information Theory 2005, ISIT 2005*, Sep. 2005, pp. 137–141.

[162] R. Annavajjala and C. R. Murthy, "Pilot-assisted distributed co-phasing for wireless sensor networks," in *Proceedings of the 6th Annual IEEE communications society conference on Sensor, Mesh and Ad Hoc Communications and Networks*, ser. SECON'09, 2009, pp. 476–483.

[163] H. Naqvi, M. Sulayman, and M. Riaz, "Adaptive beamforming in wireless sensor network in the presence of interference sources," in *Communication and Networking*, ser. Communications in Computer and Information Science, 2009, vol. 56, pp. 105–113.

[164] A. Amar, "The effect of local scattering on the gain and beamwidth of a collaborative beampattern for wireless sensor networks," *IEEE Trans. on Wireless Communications*, vol. 9, pp. 2730 – 2736, sep 2010.

[165] W. Lintz, J. McEachen, and M. Tummala, "Sensor beamforming with distributed mobile elements in a wireless sensor network," in *Canadian Conference on Electrical and Computer Engineering, 2009, CCECE '09*, May 2009, pp. 323 –328.

[166] L. Zheng and X.-D. Zhang, "Cooperative beamforming with mobile wireless sensor nodes: Performance analysis and optimal node locations," *IEEE Trans. on Communications*, vol. 58, no. 12, pp. 3375 – 3380, 2010.

[167] M. Tummala, C. C. Wai, and P. Vincent, in *Conference Record of the Thirty-Ninth Asilomar Conference on Signals, Systems and Computers, 2005.*

[168] W. Chen, D. Wang, and W. Wang, "Beamforming for information transfer in wireless sensor networks without perfect positioning," in *Microwave Conference Proceedings, 2005. APMC 2005. Asia-Pacific Conference Proceedings*, vol. 3, 2005.

[169] J.-H. Lee and C.-C. Wang, in *Adaptive array beamforming with robust capabilities under random sensor position errors.*

[170] K.-L. Kuo, H.-Y. Hsieh, and P.-C. Yeh, "A study on collaborative beamforming with protocol defects in wireless ad hoc networks," in *IEEE International Conference on Communications, 2009, ICC'09*, 2009, pp. 1 –6.

[171] M.-O. Pun, D. Brown, and H. Vincent Poor, "Opportunistic collaborative beamforming with one-bit feedback," in *Signal Processing Advances in Wireless Communications, 2008. SPAWC 2008. IEEE 9th Workshop on*, 2008, pp. 246 –250.

[172] M.-O. Pun, D. Brown, and H. Poor, "Opportunistic collaborative beamforming with one-bit feedback," *IEEE Trans. on Wireless Communications*, vol. 8, no. 5, pp. 2629 –2641, May 2009.

[173] K. Zarifi, S. Affes, and A. Ghrayeb, "Distributed beamforming for wireless sensor networks with random node location," in *IEEE International Conference on Acoustics, Speech and Signal Processing 2009, ICASSP 2009*, Taipei,, Apr. 2009, pp. 2261–2264.

[174] ——, "Distributed null-steering beamforming for wireless sensor networks," in *IEEE Global Telecommunications Conference, Globecom 2009*, Honolulu, Hawaii, Nov./Dec. 2009.

[175] S. Betz and H. Poor, "Energy efficient communication using cooperative beamforming: A game theoretic analysis," in *Personal, Indoor and Mobile Radio Communications, 2008. PIMRC 2008. IEEE 19th International Symposium on*, 2008, pp. 1 –5.

[176] C. Lin, V. Veeravalli, and S. Meyn, "A random search framework for convergence analysis of distributed beamforming with feedback," *Information Theory, IEEE Trans. on*, vol. 56, no. 12, pp. 6133 –6141, 2010.

[177] M. Johnson, M. Mitzenmacher, and K. Ramchandran, "Distributed beamforming with binary signaling," in *Information Theory, 2008. ISIT 2008. IEEE International Symposium on*, 2008, pp. 890 –894.

[178] S. Zaidi, K. Zarifi, S. Affes, and A. Ghrayeb, "A decentralized collaborative receive beamforming technique for wireless sensor networks," in *Vehicular Technology Conference (VTC 2010-Spring), 2010 IEEE 71st*, May 2010, pp. 1 –5.

[179] B. Banitalebi, S. Sigg, and M. Beigl, "On the feasibility of receive collaboration in wireless sensor networks," in *Personal Indoor and Mobile Radio Communications (PIMRC), 2010 IEEE 21st International Symposium on*, Sept. 2010, pp. 1608 – 1613.

[180] C. A. Balanis, *Antenna Theory: Analysis and Design*. New York, USA: Wiley, 1997.

[181]

[182] F. Haber, "Statistical properties of a random array of acoustic sensors in a multipath environment," 1977.

[183] D. A. S. Fraser, "Generalized hit probabilities with a gaussian target," *Ann. Math. Statist.*, vol. 22, no. 2, pp. 248–225, 1951.

[184] A. Papoulis, *Probability, Random Variables, and Stochastic Processes*, 3rd ed. Mc-Graw Hill, 1991.

[185] T. Rappaport, *Wireless Communications: Principles and Practice*, 2nd ed. Upper Saddle River, NJ: Prentice Hall PTR, 2001.

[186] J. G. Proakis, *Digital Communications*, 4th ed. McGraw-Hill, 2001.

[187] B. Sklar, "Rayleigh fading channels in mobile digital communication systems .i. characterization," *IEEE Communications Magazine*, vol. 35, no. 7, pp. 90 – 100, Jul. 1997.

[188]

[189] I. F. Blake and W. C. Lindsey, "Level crossing problems for random processes," *IEEE Transactions on Information Theory*, vol. 19, no. 3, pp. 295–315, May 1973.

[190] H. Cramer and M. R. Leadbetter, *Stationary and Related Stochastic Processes.* New York: Wiley, 1967.

[191] M. F. A. Ahmed and S. A. Vorobyov, "Beampattern random behavior in wireless sensor networks with gaussian distributed sensor nodes," in *Canadian Conference on Electrical and Computer Engineering 2008, CCECE '08*, May 2008, pp. 257–260.

[192] H. L. Van Trees, *Optimum Array Processing (Detection, Estimation, and Modulation Theory, Part IV)*, 1st ed. New York, USA: Wiley, Mar. 2002.

[193] D. T. Hughes and J. G. McWhirter, "Sidelobe control in adaptive beamforming using a penalty function," in *Proc. ISSPA*, 1996.

[194] J. Yindi and H. Jafarkhani, "Network beamforming using relays with perfect channel information," in *Proc. IEEE ICASSP*, Apr. 2007, pp. 473–476.

[195] V. Havary-Nassab, S. Shahbazpanahi, A. Grami, and L. Zhi-Quan, "Distributed beamforming for relay networks based on second-order statistics of the channel state information," *IEEE Trans. Signal Processing*, vol. 56, no. 9, pp. 4306–4316, 2008.

[196] I. Cosovic and T. Mazzoni, "Suppression of sidelobes in ofdm systems by multiple-choice sequences," *European Trans. Telecommun.*, vol. 17, no. 6, pp. 623–630, June 2006.

[197] J. M. Molina-Garcia-Pardo, A. Martinez-Sala, M. V. Bueno-Delgado, E. Egea-Lopez, L. Juan-Llacer, and J. Garca-Haro, "Channel model at 868 mhz for wireless sensor networks in outdoor scenarios," *IEEE Journal of Communication and Networks*, vol. 7, no. 4, pp. 401–407, Dec. 2005.

[198] G. Zhou, T. He, S. Krishnamurthy, and J. A. Stankovic, "Models and solutions for radio irregularity in wireless sensor networks," *ACM Trans. on Sensor Networks*, vol. 2, no. 2, pp. 221–262, May 2006.

[199] H. Yang, A. P. Petropulu, X. Yang, and T. Camp, "A novel location relay selection scheme for ALLIANCES," *IEEE Trans. on Vehicular Technology*, vol. 57, no. 2, pp. 1272–1284, Mar. 2008.

[200] E. L. Crow and K. Shimizu, *Lognormal Distributions: Theory and Applications.* CRC Press, 1987.

[201] D. C. Montgomery and G. C. Runger, *Applied Statistics and Probability for Engineers.* Hoboken, NJ: Wiley, 2007.

[202] C. W. Helstrom, *Probability and Stochastic Processes for Engineers.* New York, USA: Macmillan Publishing Company, 1984.

[203] E. Stavrou and A. Pitsillides, "A survey on secure multipath routing protocols in wsns," *Comput. Netw.*, vol. 54, pp. 2215–2238, September 2010.

[204] Y. Sankarasubramaniam, I. F. Akyildiz, and S. W. McLaughlin, "Energy efficiency based packet size optimization in wireless sensor networks," in *First IEEE International Workshop on Sensor Network Protocols and Applications, 2003*, Jun. 2003, pp. 1–8.

[205] Z. Shelby, C. Pomalaza-Rez, H. Karvonen, and J. Haapola, "Energy optimization in multihop wireless embedded and sensor networks," *International Journal of Wireless Information Networks*, vol. 12, pp. 11–21, 2005.

[206] P. Dukes, V. Syrotiuk, and C. Colbourn, "Ternary schedules for energy-limited sensor networks," *Information Theory, IEEE Transactions on*, vol. 53, no. 8, pp. 2791 –2798, 2007.

[207] S. Tokunaga, Y. Kawakami, K. Hashimoto, S. Tomisato, S. Denno, and M. Hata, "Power saving effect of sensor collaborative beamforming for wireless ubiquitous network systems," in *14th Asia-Pacific Conference on Communications, 2008, APCC 2008*, 2008, pp. 1 –5.

[208] J. Feng, C.-W. Chang, S. Sayilir, Y.-H. Lu, B. Jung, D. Peroulis, and Y. Hu, "Energy-efficient transmission for beamforming in wireless sensor networks," in *7th Annual IEEE Communications Society Conference on Sensor Mesh and Ad Hoc Communications and Networks, 2010, SECON'10*, 2010, pp. 1 –9.

[209] K. Cohen and A. Leshem, "A time-varying opportunistic approach to lifetime maximization of wireless sensor networks," *Signal Processing, IEEE Transactions on*, vol. 58, no. 10, pp. 5307 –5319, 2010.

[210] M. Perillo and W. Heinzelman, "An integrated approach to sensor role selection," *IEEE Trans. on Mobile Computing*, vol. 8, no. 5, pp. 709 –720, May 2009.

[211] M. Mallinson, S. Hussain, and J. H. Park, "Investigating wireless sensor network lifetime using a realistic radio communication model," in *International Conference on Multimedia and Ubiquitous Engineering, 2008, MUE 2008*, 2008, pp. 433 –437.

[212] M. Noori and M. Ardakani, "A probabilistic lifetime analysis for clustered wireless sensor networks," in *IEEE Wireless Communications and Networking Conference, 2008. WCNC 2008*, 31 2008.